FINITE ELEMENT MODELLING OF OIL-OPERATED PISTON-CYLINDER PRESSURE BALANCES: DETERMINING UNCERTAINTIES IN DISTORTION COEFFICIENT PREDICTIONS USING THE FINITE ELEMENT METHOD

T.J. Esward
Centre for Mechanical and Acoustical Metrology
National Physical Laboratory

ABSTRACT

This report documents the results of two projects which set out to use finite element methods to investigate the manner in which the pistons and cylinders of oil-operated pressure balances distort when they are subject to high pressure. It sets out the results of predictions of piston-cylinder distortion coefficients for three pressure balances operated by the UK's National Physical Laboratory and one operated by Germany's Physikalisch-Technische Bundesanstalt. It derives uncertainty budgets for distortion coefficients based on calculations of variations in the output of finite element models as the input parameters are varied. The results show clearly that accurate modelling requires precise knowledge of the elastic properties of the components of the balance and of the boundary conditions to be applied to the model. Finally, the report reviews the feasibility of three-dimensional modelling of pressure balances and makes recommendations for future research.

ISSN 1369-6785

National Physical Laboratory
Queens Road, Teddington, Middlesex, TW11 0LW

Approved on behalf of the Managing Director, NPL
by Dr R C Preston, authorised by Head of Centre,
Centre for Mechanical and Acoustical Metrology

CONTENTS

ABSTRACT 1
1 INTRODUCTION 5
1.1 BACKGROUND TO THE PROJECTS 5
1.2 THE IMPORTANCE OF DISTORTION COEFFICIENTS 5
1.3 THE AIMS OF THE PROJECTS 6
1.4 THE NPL PROJECT 7
1.5 THE EUROMET PROJECT NO 463 7
1.6 STRUCTURE OF THE REPORT 8
2 FINITE ELEMENT ANALYSIS OF PRESSURE BALANCES: BACKGROUND 9
2.1 ANALYTICAL METHODS OF UNDERSTANDING PRESSURE BALANCES 9
2.2 WHY FEA METHODS ARE PREFERRED 10
2.3 EARLIER FEA WORK AT NPL 11
2.4 KEY ISSUES (1): MATERIAL PROPERTIES 11
2.5 KEY ISSUES (2): GEOMETRY 13
2.6 KEY ISSUES (3): BOUNDARY CONDITIONS 13
2.7 KEY ISSUES (4): LIMITATIONS OF THE MODELS 14
3 SETTING UP THE ANSYS MODELS 16
3.1. THE ANSYS PARAMETRIC DESIGN LANGUAGE 16
3.2 PRE-PROCESSING 17
3.3 THE SOLUTION AND POST-PROCESSING 17
3.4 ANALYSING THE RESULTS 18
3.5 MODELLING THE FLUID 18
4 TESTING THE ANSYS APPROACH 20
4.1 INTRODUCTION 20
4.2 THE EUROMET 256 PROJECT BALANCE MODEL 20
4.3 RESULTS OF COMPARISON 21
5 THE BASIC FEA MODELS: SPECIFICATIONS AND INITIAL TESTS 26
5.1 INTRODUCTION 26
5.2 B2-816 26
5.3. B2-817 28
5.4 CITY UNIVERSITY RESULTS FOR B2-816 AND B2-817 29
5.5 B2-816: COMPARISON WITH CITY UNIVERSITY RESULTS 30
5.6 B2-817: COMPARISON WITH CITY UNIVERSITY RESULTS 34
5.7 VARYING THE LINE PRESSURE FOR B2-816 AND B2-817 36
5.8 D&H SERIAL NO 1000 38
5.9 THE EUROMET 463 PROJECT BALANCE 41
6 VARYING THE INPUTS 44
6.1 B2-816 44
6.2 B2-817 47
6.3 D&H SERIAL NO 1000 50
6.4 THE EUROMET 463 PROJECT BALANCE 54
7 COMPARISON WITH EXPERIMENT AND UNCERTAINTY BUDGETS 66
7.1 B2-816, B2-817 and D&H SERIAL NO. 1000: EXPERIMENT 66
7.2 THE EUROMET 463 PROJECT BALANCE: EXPERIMENT 67
7.3 UNCERTAINTY BUDGET: EUROMET PROJECT 463 BALANCE 70

7.4 UNCERTAINTY BUDGETS: NPL PRESSURE BALANCES 80
8 FEASIBILITY OF THREE-DIMENSIONAL MODELLING 85
8.1 INTRODUCTION 85
8.2 DEFINING THE UNDISTORTED AREA 85
8.3 AXIAL SYMMETRY AND 3-D MODELLING 86
8.4 THE EUROMET 463 EXPERIENCE 86
8.5 USING MEASURED PROFILE DATA: CONCLUSIONS 92
9 CONCLUSIONS 94
9.1 SUMMARY OF CONCLUSIONS OF CURRENT PROJECT 94
9.2 RECOMMENDATIONS FOR FUTURE WORK 95
10 ACKNOWLEDGEMENTS 97
REFERENCES 98
APPENDIX A: DIAGRAMS OF MODELLED BALANCES 100

1 INTRODUCTION

1.1 BACKGROUND TO THE PROJECTS

This report documents the main results of two of the mathematical modelling projects which formed part of the Department of Trade and Industry's National Measurement System (NMS) Mass Programme during the three years ending 30th September 2002. Both projects were concerned with the finite element modelling of piston-cylinder pressure balances, and in particular with the modelling of pressure balances to determine the manner in which the pistons and cylinders distort at high pressures. One project (reference number MA033050) had the aim of developing and improving existing NPL finite element modelling techniques to allow a theoretical prediction of uncertainties in the determination of piston-cylinder distortion coefficients (see section 1.2 for a definition of this term). The second project (reference number MA033090) was a collaborative Euromet activity to compare the distortion coefficient predictions derived from the different modelling methods adopted in a range of European National Metrology Institutions, with a particular emphasis on modelling which takes into account real piston and cylinder shapes, rather than the ideally round and straight piston and cylinders which are more commonly analysed.

1.2 THE IMPORTANCE OF DISTORTION COEFFICIENTS

The calculation of the pressure generated by a piston-cylinder pressure balance or deadweight tester requires one to know both the force and the area over which it is applied. However, the piston and cylinder assembly is itself distorted by the pressure generated in the pressure balance fluid, and accurate determination of the generated pressure requires this distortion to be taken into account. In other words, it is necessary to know the effective area over which the force is applied in practice. Elastic distortion theory (Dadson, Lewis and Peggs, 1982) shows that for simple piston-cylinder geometries the effective area is given by:

$$A_{eff} = A_O(1 + \lambda P) \qquad (1)$$

where A_{eff} is the effective area of the piston-cylinder combination, A_O is the effective area at atmospheric pressure, P is the applied pressure and λ is the distortion coefficient. Where the radii of the piston and cylinder vary as a function of position along the engagement length of the cylinder, but circular symmetry about a common vertical axis is retained, Dadson, Lewis and Peggs (1982, pp 28-30) derive equations whereby the distortion coefficient may be calculated by means of integration along the engagement length. NPL uses finite element methods to predict the pressure distribution along the engagement length of the piston and cylinder, and consequently the local distortion of the piston and cylinder components, and then derives the distortion coefficient by using the outputs of the modelling as inputs to Dadson et al's equations and other related equations. Currently, we employ an uncoupled solution technique, so that the fluid-flow finite element problem is solved to derive a pressure distribution, which is then used as the stress input to the finite element calculation of the

piston and cylinder strain. The distortion results are then utilised in the next iteration of the fluid-flow calculation and this process is repeated until convergence is achieved.

NPL's preferred approach to the finite element modelling of pressure balances is to employ ANSYS finite element software to calculate both the pressure distribution in the fluid and the distortion of the individual pressure balance components. A suite of macros in the ANSYS Parametric Design Language has been developed to handle all pre-processing, problem solution, and post-processing aspects of the finite element analysis. The method has been standardised so that it is only necessary to produce a single, new pre-processing macro to model a new pressure balance or to investigate a new pressure balance geometry. All other aspects of the modelling method remain the same. We have validated our methods by comparison with the predictions of other laboratories in the course of EUROMET projects, including the project reported here, and by comparisons with models of the same balance produced using alternative finite element methods. For simple piston-cylinder structures operated in free deformation mode we also compare our distortion coefficient predictions with the results of analytical models.

1.3 THE AIMS OF THE PROJECTS

The purpose of the two projects is to investigate the sensitivity of the output of finite element models of pressure balances to changes in input parameters. Distortion coefficients are predicted for a base line model using finite element methods. Input parameters are then varied and new predictions of distortion coefficient are obtained. Systematic investigation of the input parameter space leads to the evaluation of the sensitivity of the output to variations in specific input parameters. In this way an "uncertainty budget" can be developed for the model which identifies the range of predicted values which might be expected when input parameters cannot be determined exactly or are themselves expressed as a value with an associated uncertainty.

The inputs which are of most interest include the properties of the materials which form the piston and cylinder. These are typically tungsten carbide with added cobalt, or steel. In some cases a piston and cylinder may be manufactured from tungsten carbide, but the cylinder may be encased in a steel sleeve so that both materials may be present in the same structure. For the purposes of finite element modelling, the Young's modulus and Poisson's ratio of the material must be known. Other important inputs are geometrical (the radii of the piston and cylinder and the size of the gap between them), boundary conditions (where the structure is free to move and where it is constrained), and loading (where and with what accuracy are pressures applied to the structure). For oil-operated balances (which is the case for all balances discussed in this report) the viscosity and density of the fluid as a function of pressure must also be known. Finally, the mathematical modelling techniques themselves contribute uncertainties to the output predictions. Examples of sources of "mathematical modelling uncertainty" include variations in finite element model mesh densities, the choice of elements to represent a particular structure, and the choice of equations to represent the pressure-dependent behaviour of the fluid. By combining the results for each input parameter which is varied, it is possible to specify both the predicted distortion coefficient and the uncertainty on the determination of the coefficient for any particular pressure balance structure which is modelled.

1.4 THE NPL PROJECT

Project MA033050 had the aim of investigating some specific pressure balances which were employed at NPL as primary standards. The balances are all operated in free-deformation mode. Finite element models of three balances were prepared and validated. Predictions of the distortion coefficients of the individual models were calculated, the inputs to the models were varied and the sensitivities of the distortion coefficients to changes in the inputs were determined.

The balances in question were: B2-816, which is a tungsten carbide RUSKA 395 oil-operated simple piston-cylinder balance with a maximum operational pressure of 140 MPa, and B2-817, which is a similar balance made from hardened steel. These two balances were chosen because experimentally determined values of the distortion coefficient are available, the diameters of the pistons and cylinders had been measured at NPL in 1994, and they had been modelled previously by the City University School of Engineering. The results of the City University modelling are described in a report prepared for NPL by the City University School of Engineering dated May 1991 (City University, 1991). The third model is of a D&H type 5300 deadweight pressure tester, serial no. 1000, which is made of tungsten carbide and for which substantial experimental data exists, it having been calibrated against other pressure balances, such as B2-816. It had also been employed in the Euromet project no. 389 as a transfer standard.

Comparisons between the predicted distortion coefficients and those obtained from laboratory calibrations of the balance in question were a carried out to identify to what extent the finite element modelling results could be regarded as a true indicator of the behaviour of a balance under experimental conditions.

Finally, to provide an independent check on the validity of the modelling methods, a model of a BNM-LNE 200 MPa piston-cylinder was prepared. This balance had been studied during the Euromet project no. 256 (Molinar et al, 1998) by NPL, the Physikalisch-Technische Bundesanstalt (PTB, Germany) and the Istituto di Metrologia “G. Colonetti” (IMGC, Italy). During that project NPL had employed an alternative finite element modelling technique, so that there was an independent source of results with which to compare the ANSYS predictions derived during the work reported here. In addition, the PTB had employed ANSYS for the Euromet project no. 256, so that comparisons with results from another ANSYS realisation of the model were possible.

1.5 THE EUROMET PROJECT NO 463

The second project which is discussed in this report is the successor to the Euromet project no. 256. It is entitled “Calculation of elastic distortion and associated uncertainty in piston cylinders operating up to 1 GPa”. The main aim of the project is to model a 1 GPa Désgranges and Huot type 7594 controlled-clearance pressure balance and to develop an uncertainty budget for theoretical prediction of the distortion coefficient based on finite element modelling. The basic FEA models are also to be extended to take into account three-dimensional measurements of the real profiles of the piston and cylinder. Five laboratories are taking part in this project: PTB (Germany), BNM-LNE (France), IMGC-CNR (Italy), UME (Turkey) and NPL and, as at the date of this report, the project is yet to be completed.

This report documents NPL's contribution to the Euromet project. The results are of direct relevance to the work on NPL's own pressure balances. In particular, the investigation of problems associated with taking into account measured piston and cylinder profiles is important in helping to determine the future direction of finite element modelling of pressure balances at NPL.

1.6 STRUCTURE OF THE REPORT

Chapters two to five of this report describe respectively the background to finite element modelling of pressure balances, including the reasons for its current status as the preferred numerical technique for understanding pressure balance behaviour, how the ANSYS finite element models are prepared and processed, and the basic specifications of each of the models.

Chapters six and seven set out the results of varying the inputs to the FEA models and present uncertainty budgets derived from the sensitivity analyses for each balance. Chapter eight reviews the problems associated with three-dimensional modelling of pressure balances in the light of the experience of the Euromet 463 project and chapter nine draws conclusions and makes recommendations for future work.

2 FINITE ELEMENT ANALYSIS OF PRESSURE BALANCES: BACKGROUND

2.1 ANALYTICAL METHODS OF UNDERSTANDING PRESSURE BALANCES

Although it was published 20 years ago, the most comprehensive account of the theory and practice of pressure balances is the text by Dadson, Lewis and Peggs (1982). In addition, an earlier paper by Dadson, Greig and Horner (1964) provides a useful summary of the basic principles underlying pressure balance calibration. The principles and experimental techniques described are still relevant today.

Much of the early research on the theory of piston-cylinder pressure balances was concerned with the derivation of simple equations to allow the effective area of a balance to be calculated from knowledge of the materials from which the balance was manufactured and the radii of its components. In the case of what are known as balances of the "simple" type (that is, the applied pressure acts on the lower cross-section of the inner component or piston, which rotates relative to the outer component or cylinder), Dadson, Lewis and Peggs (1982, p 100) conclude, after having made simplifying assumptions concerning axial symmetry and the pressure-dependent behaviour of the distorted piston and cylinder components, that the effective area, A_P, of a simple piston-cylinder balance in free-deformation mode is given by:

$$A_P = A_O\left\{1+\frac{P}{2E}(3\sigma-1)+\frac{P}{2E'}\left\{\frac{(1+\sigma')R'^2+(1-\sigma')R^2}{R'^2-R^2}\right\}\right\} \quad (2)$$

where E, E' and σ, σ' are the respective values of Young's modulus and Poisson's ratio for the piston and cylinder, R is the internal radius of the cylinder, and R' is the external radius of the cylinder. A_O is the undistorted area.

In the case of controlled clearance balances, Dadson, Lewis and Peggs (1982, p 110) provide the following simplified effective area equation:

$$A_P = A_O\left\{1+\frac{P}{E}(3\sigma-1)\right\} \quad (3)$$

It is of interest to note that equation 3 for controlled clearance balances predicts that the effective area is independent of material properties in the case where the Poisson's ratio of the material is 0.33, and is determined solely by the geometry of the assembly.

2.2 WHY FEA METHODS ARE PREFERRED

To derive the effective area of a particular cylinder, one needs to be able to calculate the forces acting on the piston due to the fluid pressure. These are (Dadson, Lewis and Peggs, 1982, p 108):

1. the pressure due to the applied line pressure acting on the cross-sectional area of the lower end of the piston, allowing for the change of cross-section at that end due to the combined effects of axial and radial compression;
2. the vertical component of the force due to the pressure (which normally decreases progressively from the applied pressure, P, to zero or to atmospheric pressure) acting on the sides of the piston;
3. the upward frictional forces due to the movement of the fluid between the piston and cylinder surfaces.

Assuming axial symmetry and laminar flow of a viscous pressure transmitting fluid, the above three forces lead to an expression for the effective area of a piston-cylinder pressure balance in the following form (Dadson, Lewis and Peggs, 1982, p 97).

$$S_P = \pi r_O^2 \left\{ 1 + \frac{h_O}{r_O} + \frac{u_O + U_O}{r_O} + \frac{1}{r_O P} \int_0^l (p - p_2) \frac{d(u+U)}{dx} dx \right\} \qquad (4)$$

where r_O is the radius of the undistorted piston, h_O is the undistorted gap width, u and U are the differences between the distorted and undistorted radii of the radii piston and cylinder respectively along the engagement length, and u_O and U_O are the values these differences take at the applied pressure end of the engagement length, x is distance along the engagement length, P is the line pressure, p is the pressure at each x value, and p_2 is the pressure at the top of the engagement length (atmosphere or vacuum, for example).

To solve this equation it is necessary to determine p, u and U along the engagement length of the piston and cylinder. However, the pressure distribution along this gap, and therefore also u and U, are dependent on the distortions of the piston and cylinder assembly and on the pressure dependence of fluid viscosity. A closed-form analytical solution of equation 4 is not possible unless one makes some simplifications, such as assuming that the x-dependent part of the radial distortions of the structure at each axial position is proportional to the actual applied pressure at the same position. This approach can only be applied in limited circumstances (Dadson, Lewis and Peggs, 1982, pp 99-100). A general solution, which takes into account the actual structure of the piston and cylinder assembly and the manner in which it is loaded or restrained can only be achieved by numerical methods, and it is here that finite element methods can make a major contribution. Note, however, that the finite element method is used simply to evaluate the integral term and the values of u_O and U_O in equation 4. All the modelling assumptions, including axial symmetry and laminar flow of a viscous fluid, which went into the derivation of this equation, are still present in the finite element modelling results.

2.3 EARLIER FEA WORK AT NPL

At NPL the first attempts to apply finite element modelling to piston-cylinder pressure balances began in the late 1980s and were carried out jointly with London's City University. This led to the development of finite element software and the analysis of the distortion coefficients of a number of NPL-owned balances. The work is documented in a Ph D thesis entitled *Mathematical modelling of instruments for pressure metrology* (Samaan, 1990). Comparisons of Samaan's results with some of those obtained in the current NPL project are given later in this report.

Following completion of Samaan's work, NPL began to develop its own finite element software. Readers who require further information are referred to Robinson (1996, 1997). NPL's contribution to the Euromet project no. 256, which was an inter-laboratory comparison of numerical methods of calculating distortion coefficients, was carried out with this software. The Euromet study is documented in Molinar et al (1998).

Since 1996 NPL has also been developing finite element routines to study pressure balance distortion which are based on the ANSYS finite element software package. The work reported here has been carried out with this ANSYS software. We currently employ ANSYS 5.4 which we use both to solve the piston-cylinder fluid-flow and structural distortion problems.

It is worth pointing out that all these finite element approaches have been based on the assumption of axial symmetry. To date, no attempt has been made to develop a three-dimensional solution to the distortion problem. However, the limitations of the current methodology and the feasibility of moving to a full three-dimensional solution are reviewed later in this report, especially in relation to incorporating measurements of piston-cylinder roundness and straightness into the finite element modelling.

2.4 KEY ISSUES (1): MATERIAL PROPERTIES

As can be understood from equations 2 and 3 above, even the simplest analytical equations for predicting distortion coefficients require knowledge of the Young's modulus and Poisson's ratio of the piston and cylinder materials. This information is naturally also necessary for finite element models. In addition, to model the fluid and derive the pressure distribution along the engagement length, the density and viscosity of the pressure transmitting fluid must be known as functions of pressure.

The materials employed for the piston-cylinder structures which are analysed in this report are tungsten carbide with added cobalt, and steel. In the case of controlled-clearance balances to be operated at relatively high pressures, a tungsten carbide cylinder is often encased in a steel sleeve. For operation at high pressures (100s of megapascals) tungsten carbide is preferred as its Young's modulus is three times that of steel, making it less susceptible to large distortions at high pressure. However, the addition of cobalt to the tungsten carbide contributes an extra source of uncertainty to the determination of the appropriate Young's modulus value to use for mathematical modelling purposes. Doi et al (1970) have published data on the variation of Young's modulus of tungsten carbide cobalt with the volume fraction of cobalt. Figure 1 presents their results. It is important to understand that data points in this figure are averaged results and that for a given volume fraction of cobalt, materials from different manufacturers may display variations in actual values of Young's modulus.

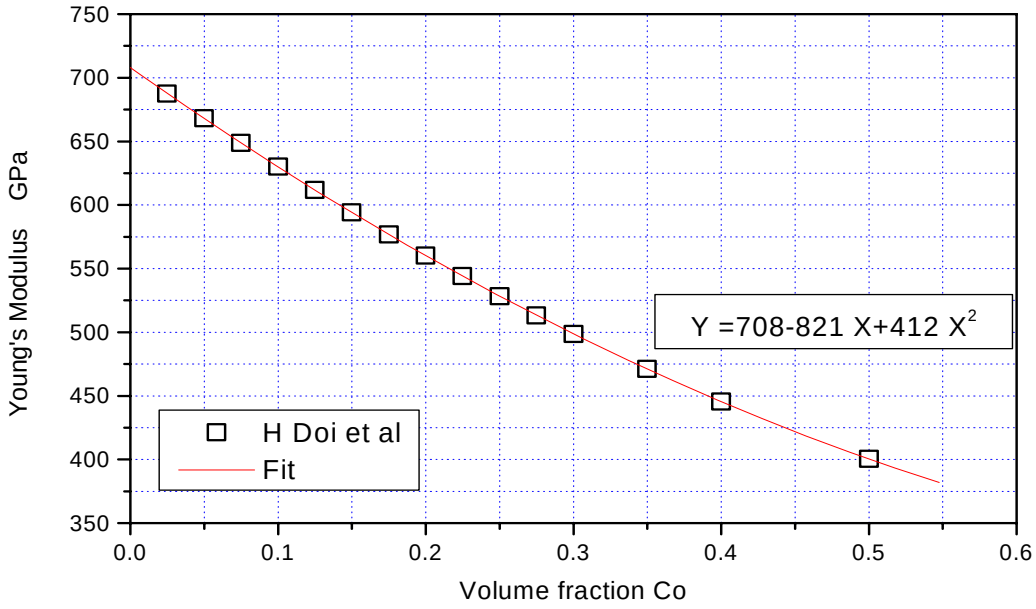

Figure 1: Young's modulus of tungsten carbide as a function of volume fraction of cobalt

For the most reliable modelling results, and especially when comparing model predictions with experiment, it is essential that material properties are known as accurately as possible. It would be preferable if properties could be determined at the time the balance is manufactured. This requirement may, however, pose some difficulties as it is the practice of manufacturers to prepare a cylinder and then to find the most suitable piston to fit the cylinder in question from a batch of pistons, which may not have identical properties. Measurement of all components' properties and accurate record keeping are required to ensure traceable data for each piston and cylinder pair.

Measurement of the properties of a completed assembly carries the risk that the components may be damaged during the measurement process. However, Sabuga (2001) has shown that it is possible to make measurements of the Young's modulus and Poisson's ratio of pistons to an accuracy of ± 1% using strain gauges and without damage to the piston undergoing the test.

Data on the viscosity and density of pressure-transmitting fluids are often difficult to obtain over wide pressure ranges, as one is entirely dependent on what empirical data have been published in the literature. For all the analyses described in this report, the pressure transmitting fluid has been assumed to be diethyl-hexyl-sebacate (DHS) where the dynamic viscosity, η, was taken to be:

$$\eta = 0.021554\left(1+1.90036\text{x}10^{-3}\,p_1\right)^{8.81} \quad \text{Pa s,} \qquad (5)$$

where p_1 is the pressure in MPa (Molinar et al, 1998). This equation appears to cover the pressure range up to approximately 600 MPa. Above that pressure, data are less readily available.

Molinar et al (1998) also quote an equation for the pressure-dependent density of DHS. However, the data for this equation appear to have been obtained from compressibility measurements. It is not clear whether such data are appropriate for the case when the fluid is free to flow along the gap under the influence of the pressure gradient. In such a case it may be preferable to treat the fluid as incompressible. In the analyses described in this report the density of DHS was held constant at 912.67 kg m^{-3}, although a brief investigation of the effect of Molinar et al's equation was carried out. The effect on distortion coefficient predictions of employing a pressure-dependent density term was shown to be negligible for the balances modelled.

2.5 KEY ISSUES (2): GEOMETRY

The simplified equations 2 and 3 require one to know the radius of the piston and the external radius of the cylinder. Equation 4 requires that the undistorted piston radius and gap width be known. In all cases these are single-valued terms taken to be characteristic of the component in question. Although NPL commonly has its dimensional metrologists determine in detail the roundness and straightness of pressure balance components, their results are reduced to a single value with an associated uncertainty for the piston and cylinder radii. In most finite element modelling of pressure balances it is the case that the undistorted piston and cylinder are taken to be ideally round and straight. It should be noted that equation 4 implicitly assumes an initially ideally round and straight undistorted piston and cylinder, or at least that single values can be stated for the undistorted piston radius and gap width, r_O and h_O. However, the integral term in equation 4 does not itself rely directly this assumption, but requires only that the changes from the undistorted values be known as a function of position along the engagement length and that the structure be regarded as axisymmetric.

The shape of the piston and cylinder in the region of the engagement length – any steps, relieved sections, counterbores, tapers and so on – affect the manner in which the assembly distorts along its engagement length and also the values to be used in equation 4 for u_O and U_O, the distortions at the applied pressure end of the piston-cylinder gap. Only finite element modelling can take this structural detail into account.

2.6 KEY ISSUES (3): BOUNDARY CONDITIONS

In any real device it will not be possible to deliver the applied line pressure directly to the bottom of the piston-cylinder gap and to nowhere else in the pressure-balance structure. Inevitably there will be surfaces which experience loading from the applied pressure, including those portions of the piston and cylinder which extend below the engagement length. The effects of these loads on the manner in which the balance distorts must also be understood. In the case of controlled-clearance designs, the exact definition of the external region over which the jacket pressure is applied becomes important, as does the effect of oil seals in this part of the structure. Finite element modelling results will be presented later in this report which will demonstrate how sensitive the predicted distortion coefficient of controlled-clearance balances is to the definition of the surface over which jacket pressure is applied.

The second aspect of boundary condition determination concerns the definition of surfaces to which movement restraints are to be applied. In axisymmetric structures such restraints limit either axial or radial movement or both axial and radial movement at particular points of the pressure-balance structure or over particular surfaces within the structure. The identification of such surfaces often requires both the study of the balance's engineering drawings and also an understanding of the manner in which the balance is used in practice.

Once again, the finite element technique provides an effective way of including pressure loading and restraint boundary conditions in the mathematical model and of investigating the sensitivity of the predictions of the model to changes in these boundary conditions.

2.7 KEY ISSUES (4): LIMITATIONS OF THE MODELS

Whether one uses the simplified equations 2 and 3 or employs numerical methods, including finite element analysis, to solve the integral term in equation 4, there are a number of features of real piston-cylinder balances which are ignored. It has already been pointed out that, in all the cases with which we are concerned, axial symmetry of the piston-cylinder structure is assumed. In addition, for oil-operated balances, all fluid flow is assumed to be the laminar flow of a viscous fluid in response to a one-dimensional pressure gradient.

The third simplification relates to the movement of the balance. The models assume that the piston and cylinder remain stationary, both in terms of their positions or heights relative to each other (that is, the effect of the piston falling or the cylinder rising is ignored), and that the cylinder and piston do not rotate. In reality, either the piston or cylinder is rotated with respect to the other component. The motivation for this form of operation is to overcome friction arising from direct contact between the floating and fixed elements of a pressure balance structure. Typically, the floating element including the attached load is rotated steadily by some form of mechanical drive. However, for the highest precision work free rotation is preferred to avoid the introduction of extraneous forces into the system, especially at the lower end of the pressure range. A full discussion of rotation effects can be found in Dadson, Lewis and Peggs (1982, pp 34-45).

Modelling the effects of rotation is possible, and is a task commonly undertaken by manufacturers and designers of journal bearings. However, it has to the author's knowledge never been applied to the modelling of pressure balances. In any case, the motivation for journal bearing designers is different, in that they are concerned chiefly with lubrication questions, whereas the users of piston-cylinder pressure balances are interested in the details of structural distortion.

Ignoring rotation may also have consequences for a full understanding of the behaviour of the pressure-transmitting fluid. Diethyl-hexyl-sebacate is a long-chain molecule and the flow of such molecules will depend on their orientation. It has been suggested that for a large molecule to flow under a pressure gradient, it must first rearrange its segments into an easy flow configuration and then move in segments of a fixed size (Min and Lamb, 1985). Note also that the direction of easy flow for a long-chain molecule must be different for the rotating and non-rotating case, as the preferred easy-flow direction must be in the direction of the governing flow regime. It may be that different equations for pressure-dependent viscosity are required for the rotating and non-rotating cases.

3 SETTING UP THE ANSYS MODELS

3.1. THE ANSYS PARAMETRIC DESIGN LANGUAGE

Relatively straightforward finite element analyses, such as the solution of a linear stress problem, can often be carried out using the graphical user interface routines of finite element software. These routines typically allow the user to "draw" the various engineering components on the VDU screen in a manner analogous to computer-aided design software, to assign loads and restraints graphically, to select the solution methods required from drop-down menus, and to display results graphically. For standard types of analysis, or when many iterations of the model are not required, this is often the most efficient means of carrying out a finite element analysis.

In the case of pressure-balance modelling however, the finite element analysis simply provides the raw data needed for the solution of equation 4, and for the work reported here, the solution method is an iterative one, as the fluid flow problem and the structural strain problem are solved in an uncoupled manner. The method requires one to make an initial guess at the pressure distribution along the gap (the simplest approach being to assume an initial linear pressure distribution) and to use this pressure distribution as input to a solution of the structural deformation problem. The structural deformation solution is then used to make a new prediction of the pressure distribution in the fluid, which is again used as input to the structural problem, which is then re-solved. This process continues until convergence is reached. It is also the case that knowledge of the structural deformation is simply a means towards the end of calculating the distortion coefficient and the piston fall-rate (the piston moves downward as fluid leaks out at the top if the engagement length), and such calculations are naturally not part of standard finite element software routines.

Furthermore, we need not only to solve an uncoupled problem iteratively but also need to be able to make changes to model input parameters and geometries without having to re-work the whole model from the beginning. One of the disadvantages of finite element methods is that they only solve a particular problem and do not provide solutions to a set or class of problems. To make small structural, materials property, or boundary condition changes to a finite element model, such as are required when performing sensitivity analyses, can be time-consuming if it is always necessary to re-work a model completely. This problem can be avoided if non-graphical methods of data generation and analysis are employed. ANSYS provides the facility to define and carry out analyses using the ANSYS Parametric Design Language (APDL). This high-level language has a FORTRAN-like structure and allows the user to define and re-define parameters, to generate macros, initiate solution routines, and write macros to analyse results, in the same manner as one writes a typical piece of line-by-line computer code. In our case we employ ADPL to control all three aspects of the finite element analysis: pre-processing of the initial definition of the problem, the solution of both the structural and fluid flow problem, and the post-processing stages of evaluating convergence criteria, calculating the predicted distortion coefficient and displaying pressure profiles and gap profiles graphically.

The use of APDL allows us to prepare a series of macros to carry out each stage of the analysis. The solution and post-processing stages are common to all the finite element analyses we carry out. To prepare a new model it is only necessary to generate new pre-

processing macros. In practice, the pre-processing macros are all very similar and the differences between balances relate only to geometry, materials properties and boundary conditions. The structure of the macros themselves remains the same from one analysis to another.

The main macros needed for each stages of the analysis process are described below.

3.2 PRE-PROCESSING

The pre-processing stages are typically separated into two macros. The first sets up the global variables for the analysis in question - materials properties, co-ordinates of key points, and line pressure value, for example. The second macro turns the above data into a meshed model with all the elements and boundary conditions defined.

Once these two macros have been run then one may begin the solution of the FE problem. At this stage ANSYS itself will have carried out a number of important checks to ensure that key features of the modelling are valid. It performs geometry validation, including checking that areas and volumes are closed, that the element types are consistent with the required analysis, and warnings are produced if aspect ratios of elements are unreasonable.

For any new model these two macros are the most crucial, as they are the ones which need the most work and which define the key parameters of the model. They will be unique to each model, whereas many of the macros which are used during the solution and post-processing stages may be common to all or to most FE analyses. In some cases, for example, when analysing a piston-cylinder whose geometry bears no relation to devices which have been modelled previously (e.g. the pressure balance for the Euromet project no. 463), it may be preferable to combine these two macros together into one file, rather than follow the two macro system.

3.3 THE SOLUTION AND POST-PROCESSING

In the case of the ANSYS models of piston-cylinder pressure balances, it is difficult to separate the solution and post-processing stages as the finite element problem is solved many times iteratively. At each cycle of the iteration some mathematical analysis is carried out in what are technically post-processing routines to define the input for the next cycle of the iteration. This process continues until the model being analysed converges to a solution. The mathematical analysis routines, which are written by NPL and not part of the ANSYS software package, are technically post-processing routines in finite element terms.

Separate macros carry out the following tasks:

1. apply the pressure loads to the relevant boundary;
2. start the ANSYS solver and test results for convergence after each loop;
3. set up the necessary post-processing mathematics, including calculation of distortion coefficient and pressure loads for the next iteration;
4. write the pressures and displacements at each node along the engagement length to a text file after each iteration;

5. write the results of the calculations of effective area, distortion coefficient, fall rate to a file after each iteration;
6. graphical display of results, including charts of the profile of the distorted gap, the pressure along the engagement length, the distorted piston profile, the distorted cylinder profile, viscosity of fluid along the gap, effective area as a function of iteration number, distortion coefficient as a function of iteration number, the fall rate as a function of iteration number, and the value of the convergence test parameter. In addition it is possible produce two-dimensional colour plots of the distorted structure, x-direction displacements of all components in the distorted structure, strain distribution in the distorted structure, and stress distribution in distorted structure.

3.4 ANALYSING THE RESULTS

Although the purpose of the modelling is to produce a prediction of the distortion coefficient for the pressure balance being modelled, it is essential to be able follow the history of a particular solution and also to examine detailed results of predicted pressure distributions and structural distortions along the engagement length. The purpose of writing the pressure and displacement data to text files at stages four and five of the analysis is to allow such examinations to be performed at any time after an analysis has been completed, without the need to repeat the analysis itself. As it may take 100 iterations or more and several hours for an analysis to converge to a solution, it is important to retain as many results of the analysis as possible to avoid the need to repeat calculations.

The use of text files also allows data to be imported into other software packages such as Excel or Matlab, thus facilitating alternative methods of data analysis, including the production of graphical output. Another benefit is that it renders the user independent of ANSYS's own graphics capabilities. All the figures in this report showing pressure distributions or gap profiles have been produced in this way.

3.5 MODELLING THE FLUID

To model the fluid flow and therefore the pressure distribution along the gap between the piston and cylinder we employ an analogy between fluid flow and thermal flow, which allows us to use thermal finite elements within our ANSYS model. The model of fluid flow we employ in the gap is steady-state viscous laminar flow of a fluid moving laterally between two plates whose length and width are much greater than the distance separating them. This can also be applied to flow in the gap between a piston and cylinder provided the gap is small. As Drysdale et al (1925, p 116) point out, in such a case the total fluid flow across a unit width perpendicular to the flow direction is equal to the rate of decrease of pressure in that direction multiplied by the constant $h^3/12\mu$, where h is the gap width and μ is the coefficient of viscosity. In the case of one-dimensional heat flow, the heat flux is equal to the rate of decrease of temperature in the direction of interest multiplied by KA, where K is the thermal conductivity and A is the cross-sectional area.

The LINK32 ANSYS finite element is a uniaxial conducting bar element with a single degree of freedom, temperature, at each node point and can be used for plane or axisymmetric

analyses. The element is defined by two nodes, a cross-sectional area and the material properties. For steady-state solutions, density and specific heat of the bar material are ignored, so that only the thermal conductivity and the cross-sectional area of the element are required. Thus this element can be used to calculate pressure distributions in the case under consideration provided the thermal conductivity value is replaced by the appropriate value for the fluid flow problem. The "thermal" finite element problem is solved independently of the structural FE problem and its results are used as the input to the next iteration of the structural problem. The solution of the structural finite element analysis then provides the information on the gap width, and therefore area, needed for the next iteration of the "thermal" analysis.

The solution and post-processing macros also calculate the rate which the piston falls as a result of fluid flow. For this purpose it is simply necessary to determine the volume flow rate of the fluid through the annular gap using equation 6 (see below) given by Molinar et al (1998), in which the piston is considered to fall at the rate at which the volume of fluid it displaces equals the volume of fluid flowing through the gap.

$$v_F = \frac{Q_m}{\pi r^2 \rho(p_1)} \qquad (6)$$

where Q_m is the mass flow in the gap, given by equation 7, and v_F is the piston fall rate:

$$Q_m = -\frac{\pi r h^3(x)\rho(p)}{6\eta(p)}\frac{dp}{dx} \qquad (7)$$

From what has been described above, it is clear that our current modelling approach can only be regarded as strictly valid in the case where the fluid flow regime and the pressure distribution in the fluid can be described using the simplifications built into the model. These are of course those assumptions which are also adopted by Dadson, Lewis and Peggs (1982). In cases where gaps become very small indeed, where molecular effects become important, or to model rotation or three-dimensional flow, alternative methods of fluid modelling would have to be adopted for the most accurate results. There may be limited advantage for computational purposes only in describing fluid properties by an "effective viscosity" coefficient in some cases, but such an approach would necessarily obscure the underlying physics of the problem. In fact, it will be seen that the current finite element models are relatively insensitive to changes in fluid viscosity and this seems to be a natural consequence of the assumptions built into the modelling method itself, which is also true of the simplified equations 2 and 3 quoted earlier in this report.

4 TESTING THE ANSYS APPROACH

4.1 INTRODUCTION

To test the results of the ANSYS models against previously validated work it was decided to investigate an ANSYS model of one of the pressure balances which was modelled during the course of the Euromet project no. 256. The outcome of this project is described in Molinar et al (1998). NPL's contribution to the project is documented in Robinson (1996, 1997).

The balance chosen for the ANSYS model was the BNM-LNE 200 MPa pressure balance defined as assembly no. 4 and the ANSYS results for free deformation mode and controlled clearance mode were compared with the published results from this project, including the earlier modelling at NPL using alternative finite element software. Full details of the pressure balance, its geometry and the results of the Euromet comparison are set out in Molinar et al (1998) to which the reader is referred for further information.

4.2 THE EUROMET 256 PROJECT BALANCE MODEL

For this model and indeed also for the balances described in sections 5.2, 5.3 and 5.8 of this report a simple mesh structure was employed. The piston and cylinder were modelled in the region of the engagement length only. Appendix A includes figures showing shows the outline of the ANSYS model and the meshing for this balance and the other balances modelled during the course of the current work.

Basic control of the mesh density is achieved by specifying the number of radial (horizontal direction) divisions required across the piston and cylinder structures. The model is designed so that the number of divisions can easily be varied. In the axial (vertical direction) a variable meshing technique is employed to allow a higher mesh density to be obtained at the top and bottom of the engagement length than in the centre. The steepest pressure gradients are obtained at the top of the piston-cylinder engagement length and the increased mesh density in the region allows greater accuracy to be achieved in representing piston-cylinder behaviour. Once the radial and axial divisions has been defined, automatic meshing techniques are employed to generate the complete model.

Table 4 in Molinar et al (1998) sets out the key structural characteristics of the BNM-LNE 200 MPa balances which were modelled in the Euromet study. The balance in question was no. 4, which has a piston diameter of 8 mm and an undistorted gap clearance of 0.57 μm. The balance is made of tungsten carbide with a Young's modulus of 630 GPa and a Poisson's ratio of 0.218. A schematic diagram of the balance is given in figure 5(b) of Molinar et al (1998) and table 2 in the same reference gives the positional co-ordinates of the key points of the piston and cylinder structure as identified in figure 2 of that paper. For the purposes of the comparison of mathematical modelling results, calculations were performed for this balance in both free deformation and controlled clearance mode at 200 MPa and 120 MPa line pressures. In controlled clearance mode the jacket pressure is applied along the line joining key points 5 and 6 in figure 5(b) of the Molinar reference. Note that the jacket pressure is taken to be 25% of the applied line pressure.

For the Euromet project no. 256 study, the Physikalisch-Technische Bundesanstalt (PTB, Germany) carried out its calculations using ANSYS, the Istituto di Metrologia "G. Colonetti" (IMGC, Italy) used its own, non-finite-element-based numerical methods and NPL employed Robinson's finite element software (1996,1997). For the purpose of the current work, it is instructive to compare the PTB's ANSYS results with NPL's ANSYS results. Figure 5 (b) of Molinar et al (1998) shows that PTB and NPL used a different approach to the modelling of the cylinder structure in the regions above and below the engagement length. PTB incorporated the stepped features at the top and bottom of the cylinder into its model, whereas the NPL and IMGC approaches considered the undistorted cylinder to be perfectly round and straight throughout. The perfectly round and straight cylinder model was employed for the NPL ANSYS work reported here so that the results are exactly comparable.

4.3 RESULTS OF COMPARISON

Tables 5 and 6 of Molinar et al (1998) give the results of the comparison of the numerical modelling predictions. The model output parameters which were compared were the prediction of the distortion coefficient and fall rate of the piston at both 200 MPa and 120 MPa and the predicted radial distortions of the cylinder and piston (departures from the undistorted radii) and the annular gap width at the top and bottom of the engagement length. For the comparison with the NPL ANSYS model, the relevant data for the balance in question were extracted from the paper and new comparison tables were generated and are set out below. Note that for the purposes of this report, the fall rate results have been expressed as mm/min rather μm/s as this a more realistic unit for experimental purposes and is, in fact, the unit used in the current ANSYS macros. Table 1 gives the radial distortion and gap width results for the analysis of the balance in free deformation mode at 120 MPa and 200 MPa. Table 2 gives the same data for the controlled clearance case at the same two pressures. In both these cases the upper section of the table summarises the results from the original Euromet project no. 256, whereas the lower half of the table repeats these results but with the original NPL data replaced by the results of the ANSYS modelling of the balance in question. For the free deformation case only, it was possible to make predictions using simplified distortion theory as set out in Dadson, Lewis and Peggs (1982), that is, the assumption that that the local radial distortions of the piston and cylinder are proportional to the local pressure in the clearance. The results of prediction using this approach have also been included in table 1 with the identifier "simple". Table 3 compares the distortion coefficients and fall rates for both the free deformation and controlled clearance cases, once again with the original results in the upper half of the table. In tables 1 and 2 the maximum difference between the IMGC, PTB and NPL calculations is also presented for each parameter which was investigated.

The results of the recalculations using the NPL ANSYS model are instructive. In tables 1 and 2 NPL ANSYS results are now much closer to the PTB results than the original NPL results. The maximum differences between the data have also been reduced, except for those few cases where the maximum difference is due to an outlying IMGC result. The improvements arising from the NPL ANSYS model are particularly noticeable at the top of the engagement length, which is the region where pressure gradients are the greatest. In the free deformation case at 120 MPa, the PTB predicted a radial distortion of 0.084 μm for the cylinder, whereas the original NPL prediction was 0.079 μm. The new ANSYS prediction produces a value of 0.085 μm. For the gap width at the same position and pressure PTB obtained 0.510 μm and NPL original version predicted 0.505 μm . The NPL ANSYS prediction is 0.512 μm. For the

200 MPa free deformation model the original results for the cylinder and piston distortion and gap width at the top of the engagement length all show closer agreement between the NPL ANSYS results and the PTB results than were achieved with the original NPL software.

Table 2, the controlled clearance case, also shows the improved agreement between the NPL ANSYS model and the PTB model. This is most noticeable again at the top of the engagement length. The predicted 200 MPa controlled clearance cylinder distortion was: PTB, -0.140 μm, NPL, -0.109 μm. The NPL ANSYS value is –0.135 μm. The same pattern is repeated for the piston distortion, where the original results were: PTB, 0.191 μm, NPL, 0.186 μm. The NPL ANSYS results is 0.192 μm. There is also a marked improvement in the prediction of the gap width at the top of the engagement length: PTB 0.240 μm, NPL original results 0.275 μm, NPL ANSYS result 0.242 μm.

In table 3, the results of the NPL ANSYS model show fall rates for both pressure and both modes which are in all cases in closer agreement with the PTB results than the original NPL work. As the same flow equations (6 and 7 above) were used by all the original Euromet project 256 models and by the revised NPL model, the better agreement with the PTB achieved by the NPL ANSYS results gives confidence in the NPL ANSYS model. In the case of distortion coefficients, the controlled clearance results show better agreement between the PTB model and the NPL ANSYS model at 120 MPa (PTB, 0.093 ppm/MPa, NPL original 0.083 ppm/MPa, NPL ANSYS, 0.088 ppm/MPa). At 200 MPa the ANSYS results differ from the original NPL results by 0.001 (PTB, 0.117 ppm/MPa, NPL original 0.111 ppm/MPa, NPL ANSYS 0.110 ppm/MPa). For the free deformation case the PTB and NPL ANSYS results differ more than the PTB and NPL original results. At 200 MPa the results were: PTB 0.803 pm/MPa, NPL original 0.800 ppm/MPa, NPL ANSYS 0.797 ppm/MPa and at 120 MPa the equivalent figures were: PTB 0.802 pm/MPa, NPL original 0.801 ppm/MPa, NPL ANSYS 0.796 ppm/MPa. Note however that neither the original NPL model nor the PTB model took into account the specific contribution to the distortion coefficient of the distortion of the high pressure end of the cylinder and piston - see equation 5 in Molinar et al (1998), as compared to equation 4 above.

In the light of the findings summarised above, it appeared reasonable to accept that the approach to modelling pressure balances which was embodied in the NPL ANSYS macros was producing acceptable results. Indeed, if these results had been available at the time the Euromet project no. 256 was being carried out, the participants would have achieved better agreement in their modelling results than was, in fact, actually obtained during the project.

Table 1: Free deformation mode at 120 MPa and 200 MPa

Radial distortion of cylinder (U), piston (u), and annular gap width (h) at the bottom and top of the piston-cylinder engagement length

Original results from Euromet project no. 256, table 5, Molinar et al (1998)

Pressure	Method	Bottom			Top		
		U	u	h	U	u	h
MPa		m/E-6	m/E-6	m/E-6	m/E-6	m/E-6	m/E-6
120	PTB	1.074	-0.428	2.071	0.084	0.144	0.510
	NPL	1.021	-0.428	2.019	0.079	0.144	0.505
	simple	1.030	-0.430	2.030	0.000	0.166	0.404
	max. diff	**0.053**	**0.000**	**0.052**	**0.005**	**0.000**	**0.005**
200	IMGC	1.731	-0.712	3.013	0.179	0.179	0.579
	PTB	1.756	-0.712	3.038	0.159	0.231	0.498
	NPL	1.7	-0.712	2.983	0.154	0.227	0.496
	simple	1.716	-0.716	3.003	0	0.277	0.293
	max. diff	**0.056**	**0**	**0.055**	**0.025**	**0.052**	**0.083**

Revised results with NPL ANSYS predictions replacing original NPL data

Pressure	Method	Bottom			Top		
		U	u	h	U	u	h
MPa		m/E-6	m/E-6	m/E-6	m/E-6	m/E-6	m/E-6
120	PTB	1.074	-0.428	2.071	0.084	0.144	0.510
	NPL	1.031	-0.428	2.028	0.085	0.144	0.512
	simple	1.030	-0.430	2.030	0.000	0.166	0.404
	max. diff	**0.043**	**0.000**	**0.043**	**0.001**	**0.000**	**0.002**
200	IMGC	1.731	-0.712	3.013	0.179	0.179	0.579
	PTB	1.756	-0.712	3.038	0.159	0.231	0.498
	NPL	1.722	-0.713	2.998	0.160	0.230	0.499
	simple	1.716	-0.716	3.003	0.000	0.277	0.293
	max. diff	**0.034**	**0.001**	**0.040**	**0.019**	**0.052**	**0.081**

Table 2: Controlled clearance mode at 120 MPa and 200 MPa

Radial distortion of cylinder (U), piston (u), and annular gap width (h) at the bottom and top of the piston-cylinder engagement length

Original results from Euromet project no. 256, table 5, Molinar et al (1998)

Pressure	Method	Bottom			Top		
		U	u	h	U	u	h
MPa		m/E-6	m/E-6	m/E-6	m/E-6	m/E-6	m/E-6
120	PTB	0.640	-0.428	1.639	-0.120	0.134	0.315
	NPL	0.613	-0.428	1.611	-0.106	0.135	0.329
	max. diff	**0.027**	**0.000**	**0.028**	**0.014**	**0.001**	**0.014**
200	IMGC	1.038	-0.710	2.318	-0.082	0.149	0.339
	PTB	1.040	-0.714	2.323	-0.140	0.191	0.240
	NPL	1.021	-0.714	2.305	-0.109	0.186	0.275
	max. diff	**0.019**	**0.004**	**0.018**	**0.058**	**0.042**	**0.099**

Revised results with NPL ANSYS predictions replacing original NPL data

Pressure	Method	Bottom			Top		
		U	u	h	U	u	h
MPa		m/E-6	m/E-6	m/E-6	m/E-6	m/E-6	m/E-6
120	PTB	0.640	-0.428	1.639	-0.120	0.134	0.315
	NPL	0.614	-0.428	1.612	-0.116	0.134	0.320
	max. diff	**0.026**	**0.000**	**0.027**	**0.004**	**0.000**	**0.005**
200	IMGC	1.038	-0.710	2.318	-0.082	0.149	0.339
	PTB	1.040	-0.714	2.323	-0.140	0.191	0.240
	NPL	1.023	-0.714	2.307	-0.135	0.192	0.242
	max. diff	**0.017**	**0.004**	**0.016**	**0.058**	**0.043**	**0.099**

Table 3: Euromet project no. 256: distortion coefficient and fall rate predictions at 120 MPa and 200 MPa

Original results from table no. 6, Molinar et al (1998)

		Free deformation		Controlled Clearance	
Pressure	**Method**	**Distortion coefficient**	**Fall rate**	**Distortion coefficient**	**Fall rate**
MPa		**ppm/MPa**	**mm/min**	**ppm/MPa**	**mm/min**
120	PTB	0.802	0.242	0.093	0.096
	NPL	0.801	0.238	0.083	0.093
200	IMGC	0.844	0.516	0.143	0.163
	PTB	0.803	0.508	0.117	0.164
	NPL	0.800	0.504	0.111	0.159

Revised results with NPL ANSYS predictions replacing original NPL data

		Free deformation		Controlled Clearance	
Pressure	**Method**	**Distortion coefficient**	**Fall rate**	**Distortion coefficient**	**Fall rate**
MPa		**ppm/MPa**	**mm/min**	**ppm/MPa**	**mm/min**
120	PTB	0.802	0.242	0.093	0.096
	NPL	0.796	0.239	0.088	0.095
200	IMGC	0.844	0.516	0.143	0.163
	PTB	0.803	0.508	0.117	0.164
	NPL	0.797	0.509	0.110	0.163

5 THE BASIC FEA MODELS: SPECIFICATIONS AND INITIAL TESTS

5.1 INTRODUCTION

In this chapter the specifications of four pressure balances which have been modelled using the ANSYS software are given. All four FEA models have been used to investigate the sensitivity of model outputs to variations in input parameters.

Three of these are models of NPL piston-cylinder pressure balances: B2-816, which is a tungsten carbide RUSKA 395 oil-operated simple piston-cylinder balance with a maximum operational pressure of 140 MPa, and B2-817, which is a similar RUSKA balance made from hardened steel. These two balances were chosen because experimentally-determined values of the distortion coefficient are available, the diameters of the pistons and cylinders had been measured at NPL in 1994, and they had been modelled previously by the City University School of Engineering. The results of the City University modelling are described in the May 1991 report prepared for NPL by the City University School of Engineering. The third model is of a D&H type 5300 deadweight pressure tester, serial no. 1000, which is made of tungsten carbide and for which substantial experimental data exists, as it had been calibrated against other pressure balances, such as B2-816. It had also been employed in the Euromet project 389 as a transfer standard. The fourth model is the PTB's 1 GPa D&H controlled-clearance piston-cylinder which was investigated for the Euromet project no. 463.

In the case of the B2-816, B2-815 and D&H models, this chapter also presents some results of initial tests of the model, including, in the case of the B2-816 and B2-817, comparisons with the City University results.

5.2 B2-816

The piston and cylinder of this balance had been dimensioned at NPL in August 1994. The relevant NPL certificates are 08B071/B82/90 (pistons for B2-816 and B2-817) and 08B071/B82/75 (cylinders for B2-816 and B2-817). The measured diameter of the piston at its middle position was 4.62305 mm ± 0.00015 mm at the 95% confidence level at 20^{O}C. For the purposes of an axisymmetric model, the radius is taken to be 2.311525 mm ± 0.000075 mm. Diametral measurements were also made at a minimum of five positions along the surface of the piston and the maximum variation of these measurements from the mid-position diameter was 0.00025 mm. The diameter of the cylinder was measured at five positions along its length and the results of the five measurements are set out in table 4 below where the uncertainties are those at the 95% confidence level.

Position	Measured diameter at 20°C mm	Uncertainty of diameter measurement mm	Departure from roundness mm
A	4.62505	± 0.00025	0.00005
B	4.62505	± 0.00025	0.00005
C	4.62505	± 0.00030	0.00005
D	4.62500	± 0.00030	0.00015
E	4.62500	± 0.00040	0.00010

Table 4: Measured diameter of cylinder of B2-816 pressure balance

The mean diameter determined from the five measurements reported in table 4 is 4.62503 mm, giving a mean radius of 2.312515 mm. The mean measured gap between the piston and cylinder is therefore 0.00099 mm.

The City University finite element models were prepared before the NPL dimensional data were available and an initial gap width of 1 μm was employed in their modelling. For the purposes of comparison between the City University results and NPL's ANSYS results a 1μm gap width has been used in the ANSYS models. The City University report does not quote the radius of either the piston or the cylinder, although the report states that the nominal area of the piston was 16.77110614872 mm^2 (City University report precision) suggesting that the radius of the piston was taken to be 2.31050 mm. For the purposes of the NPL ANSYS models, the piston radius was taken to be 2.311525 mm, in accordance with the August 1994 measurements, a value 0.001025 mm (0.044%) larger than the apparent City University value.

The position of the piston in the B2-816 balance can vary by ± 2 mm from its normal operating position. The normal operating position for this balance gives an engagement length of 25.0 mm along the piston-cylinder interface. This position was referred to as case A in the City University Report (City University, 1991). Case B was defined as the "piston down" position where the engagement length was assumed to be 27.0 mm. Case C was the "piston up" position – an engagement length of 23.0 mm. NPL ANSYS modelling was carried out for the "normal" engagement length of 25.0 mm.

The piston and cylinder were both machined from tungsten carbide. The Young's modulus of tungsten carbide was taken to be 583 GPa, with a Poisson's ratio of 0.23. No uncertainties on these values were reported by City University.

The transmitting fluid was a sebacate oil, diethyl-hexyl-sebacate (DHS), with a dynamic viscosity of 21.1 mPa s at ambient pressure. The equation used by City University for the pressure dependence of viscosity was taken from Stuart (1989):

$$\log_{10}\eta + 1.2 = (\log_{10}\eta_O + 1.2)(1 + p/200)^z \quad (8)$$

where η_O = 21.1 mPa s, z = 0.55 and pressure is in MPa.

For the NPL ANSYS models the pressure dependence of the dynamic viscosity of DHS was taken to be in accordance with equation 3 of Molinar et al (1998), which is given as equation 5 in this report.

The City University report refers to support conditions rather than boundary conditions. The "support conditions" for the piston was "sliding support" at the top edge. In Samaan (1990, p 66) a "sliding support condition" is defined to be when a node or group of adjacent nodes is allowed to move in the radial or axial direction. The axial direction is parallel to the axis of symmetry of the model and the radial direction is perpendicular to the axial direction. For all pressure balances modelled by City University the top edge of the piston was restrained from axial direction movement, but radial movement was allowed. For the B2-816 cylinder, only radial movement was allowed at the position of the cylinder O-ring. The same boundary conditions have been applied to the NPL ANSYS models.

5.3. B2-817

The B2-817 balance differs from the B2-816 balance only in its material and its detailed dimensions. These differences are described below. Where information provided for the B2-816 balance is not repeated, it may be assumed that the details are identical to those for the B2-816 balance.

According to NPL certificate no. 08B071/B83/90 the diameter of the B2-817 piston at its middle position is 4.62440 mm ± 0.00020 mm at 20^{O} C at the 95% confidence level. The radius of the piston is therefore taken to be 2.31220 mm ± 0.00010 mm. As with the cylinder of B2-816, the diameter of the B2-817 cylinder was determined at five positions along its length and the results of these measurements are summarised in table 5 below.

Position	Measured diameter at 20^{O}C mm	Uncertainty of diameter measurement mm	Departure from roundness mm
A	4.62520	± 0.00045	0.00005
B	4.62520	± 0.00035	0.00005
C	4.62520	± 0.00050	0.00010
D	4.62535	± 0.00025	0.00005
E	4.62535	± 0.00025	0.00005

Table 5: Measured diameter of cylinder of B2-817 pressure balance

The mean diameter determined from the five measurements reported in table 5 is 4.62526 mm, implying a mean radius of 2.31263 mm. The mean measured gap between the piston and cylinder is therefore 0.00043 mm.

As was pointed out above in relation to B2-816, the City University finite element models were prepared before the NPL dimensional data were available and an initial gap width of 1 μm was employed in their modelling both for B2-816 and B2-817. For the purposes of

comparison between the City University results and NPL's ANSYS results a 1 μm gap width has been used in the ANSYS models. Note, however, that for comparison with NPL experimental results, the NPL ANSYS models were amended to employ a gap width of 0.43 μm.

In the same manner as was adopted for B2-816, the City University used a nominal piston area of 16.77110614872 mm^2 (sic) for B2-817, so that the radius of the piston was again taken to be 2.31050 mm. For the NPL ANSYS models, the piston radius employed was 2.31220 mm, in accordance with the August 1994 measurements.

5.4 CITY UNIVERSITY RESULTS FOR B2-816 AND B2-817

The City University report provides limited information about the results of its modelling of the two balances in question. Tables 4(a) and 4(b) of the report list distortion coefficients calculated for each balance for a range of line pressures between 14 MPa and 140 MPa for the three piston positions (normal, up and down). For the purposes of comparison with NPL's ANSYS results tables 4(a) and 4(b) are summarised in tables 6 and 7 below.

City University results for B2-816 piston-cylinder Material: tungsten carbide			
	Distortion coefficient λ (ppm/MPa)		
Pressure MPa	Normal	Piston down	Piston up
14	0.84	0.833	0.843
28	0.84	0.834	0.843
42	0.84	0.834	0.843
56	0.84	0.834	0.843
70	0.84	0.834	0.843
84	0.84	0.834	0.843
98	0.84	0.834	0.843
112	0.84	0.834	0.843
126	0.84	0.834	0.843
140	0.84	0.834	0.843

Table 6: City University finite element modelling results, distortion coefficient of B2-816 piston-cylinder as functions of piston position and applied line pressure

City University results for B2-817 piston-cylinder Material: steel			
	Distortion coefficient λ (ppm/MPa)		
Pressure MPa	Normal	Piston down	Piston up
14	3.000	2.980	3.008
28	3.000	2.990	3.012
42	3.011	2.990	3.018
56	3.020	3.002	3.024
70	3.023	3.007	3.030
84	3.028	3.013	3.036
98	3.033	3.017	3.042
112	3.037	3.021	3.047
126	3.041	3.025	3.051
140	3.050	3.029	3.055

Table 7: City University finite element modelling result, distortion coefficient of B2-817 piston-cylinder as functions of piston position and applied line pressure

Figures 19 and 20 of the City University report provide graphs of the pressure profile along the engagement length and of the gap profile for both the B2-816 and B2-817 balances at 140 MPa. In addition, the maximum and minimum gap widths are quoted for each balance at 140 MPa. These results are summarised in table 8 below.

City University results for B2-816 and B2-817 piston-cylinders Maximum and minimum gap widths at 140 MPa				
		B2-816 Gap width μm	B2-817 Gap width μm	
	Minimum	0.89299	0.856084	
	Maximum	1.97544	3.63073	

Table 8: City University finite element modelling results, maximum and minimum gap widths at 140 MPa for B2-816 and B2-817

5.5 B2-816: COMPARISON WITH CITY UNIVERSITY RESULTS

Following some initial investigations of variations in mesh density and in the boundary conditions applied to piston and cylinder surfaces, a basic model for the B2-816 piston-cylinder was established. The boundary conditions copy the "support conditions" for piston-

cylinders described in the City University report. However, the piston radius determined by measurement at NPL was employed in the ANSYS model, although the initial gap width was defined as 1 μm in accordance with the City University model

Figures 1 and 2 present the pressure distribution along the piston-cylinder gap and the gap profile for this model for a range of pressures from 14 MPa to 140 MPa applied pressure. The piston has been meshed with twelve elements radially and the cylinder with thirty elements radially. An axial meshing factor has been chosen which gave 288 elements along the piston-cylinder engagement length. The model converged after 21 iterations.

The distortion coefficient predicted by the NPL ANSYS model was 0.857 ppm/MPa. The maximum gap width was 2.011 μm and the minimum gap width was 0.885 μm. The NPL ANSYS distortion coefficient is 2% larger than that predicted by City University. The maximum gap width of the NPL ANSYS model is 1.8% larger than the City University maximum width, but NPL's predicted minimum gap width is 1% smaller than the City University value.

The B2-816 model was established after several tests of different mesh densities and meshing methods. In addition to the 288 elements along the piston-cylinder gap it contains 18144 PLANE42 quadrilateral elements, giving 37914 degrees of freedom. This model takes many hours to run to completion, as each iteration takes approximately 30 minutes. For testing the effect of changes in model parameters, a less densely meshed model is to be preferred. Table 9 shows the variation in distortion coefficient and in the maximum and minimum gap widths which were observed for a range of different models of B2-816. The version referred to as run no. 6 is the basic model described above. Run no. 5 differs from run no. 6 only in the reduced density of the mesh which was employed in run no. 5 for the sections of the piston and cylinder which are outside the engagement length region. In the case of run no. 7 two changes were made from the model which was employed in run no. 6 – the mesh density along the piston-cylinder engagement length was reduced to 72 elements and the City University viscosity equation was substituted for the NPL equation. Run no. 8 was identical to run no. 7 except that PLANE2 six-noded triangular elements were used to mesh the piston and cylinder structures. Run no. 9 keeps the same model and meshing (PLANE2 triangular elements) as run no. 8 but reinstates the NPL viscosity equation.

Comparison of NPL ANSYS models of B2-816 piston-cylinder pressure balance				
Run no.	Distortion coefficient ppm/MPa	Maximum gap width µm	Minimum gap width µm	Comments
6	0.857	2.010980	0.884846	Basic NPL model: highest density mesh 288 elements along engagement length
5	0.856	2.012490	0.921178	Identical to run no. 6 but reduced mesh density outside engagement length regions of model
7	0.861	2.015670	0.890719	Reduced mesh density in gap, 72 elements along engagement length, City University viscosity equation
8	0.864	2.012760	0.890271	As run no 7, but PLANE2 triangular elements
9	0.863	2.012090	0.888487	As run no 8, but NPL viscosity equation

Table 9: B2-816 distortion coefficient and gap width results for a range of NPL ANSYS models, applied pressure 140 MPa.

For the 5 models analysed in table 9 the distortion coefficient varies from a minimum value of 0.856 ppm/MPa to 0.864 ppm/MPa - the highest value being 0.8% larger than the lowest value. Note, too, that the lowest values of the distortion coefficient were obtained for runs nos. 5 & 6 where 288 elements were used along the piston-cylinder gap, rather than the 72 elements which were employed in the three remaining models. For the maximum gap width, which occurs at the lower end of the piston-cylinder gap, the lowest value 2.010980 µm was obtained from run no. 6, which had a high mesh density throughout the model both in the piston-cylinder gap and outside it. The highest value of the gap width occurred for run no. 7, which employed a reduced mesh density and the City University viscosity equation. The highest value was 0.23% larger than the lowest value. The lowest value of the minimum gap width, which is located at the top of the piston-cylinder engagement length, was obtained from run no. 6, 0.884846 µm. The largest value, 0.921178 µm came from run no. 5, the only model of the five models listed in table 5 which used a reduced mesh density in the regions of the model outside the engagement length. The largest value exceeded the smallest value by 3.7%. If the minimum gap width results from run no. 5 are excluded, then the range of values for this parameter is from 0.884846 µm to 0.890719 µm, a range of 0.7%. The results set out in table 9, and the comparisons with the City University results, suggest that for the highest accuracy, dense meshes are preferable, but that in investigating sensitivity to changes in model parameters, less dense meshes are likely to be acceptable.

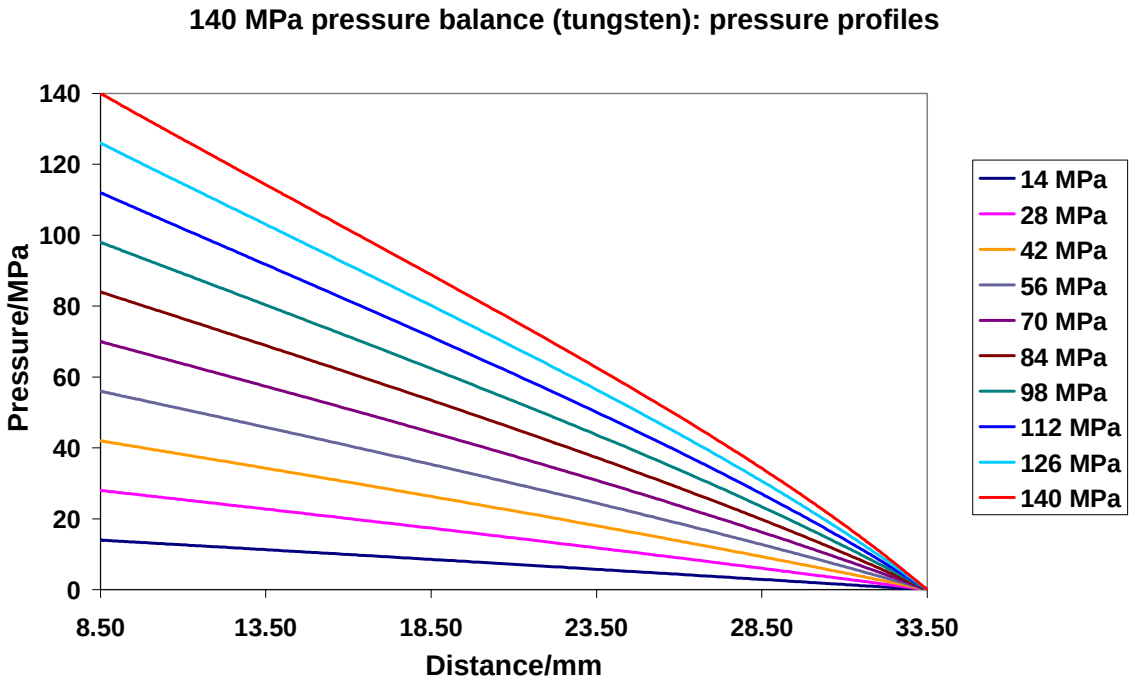

Figure 1: NPL ANSYS model of B2-816, 14 to 140 MPa applied pressure, pressure distributions along engagement length in piston-cylinder gap

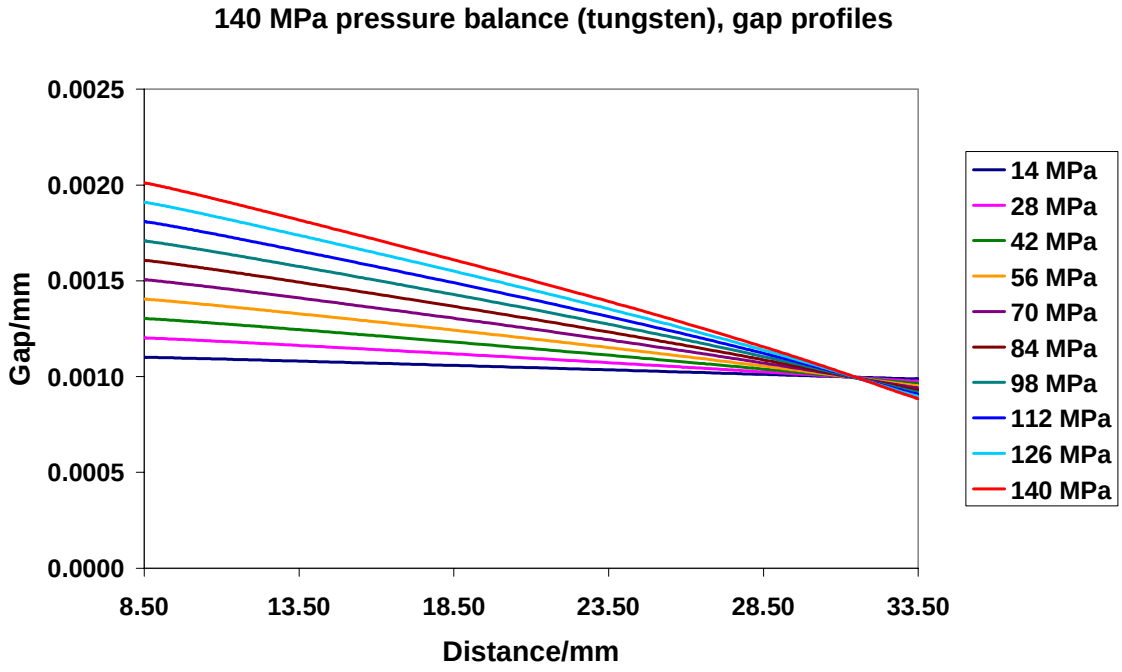

Figure 2: NPL ANSYS model of B2-816, 14 to 140 MPa applied pressure, gap profile along engagement length in piston-cylinder gap

5.6 B2-817: COMPARISON WITH CITY UNIVERSITY RESULTS

The NPL ANSYS B2-817 finite element models are based on the B2-816 models, the difference between the models being limited to the difference in material properties (B2-817 is made of steel rather than tungsten carbide) and to the difference in the measured piston and cylinder radii. Initial versions of the B2-817 model were analysed with a 1 μm piston-cylinder gap in accordance with the City University model but in later versions the measured gap width of 0.43 μm was employed. Table 10 below shows the predicted distortion coefficients and the maximum and minimum gap widths for five versions of the B2-817 model with an applied pressure of 140 MPa. Figures 3 and 4 present the pressure profiles and gap widths for pressures of 14 MPa to 140 MPa using the input parameters for run no. 4 in table 10. Note that for the steel balance with the smaller gap, both the pressure and gap results show substantial departures from linear profiles, especially at the top of the engagement length, when compared with the results from the tungsten carbide balance.

Comparison of NPL ANSYS models of B2-817 piston-cylinder pressure balance				
Run no.	Distortion coefficient ppm/MPa	Maximum gap width μm	Minimum gap width μm	Comments
1	3.10917	3.726770	0.819495	72 elements along engagement length, basic NPL model
2	3.09859	3.720190	0.805271	As run no. 1 but increased mesh density, 144 elements along engagement length
3	3.10301	3.717850	0.803736	As run no, 2 but PLANE2 triangular elements
4	3.09577	3.717820	0.799402	As run no. 2 but 288 elements along engagement length
5	3.19318	3.152990	0.454301	As run no. 4 but reduce gap to 0.43 microns

Table 10: B2-817 distortion coefficient and gap width results for a range of NPL ANSYS models, applied pressure 140 MPa.

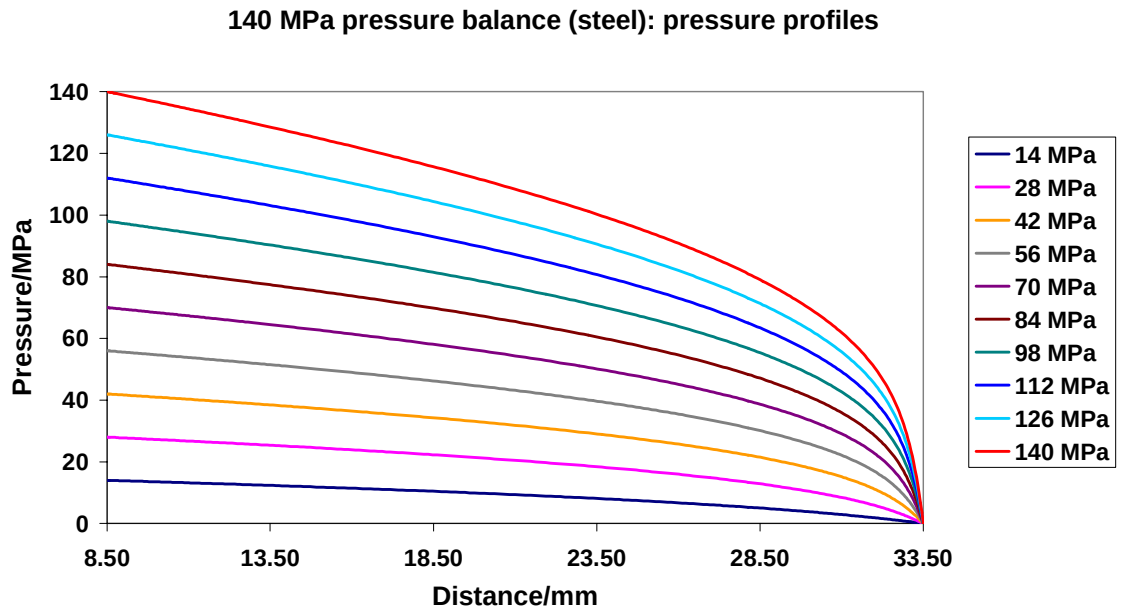

Figure 3: NPL ANSYS model of B2-817, 14 MPa to 140 MPa applied pressure, pressure distribution along engagement length in piston-cylinder gap

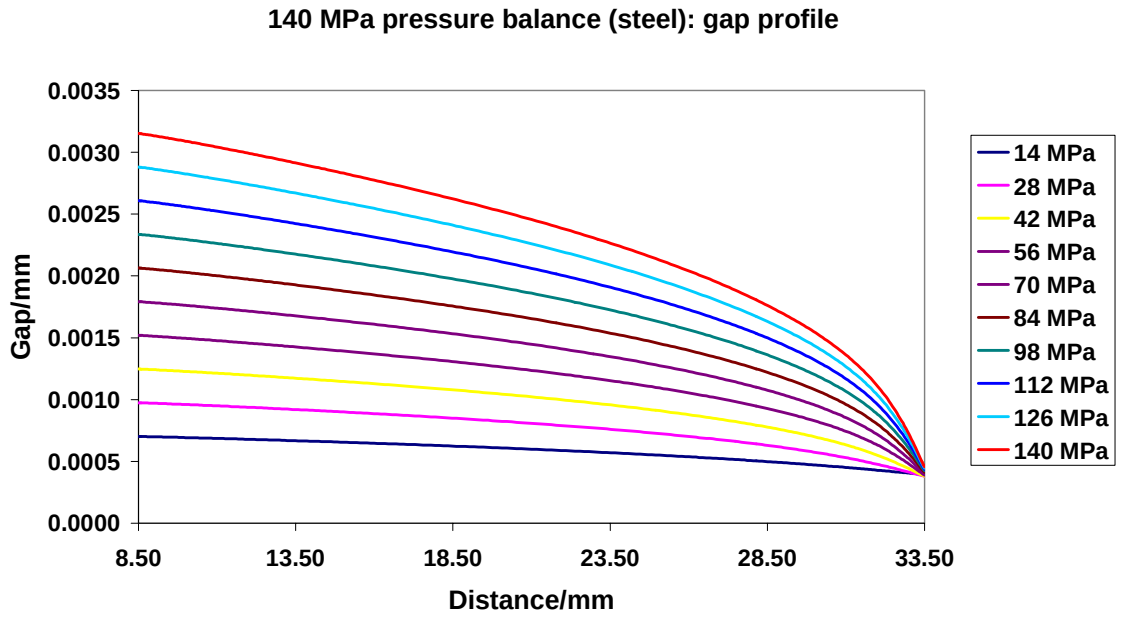

Figure 4: NPL ANSYS model of B2-817, 140 MPa applied pressure, gap profile along engagement length in piston-cylinder gap

Run no. 4 produced the lowest value of the distortion coefficient, 3.09577 ppm/MPa, of the four runs which used a nominal 1 μm gap width. The City University value at 140 MPa for

B2-817 was 3.050 ppm/MPa – the difference between this and the NPL value for run no. 4 being 1.5%. The range of the distortion coefficient values for NPL versions 1 to 4 in table 10 were from 3.09577 ppm/MPa to 3.10917 ppm/MPa, the highest value being obtained for the lowest density mesh. The highest value is 0.4% larger than the lowest value. The range of the maximum predicted gap width for runs 1 to 4 is from 3.717820 μm, obtained from the densest mesh and with quadrilateral elements, to 3.726770 μm, from the least dense mesh, the range being 0.2%. For the minimum gap width, the range is from 0.799402 μm from the highest density quadrilateral mesh to 0.819495 μm from the least dense mesh. The range in this case is 2.5%. The City University figures for maximum and minimum gap width for the B2-817 model were 3.63075 μm and 0.856084 μm respectively.

5.7 VARYING THE LINE PRESSURE FOR B2-816 AND B2-817

As mentioned above, for both of the basic NPL ANSYS models, B2-816 and B2-817, the line pressure was varied from 14 MPa to 140 MPa in intervals of 14 MPa (see figures 1 to 4 for a graphical presentation of the pressure and gap profiles). In the case of the B2-817 balance, the measured gap width of 0.43 μm was used in this process. The results of the calculations of distortion coefficient, and maximum and minimum gap width are presented in tables 11 and 12.

NPL ANSYS model of B2-816 piston-cylinder pressure balance: 1 micron gap
Variation of model output as a function of applied line pressure

Run no	Applied pressure/ MPa	Distortion coefficient ppm/MPa	Maximum gap width μm	Minimum gap width μm
B1	14	0.85731	1.10105	0.98773
B2	28	0.85730	1.20220	0.97567
B3	42	0.85730	1.30340	0.96381
B4	56	0.85731	1.40461	0.95213
B5	70	0.85733	1.50580	0.94061
B6	84	0.85734	1.60695	0.92923
B7	98	0.85737	1.70806	0.91799
B8	112	0.85740	1.80911	0.90685
B9	126	0.85735	1.91010	0.89575
6	140	0.85745	2.01098	0.88485

Table 11: Variation of distortion coefficient and maximum and minimum gap width as a function of applied pressure for the B2-816 pressure balance

NPL ANSYS models of B2-817 piston-cylinder pressure balance: 0.43 micron gap Variation of model output as a function of applied line pressure				
Run no	**Applied pressure/ MPa**	**Distortion coefficient ppm/MPa**	**Maximum gap width µm**	**Minimum gap width µm**
6	14	3.05503	0.70153	0.39387
7	28	3.08093	0.97424	0.37960
8	42	3.11064	1.24697	0.38047
9	56	3.13564	1.51961	0.38868
10	70	3.15465	1.79215	0.39982
11	84	3.16851	2.06456	0.41194
12	98	3.17842	2.33866	0.42381
13	112	3.18535	2.60903	0.43497
14	126	3.19007	2.88108	0.44518
5	140	3.19318	3.15299	0.45430

Table 12: Variation of distortion coefficient and maximum and minimum gap width as a function of applied pressure for the B2-817 pressure balance

Once again, tables 11 and 12 emphasise the effect of different materials properties and gap widths on balances of nominally identical construction. B2-816, the tungsten carbide balance has a distortion coefficient which is insensitive to changes in applied pressure, whereas the steel balance shows an increase in distortion coefficient of 4.5% between 14 MPa and 140 MPa applied pressure. In the case of the B2-817 steel balance the predicted minimum gap width at the top of the gap gets larger as pressure increases, whereas the opposite effect occurs in the tungsten carbide balance. At the bottom of the engagement length, the B2816 tungsten carbide balances shows an 83% increase in width from 1.10105 µm to 2.01098 µm as the pressure increases from 14 MPa to 140 MPa, whereas the equivalent figure for the steel balance is 449% as the gap increases from 0.71053 µm to 3.15299 µm.

5.8 D&H SERIAL NO 1000

This pressure balance had not been modelled as part of the City University research. Only limited information about its geometry exists, as it has not been dimensioned. It operates in the pressure range up to 100 MPa.

As far as can be ascertained from pressure and vacuum section records, from the D&H drawings of the assembly, and an earlier attempt to model this pressure, the key dimensions are:

Piston length: 84.56 mm
Cylinder length: 27 mm
Cylinder outside diameter: 17 mm
Undistorted area, A_O: 9.80590 mm^2
Piston radius, r_O: 1.766724 mm

The working position of the pressure balance was defined to be that in which the piston extends for 7.5 mm below the lower face of the cylinder. An initial "guess" at the gap width of 1 μm was employed in the modelling, but investigations were also carried out with a gap width of 0.3 μm. This pressure balance is made of tungsten carbide and DHS was modelled as the working fluid for this balance, as it was for B2-816 and B2-817.

As no detailed results from earlier modelling of this pressure balance exists, validation by comparison is not possible. Thus, at this stage it is only possible to present some numerical results which were obtained during the development of the ANSYS model. For this balance, two cases were investigated. The first of these was the effect of a change in the value of Young's modulus for tungsten carbide from 583 GPa to 543 GPa. The stiffness of tungsten carbide is controlled by the addition of cobalt. See figure 1 earlier in this report. The second case to be investigated was the effect of changing the initial gap width from 1 μm to 0.3 μm, with the values of Young's modulus and Poisson's ratio held constant.

Figure 5 shows the pressure profile along the engagement length for a 0.3 μm initial gap width, for two values of Young's modulus, 583 GPa and 543 GPa. The distortion coefficient, as predicted by the ANSYS software, for the 583 GPa case was 0.874 ppm/MPa and for the 543 GPa case, 0.970 ppm/MPa. A 7% reduction in Young's modulus produced a 11% rise in the predicted distortion coefficient. Figure 6 shows the gap profile along the engagement length for the same two values of Young's modulus.

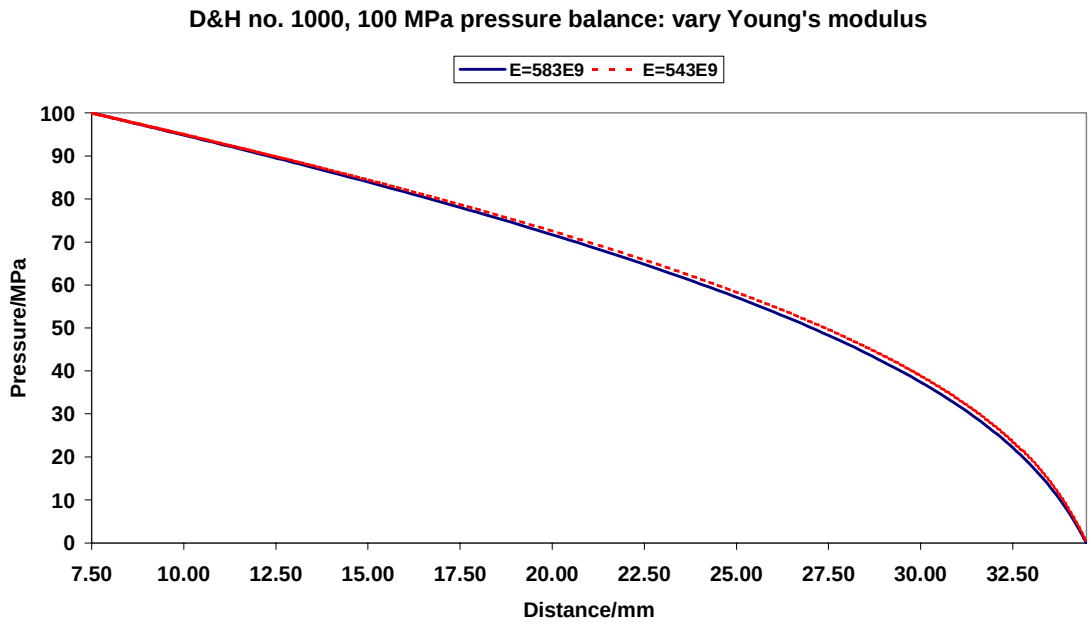

Figure 5: D&H serial no 1000, pressure profile along the engagement length for a 0.3 µm initial gap width, for two values of Young's modulus, 583 GPa and 543 GPa.

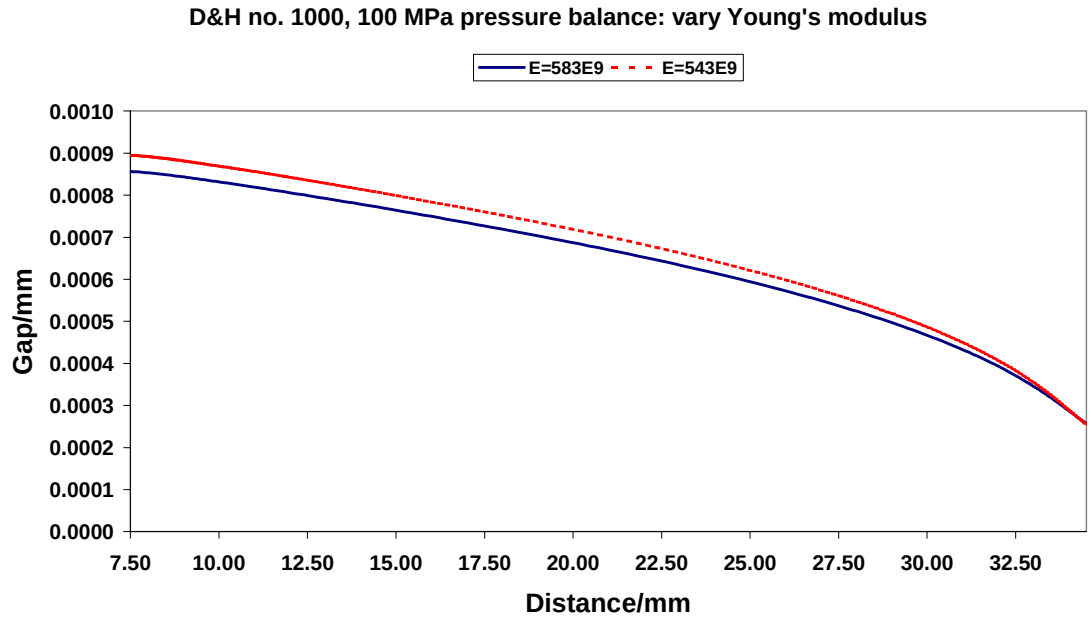

Figure 6: D&H serial no 1000, gap profile along the engagement length for a 0.3 µm initial gap width, for two values of Young's modulus, 583 GPa and 543 GPa.

Figures 7 and 8 show the effect on the output of the ANSYS model of the D&H 100 MPa pressure balance of keeping the value of Young's modulus constant at 543 GPa and varying the initial gap width from 1 µm to 0.3 µm.

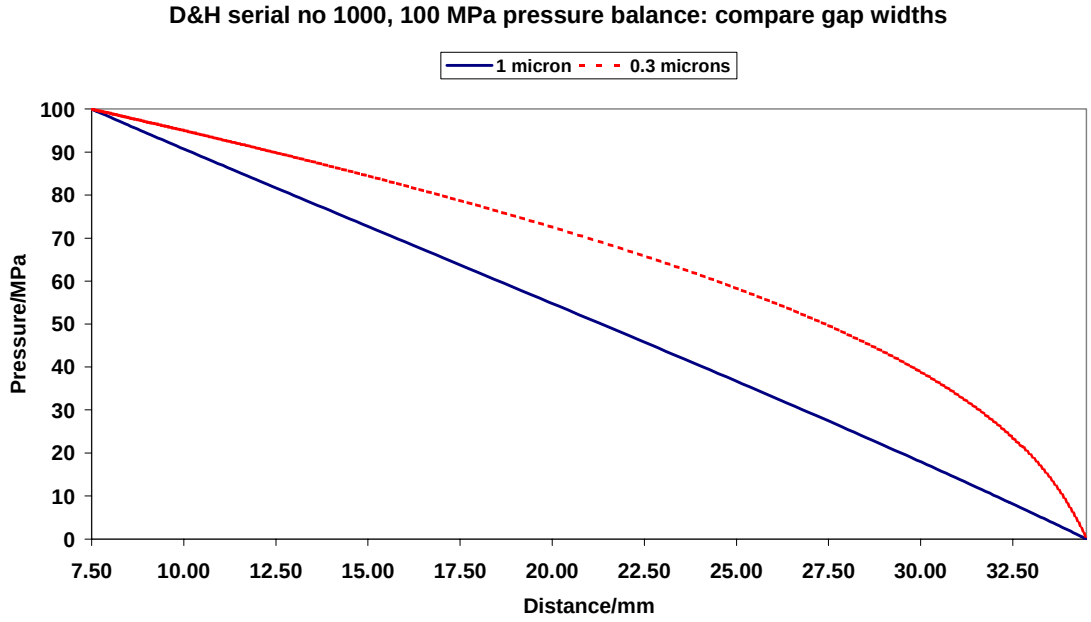

Figure 7: D&H serial no 1000 pressure balance: pressure profile, Young's modulus kept constant at 543 GPa and initial gap width varied from 1 µm to 0.3 µm.

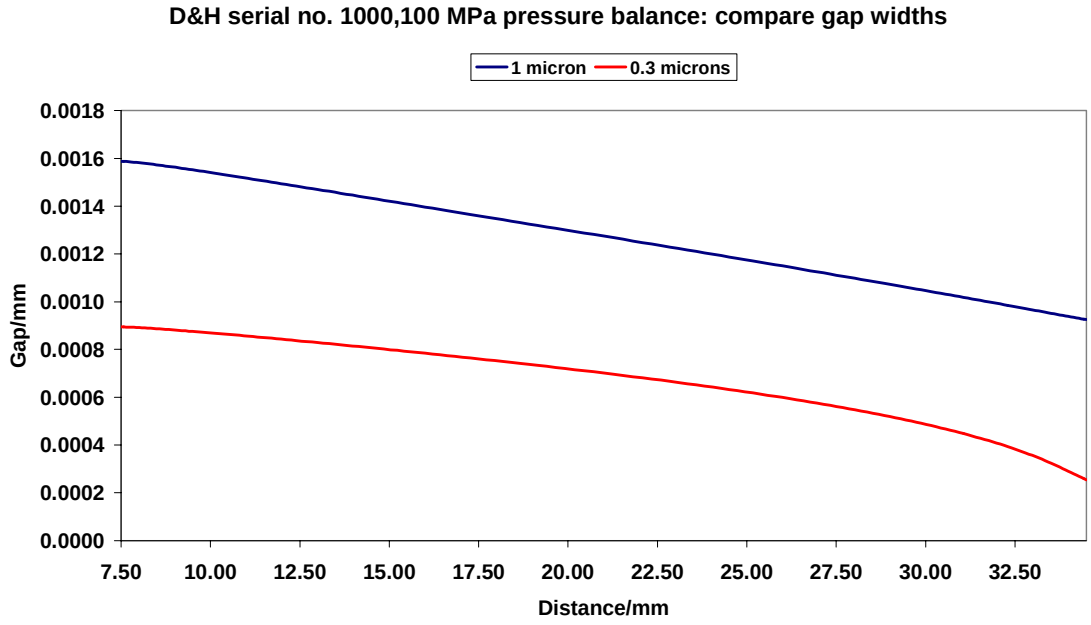

Figure 8: D&H serial no 1000 pressure balance: gap profile, Young's modulus kept constant at 543 GPa and initial gap width varied from 1 µm to 0.3 µm.

Figures 7 and 8 both underline the effect that a substantial reduction in gap width can have on the shape of the pressure and gap profiles of tungsten carbide balances. However, for the 1 µm gap the predicted distortion coefficient for the 543 GPa Young's modulus case was 0.964 ppm/MPa compared with 0.970 ppm/MPa for the 0.3 µm gap, a relatively minor change.

5.9 THE EUROMET 463 PROJECT BALANCE

The Euromet project no. 463 followed on from project no. 256 and has the aim of investigating uncertainty budgets for finite element models of pressure balances. The project, which is co-ordinated by the Physikalisch-Technische Bundesanstalt (PTB), requires the modelling of a 1 GPa controlled-clearance DH 7594 type balance, which is owned by the PTB and for which the PTB has extensive experimental data, including measurements of the roundness and straightness of the piston and cylinder units.

The nominal radius of the piston is 1.25 mm and the gap width is taken to be 0.32 ± 0.03 µm. The engagement length is 19.3 mm. The piston and cylinder are manufactured from tungsten carbide with added cobalt and the cylinder sleeve is made of steel. In controlled clearance operation a jacket pressure of one tenth of the line pressure is applied to the cylinder sleeve. Figure 9, provided by the PTB, shows a schematic diagram of the combined piston and cylinder structure. The balance has a more complex structural geometry than the balances discussed earlier in this chapter. Further information about the balance can be found on the PTB web-site at http://www.ptb.de/de/org/3/_index.htm. The results of the finite element modelling of this balance are presented in subsequent chapters of this report.

As the PTB web-site points out, this system differs from conventional piston-cylinder assemblies in a number of ways. Although this balance is designed to measure up to 1 GPa, the breaking point of tungsten carbide under a tensile stress is noticeably lower than this value. The tensile stress caused by the pressure loading is therefore compensated both by the pressure applied to the sleeve, and by the double-wall design of the cylinder, where the steel wall is shrunk onto the tungsten carbide inner cylinder to cause compressive stress in the cylinder. However, in the finite element modelling undertaken for this project, any effects or loads arising from this static compressive stress are ignored.

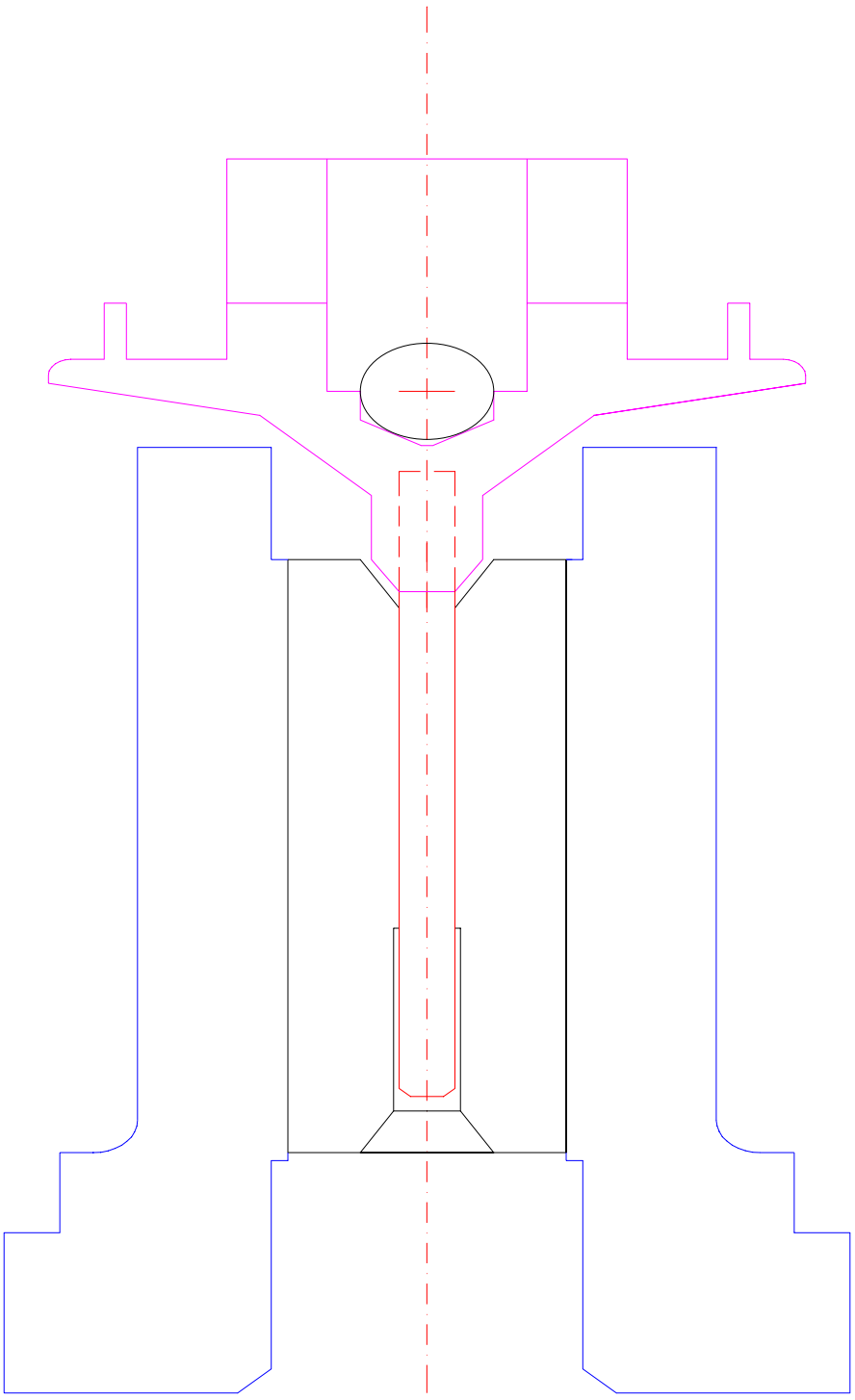

Figure 9: Schematic diagram of Euromet project no 463 1 GPa pressure balance

Initial tests on the FEA model were carried out by assuming that the pressure balance was to be operated in free deformation mode and that the piston, cylinder and cylinder sleeve all had identical material properties. In this way, distortion coefficient predictions derived from the FEA model could be compared with predictions from simple elastic theory. The cases considered were firstly an assumption that the balance had the properties defined by the PTB's experimental determination of the piston's Young's modulus and Poisson's ratio, that is, 543 GPa and 0.238 respectively, and secondly that the balance had the D&H supplied values, a Young's modulus of 630 GPa and a Poisson's ratio of 0.22. In addition, the effect of varying the boundary conditions on the conical part of the lower part of the cylinder was also examined, by calculating the results with and without the line pressure applied to this conical surface. It was assumed that omitting the application of pressure to the cone would lead to results which agreed more closely with the predictions of simple elastic theory, which was, in fact, shown to be the case. The results of the FEA predictions and the comparison with simple elastic theory are set out in table 13. The PTB had also made available its own calculation of the case in which no line pressure is applied to the cone for purposes of comparison and these results are also included in the table. The good agreement between all three methods of calculation suggest that, at least in the free deformation case, the NPL FEA model is providing reliable results.

Euromet 463 project: testing FEA in simple mode
Free deformation mode predictions of distortion

	Distortion coefficient/ppm/MPa		
	FEA		Elastic
	NPL	PTB	theory
PTB properties			
+ line 1 to 2	0.9095		0.8938
- line 1 to 2	0.9033	0.903	0.8938
D&H properties			
+ line 1 to 2	0.7265		0.7132
- line 1 to 2	0.7207	0.728	0.7132

Table 13: Euromet 463 project: compare FEA results with simple elastic theory for models with identical properties for all components of the balance.

6 VARYING THE INPUTS

In this chapter the results of varying the key model input parameters are presented. The aim was to determine the sensitivity of the prediction of the distortion coefficient in particular to changes in the model input parameters, and especially to variations in material properties.

6.1 B2-816

In the case of this balance, the study of the distortion coefficient predictions concentrated on the Young's modulus and Poisson's ratio of the piston and cylinder for an applied line pressure value of 140 MPa. Two cases were considered, the first assumed that the piston and cylinder both possessed the same properties and the second allowed the properties of the piston and cylinder to be varied independently. In addition, comparisons were made between the finite element results and the predictions of simple elastic theory for both cases.

The range of variation of Young's modulus was from 493 GPa to 673 GPa, and for Poisson's ratio, 0.195 to 0.265. These values are not intended to represent the actual properties of the balance and their associated uncertainties, but to demonstrate the changes in output which are observed when inputs are varied over such a wide range. Table 14 shows the distortion coefficient predictions from FEA modelling and from simple theory when the properties of the piston and cylinder are varied jointly. Table 15 presents similar results for Poisson's ratio variations.

Young's modulus GPa	Distortion coefficient ppm/MPa	
	FEA	Simple
493	1.0144	1.0115
508	0.9844	0.9816
523	0.9561	0.9534
538	0.9293	0.9269
553	0.9041	0.9017
568	0.8801	0.8779
583	0.8575	0.8553
598	0.8359	0.8339
613	0.8154	0.8135
628	0.7959	0.7940
643	0.7773	0.7755
658	0.7596	0.7578
673	0.7427	0.7409

Table 14: B2-816, variation of distortion coefficient as Young's modulus is varied

Poisson's ratio	Distortion coefficient ppm/MPa	
	FEA	Simple
0.195	0.7371	0.7353
0.202	0.7612	0.7593
0.209	0.7852	0.7833
0.216	0.8093	0.8073
0.223	0.8334	0.8313
0.230	0.8575	0.8553
0.237	0.8815	0.8793
0.244	0.9056	0.9034
0.251	0.9297	0.9274
0.258	0.9537	0.9514
0.265	0.9778	0.9754

Table 15: B2-816, variation of distortion coefficient as Poisson's ratio is varied

Figures 10 and 11 show the results from the two tables graphically. Note that the FEA predictions and the results from the simplified theory are hardly separable on the scale of the graphs shown here.

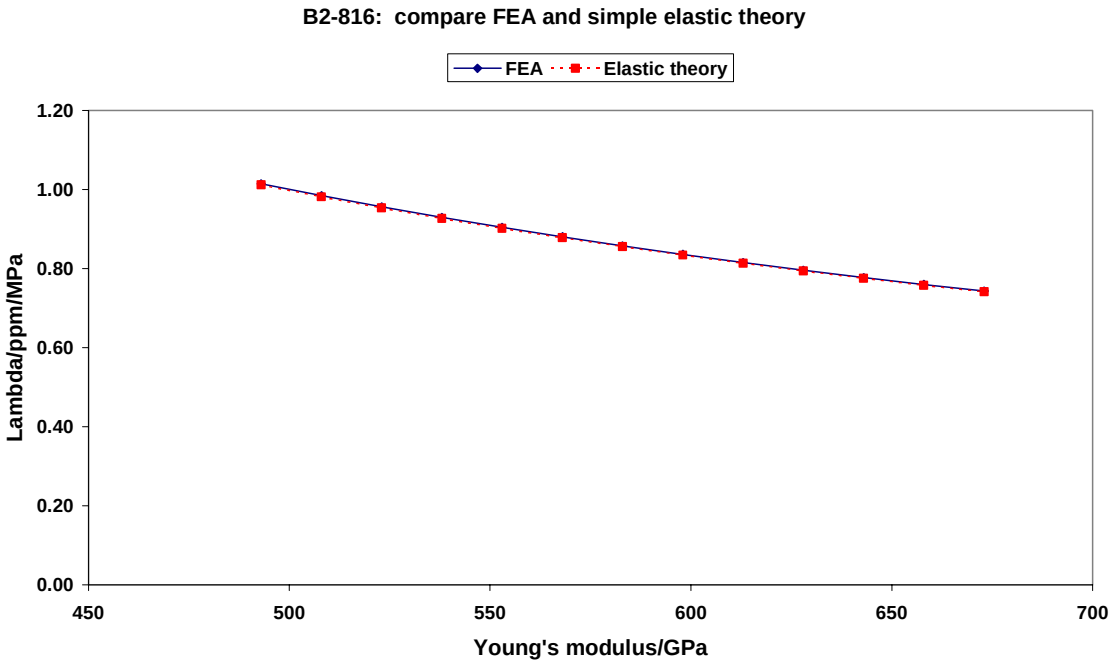

Figure 10: B2-816, variation of distortion coefficient as Young's modulus is varied

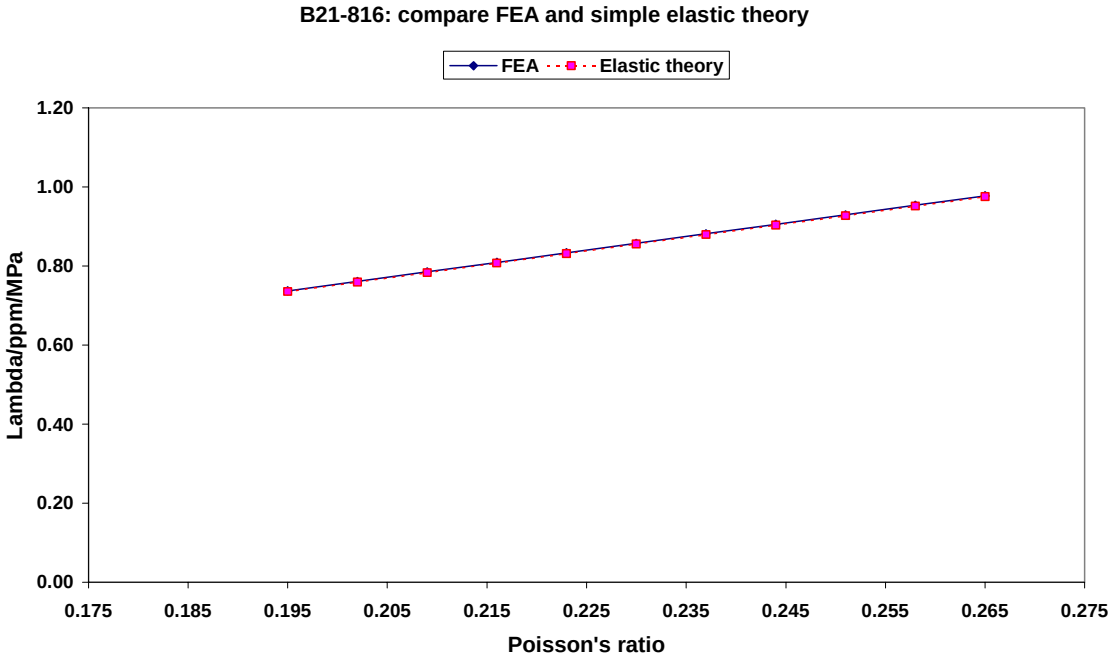

Figure 11: B2-816, variation of distortion coefficient as Poisson's ratio is varied

The next stage of the work was to investigate the effects of allowing the piston and cylinder properties to vary separately. The "reference values" for this exercise were taken to be a Young's modulus value of 583 GPa and Poisson's ratio value of 0.23. Tables 16 and 17 show the effect on the distortion coefficient of varying the Young's modulus and Poisson's ratio of the piston and cylinder separately.

Young's modulus GPa		Distortion coefficient ppm/MPa	
Piston	Cylinder	FEA	Simple
583	583	0.8575	0.8553
583	493	1.0639	1.0600
583	523	0.9873	0.9839
583	553	0.9190	0.9161
583	613	0.8025	0.8005
583	643	0.7524	0.7507
583	673	0.7066	0.7054
493	583	0.8085	0.8068
523	583	0.8268	0.8248
553	583	0.8431	0.8409
613	583	0.8709	0.8683
643	583	0.8829	0.8801
673	583	0.8938	0.8909

Table 16: B2-816, variation of distortion coefficient as Young's modulus of piston and cylinder is varied separately

		Distortion coefficient	
Poisson's ratio		ppm/MPa	
Piston	Cylinder	FEA	Simple
0.23	0.23	0.8575	0.8553
0.23	0.195	0.8275	0.8253
0.23	0.209	0.8396	0.8373
0.23	0.223	0.8517	0.8493
0.23	0.237	0.8638	0.8613
0.23	0.251	0.8759	0.8733
0.23	0.265	0.8880	0.8853
0.195	0.23	0.7675	0.7653
0.209	0.23	0.8036	0.8013
0.223	0.23	0.8397	0.8373
0.237	0.23	0.8758	0.8733
0.251	0.23	0.9118	0.9094
0.265	0.23	0.9479	0.9454

Table 17: B2-816, variation of distortion coefficient as Poisson's ratio of piston and cylinder is varied separately

The clear conclusion to be drawn from the above results is that for pressure balances of simple structure manufactured from hard metals such as tungsten carbide and, for micrometre sized gaps and pressures of the order of 100 MPa, both finite element analysis and simple theory give very similar results.

6.2 B2-817

The B2-817 balance has the same structure as B2-816. However, the balance is made from steel and the gap width is 0.43 μm. A similar investigation of the sensitivity of the FEA distortion coefficient predictions to variations in material parameters was carried out for this balance. In the case of the steel balance, the range of variation of Young's modulus was from 170 to 250 GPa, and for Poisson's ratio from 0.255 to 0.345, where the base line values were taken to be 210 GPa for Young's modulus and 0.3 for Poisson's ratio. The line pressure used throughout the analysis was 140 MPa. Once again, the aim here was not to select realistic values for the balance in question but to understand the sensitivity of model output to changes in input.

Tables 18 and 19 below give the results of the distortion coefficient predictions for the case where the piston and cylinder are assumed to have identical properties. Once again, results are compared with predictions from simple elastic theory. Figures 12 and 13 show a comparison between the FEA results and simple theory for the two cases.

Young's modulus GPa	Distortion coefficient ppm/MPa	
	FEA	Simple
170	3.9728	3.7568
180	3.7453	3.5481
190	3.5417	3.3614
200	3.3587	3.1933
210	3.1932	3.0412
220	3.0430	2.9030
230	2.9059	2.7768
240	2.7804	2.6611
250	2.6648	2.5546

Table 18: B2-817, variation of distortion coefficient as Young's modulus is varied

Poisson's ratio	Distortion coefficient ppm/MPa	
	FEA	Simple
0.255	2.7417	2.6127
0.264	2.8317	2.6984
0.273	2.9216	2.7841
0.282	3.0123	2.8698
0.291	3.1027	2.9555
0.3	3.1932	3.0412
0.309	3.2838	3.1269
0.318	3.3746	3.2127
0.327	3.4655	3.2984
0.336	3.5565	3.3840
0.345	3.6474	3.4698

Table 19: B2-817, variation of distortion coefficient as Poisson's ratio is varied

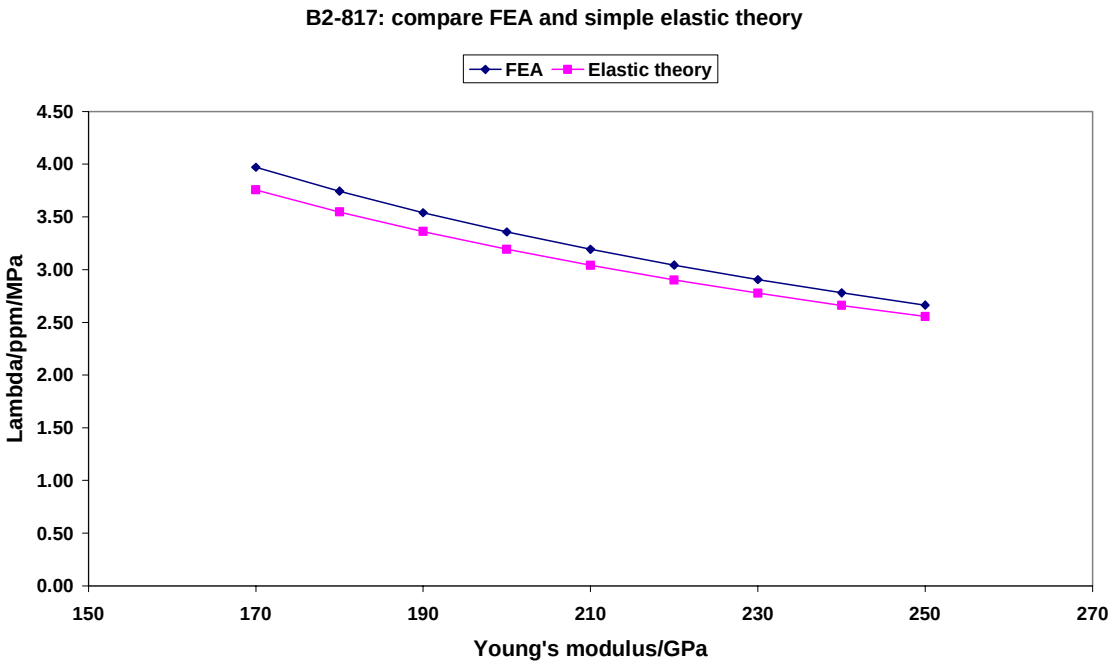

Figure 12: B2-817, compare FEA and elastic theory distortion coefficients as Young's modulus is varied

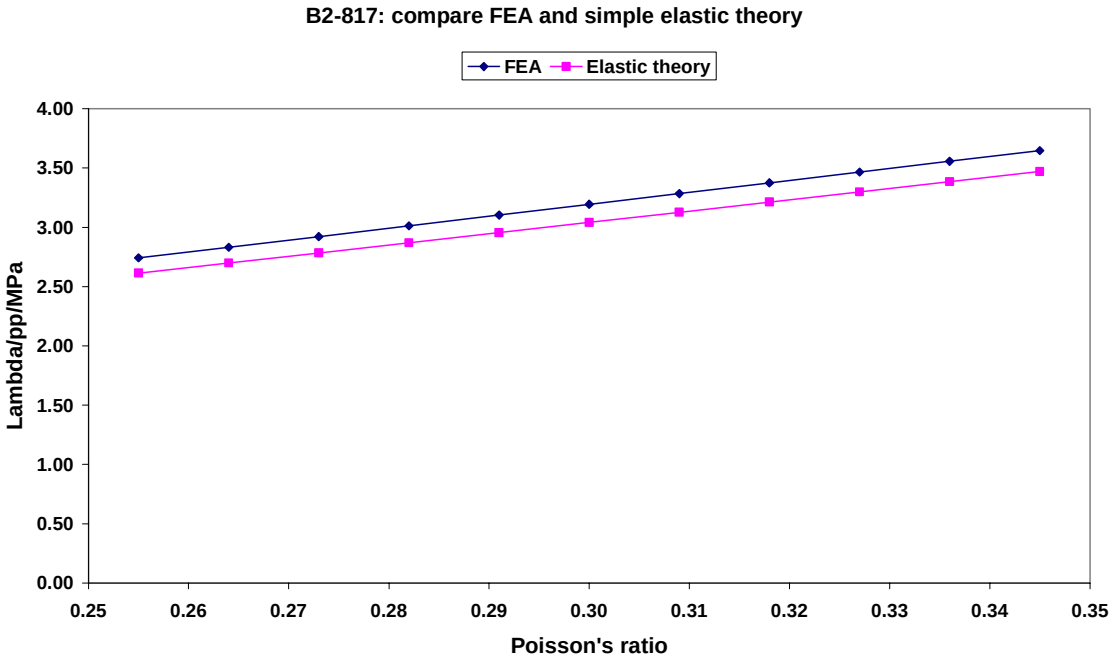

Figure 13: B2-817, compare FEA and elastic theory distortion coefficients as Poisson's ratio is varied

As before, the effect of varying the piston and cylinder properties separately was investigated**.** The "reference values" for this analysis were again taken to be: Young's modulus, 210 GPa, and Poisson's ratio, 0.3. Tables 20 and 21 below set out the results.

Young's modulus GPa		Distortion coefficient ppm/MPa	
Piston	Cylinder	FEA	Simple
210	210	3.1932	3.0412
210	170	3.9982	3.8128
210	190	3.5536	3.3864
210	230	2.8961	2.7561
210	250	2.6461	2.5165
170	210	3.1673	2.9852
190	210	3.1816	3.0162
230	210	3.2037	3.0619
250	210	3.2122	3.0793

Table 20: B2-817 variation of distortion coefficient as Young's modulus of piston and cylinder is varied separately

Poisson's ratio		Distortion coefficient ppm/MPa	
Piston	Cylinder	FEA	Simple
0.300	0.300	3.1932	3.0412
0.300	0.255	3.0799	2.9341
0.300	0.273	3.1255	2.9769
0.300	0.291	3.1708	3.0198
0.300	0.318	3.2391	3.0841
0.300	0.336	3.2847	3.1269
0.255	0.300	2.8553	2.7198
0.273	0.300	2.9904	2.8484
0.291	0.300	3.1260	2.9769
0.318	0.300	3.3295	3.1698
0.336	0.300	3.4658	3.2984

Table 21: B2-817 variation of distortion coefficient as Poisson's ratio of piston and cylinder is varied separately

In contrast to what was observed during the analysis of the tungsten carbide balance B2-816, there is poorer agreement between the FEA predictions and simple theory. The FEA distortion coefficient predictions are always higher than those given by the simple elastic model, typically by 5%. Note, however, as shown by figures 12 and 13, that agreement improves at higher Young's modulus and lower Poisson's ratio values.

6.3 D&H SERIAL NO 1000

This balance is again of simple construction with a piston of 1.76622 mm radius and a gap width of 1 µm. Its maximum line pressure, which was employed for all the analyses tabulated in this section of the report, was 100 MPa. The balance is made of tungsten carbide throughout. As with balance B2-816 the range of variation of Young's modulus was taken to be 493 GPa to 673 GPa, and the range of Poisson's ratio was from 0.195 to 0.265. Tables 22 and 23 and figures 14 and 15 set out the results for the case in which the properties of both

the cylinder and piston are regarded as being identical. Once again, the cylinder and piston material properties were allowed to vary independently of each other, with the "reference values" for the comparison being taken as 583 GPa for Young's modulus and 0.23 for Poisson's ratio. The results for this case are set out in tables 24 and 25. Note that the FEA predictions are in good agreement with those obtained by the use of simple models based on elastic theory, confirming the observation that for stiff materials, simple structures and gaps of the order of 1 μm, simple theory can give an adequate prediction of the distortion coefficient.

Young's modulus	Distortion coefficient ppm/MPa	
GPa	FEA	Simple
493	1.0269	1.0247
508	0.9965	0.9944
523	0.9679	0.9659
538	0.9409	0.9390
553	0.9154	0.9135
568	0.8912	0.8894
583	0.8707	0.8665
598	0.8465	0.8448
613	0.8257	0.8241
628	0.8060	0.8044
643	0.7872	0.7857
658	0.7692	0.7677
673	0.7521	0.7506

Table 22: D&H no 1000: variation of distortion coefficient as Young's modulus is varied

Poisson's ratio	Distortion coefficient ppm/MPa	
	FEA	Simple
0.195	0.7479	0.7464
0.202	0.7719	0.7705
0.209	0.7960	0.7945
0.216	0.8201	0.8185
0.223	0.8442	0.8425
0.23	0.8707	0.8665
0.237	0.8923	0.8905
0.244	0.9164	0.9145
0.251	0.9405	0.9386
0.258	0.9646	0.9626
0.265	0.9887	0.9866

Table 23: D&H no 1000: variation of distortion coefficient as Poisson's ratio is varied

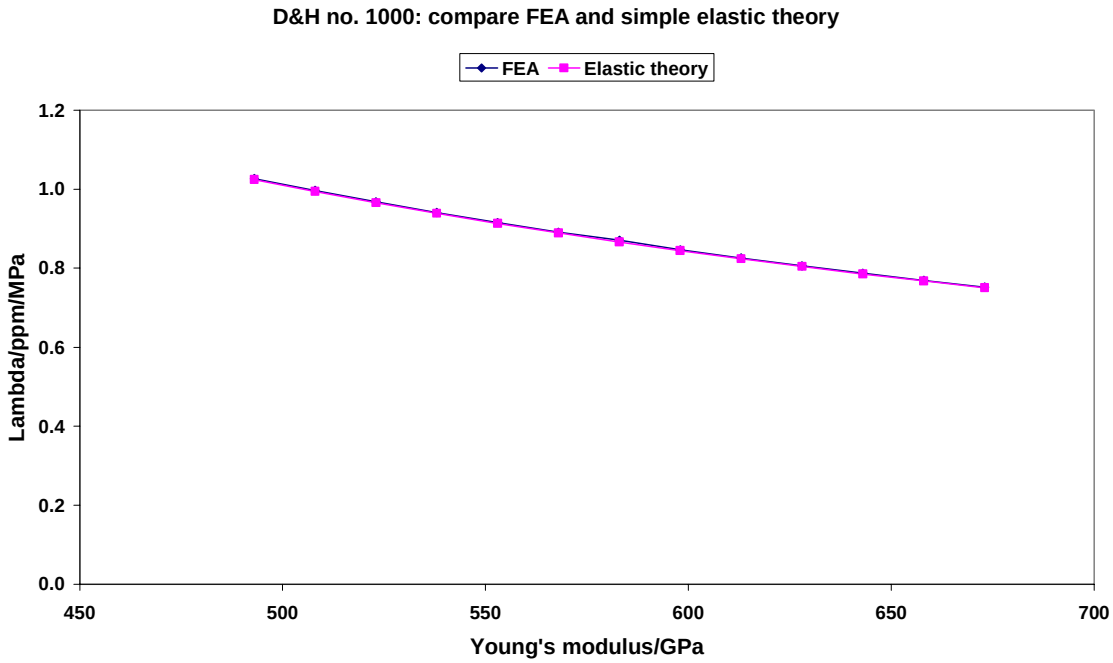

Figure 14: D&H no 1000 compare FEA and elastic theory distortion coefficients as Young's modulus is varied

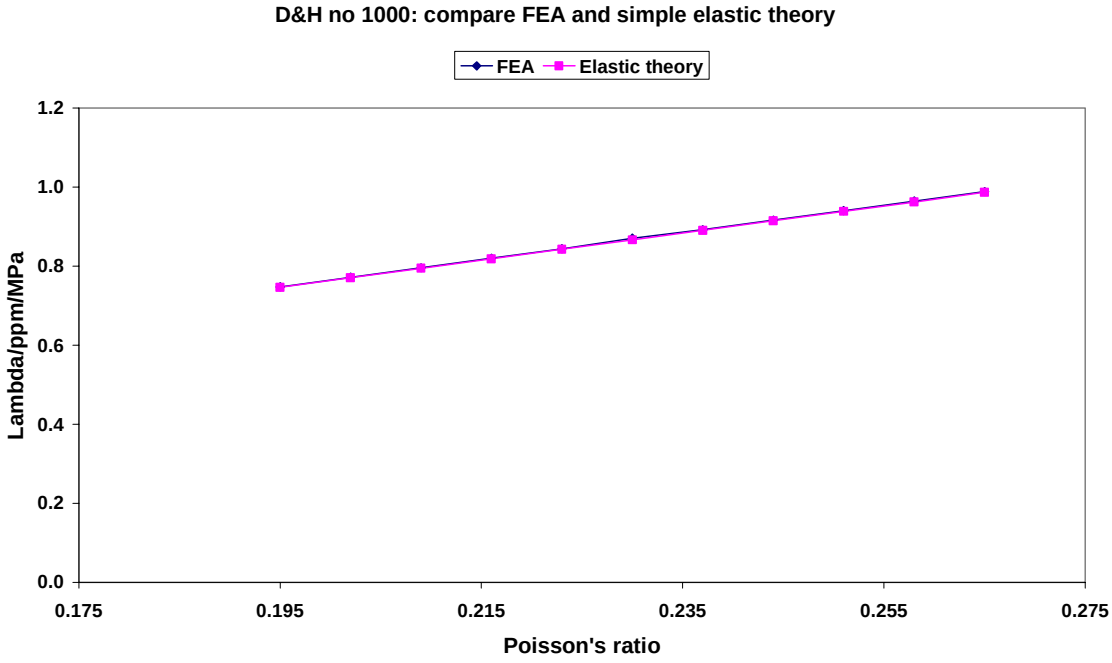

Figure 15: D&H no 1000 compare FEA and elastic theory distortion coefficients as Poisson's ratio is varied

Young's modulus GPa		Distortion coefficient ppm/MPa	
Piston	Cylinder	FEA	Simple
583	583	0.8707	0.8665
583	493	1.0766	1.0732
583	523	0.9992	0.9964
583	553	0.9302	0.9279
583	613	0.8124	0.8111
583	643	0.7618	0.7609
583	673	0.7157	0.7151
493	583	0.8186	0.8180
523	583	0.8370	0.8360
553	583	0.8535	0.8521
613	583	0.8816	0.8795
643	583	0.8937	0.8913
673	583	0.9047	0.9021

Table 24: D&H no 1000, variation of distortion coefficient as Young's modulus of piston and cylinder is varied separately

Poisson's ratio		Distortion coefficient ppm/MPa	
Piston	Cylinder	FEA	Simple
0.23	0.23	0.8707	0.8665
0.23	0.195	0.8380	0.8365
0.23	0.209	0.8501	0.8485
0.23	0.223	0.8622	0.8605
0.23	0.237	0.8743	0.8725
0.23	0.251	0.8864	0.8845
0.23	0.265	0.8985	0.8965
0.195	0.23	0.7781	0.7765
0.209	0.23	0.8142	0.8125
0.223	0.23	0.8502	0.8485
0.237	0.23	0.8863	0.8845
0.251	0.23	0.9224	0.9205
0.265	0.23	0.9584	0.9566

Table 25: D&H no 1000, variation of distortion coefficient as Poisson's ratio of piston and cylinder is varied separately

6.4 THE EUROMET 463 PROJECT BALANCE

The investigations to be performed on the model of the Euromet 463 balance were defined by the PTB. There were four tasks, two of which were to be carried out using a model with an ideally round and straight piston and two using a model which took into account measured three-dimensional piston and cylinders profiles. In this section of the report the results for the ideally round and straight case are considered. The analysis of three-dimensional data is discussed in chapter 8 of this report.

As a result of some preliminary comparisons of finite element modelling results with experimental determinations of the pressure balance's distortion coefficient and fall rate, it appeared that the piston and cylinder of the balance had been manufactured from tungsten carbide with different properties. The PTB were able to measure the Young's modulus and Poisson's ratio of the balance piston and had determined these to be 543 ± 7 GPa and 0.238 ± 0.002 respectively (Sabuga, 2001). The properties of the cylinder were taken to be those which had originally been provided by the manufacturer, Désgranges and Huot, namely a Young's modulus of 630 GPa and a Poisson's ratio of 0.22. The uncertainties on the cylinder properties were taken to be ± 10 GPa for Young's modulus and ± 0.002 for Poisson's ratio. The cylinder sleeve is made from steel and its properties were considered to be 200 ± 7 GPa for Young's modulus and 0.29 ± 0.02 for Poisson's ratio. The gap width in the ideally round and straight case was taken to be 0.32 ± 0.03 μm. In controlled clearance mode calculations of distortion coefficient and piston fall rate were to be carried out at applied pressures of 100, 250, 400, 600, 800 and 1000 MPa, with the jacket pressures exactly one tenth of these values. In free deformation mode the applied pressures to be investigated were 100, 250, 500 and 600 MPa. In addition to the calculations required by the PTB, the effect of varying boundary conditions, of using a pressure-dependent density (equation 2 from Molinar et al 1999) and of coarsening the FEA mesh were also investigated.

Figure 16 identifies the location of lines upon which specific boundary conditions were to be applied. Lines 6 to 7 and 8 to 9 were to be constrained from movement in both the axial and radial directions. The applied pressure should be applied on line 1 to 2, as well as to the piston and to higher points on the cylinder in the gap region. In the controlled clearance case, the jacket pressure was to be applied along the line from point 4 to 5. In addition, the effect of extending the region of jacket pressure application to point 3 was also investigated, as was moving point 4 lower to coincide with the location of the top of the piston-cylinder engagement length.

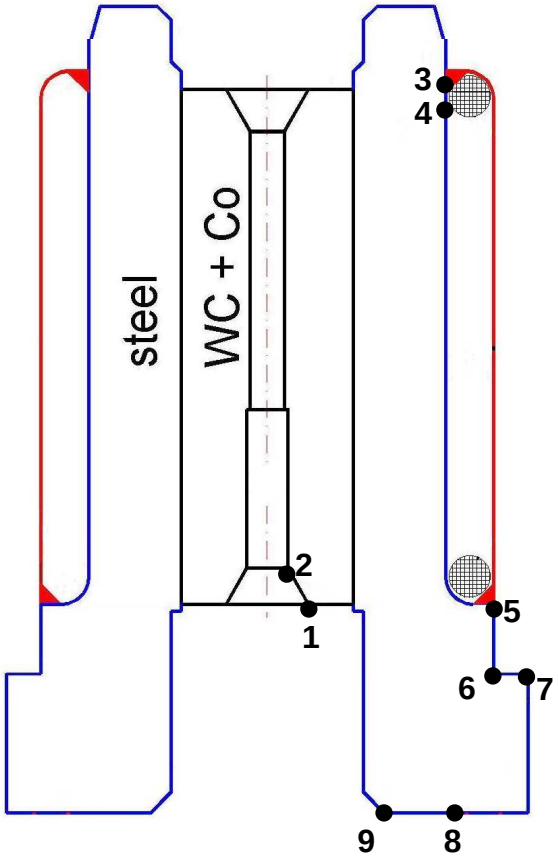

Figure 16: diagram of Euromet 463 pressure balance identifying lines to be used in defining boundary conditions

Following the analysis of the case in which the piston and cylinder are taken as having different properties, the calculations were repeated on the assumption that the cylinder had the same properties as the piston, that is, a Young's modulus of 543 ± 7 GPa and a Poisson's ratio of 0.238 ± 0.002. Table 26 sets out the predicted distortion coefficients and piston fall rates for the four base line models at a line pressure of 400 MPa (different piston and cylinder properties, (Sabuga, 2001), free deformation and controlled clearance modes; identical piston and cylinder properties, free deformation and controlled clearance modes).

The inputs to the base line models were then varied in accordance with the requirements of the PTB project co-ordinator. In the case of the materials properties for the piston, cylinder and cylinder sleeve, additional analyses were carried out for two values of each property, representing the extremes of the uncertainty range which had been quoted. Thus, in the case of the piston, the base line Young's modulus value was 543 GPa, and the two additional cases which were calculated were 536 GPa and 550 GPa. A similar approach was adopted for the other materials properties and components. In the case of the gap width, which was taken to be 0.32 µm for the base line model, additional gap widths of 0.29 µm and 0.35 µm were also analysed. In each case, two approaches to defining the revised gap were investigated. The

first was to apply the 0.03 μm adjustment needed wholly to the piston radius and the second was to apply it wholly to the cylinder internal radius.

Other variations to the 400 MPa base line model results were to vary the applied pressure from 100 MPa to 1000 MPa in the controlled clearance mode, and from 100 MPa to 600 MPa in the free deformation mode, to investigate changes in boundary conditions, to test the effect of employing a pressure-dependent density term and to vary the FEA mesh density. The boundary conditions variations which were implemented were to omit the application of the line pressure on the line between points 1 and 2 in both the controlled clearance and free deformation cases, and to vary the range over which the jacket pressure was applied in the controlled clearance case by applying it additionally between lines 3 and 4, by removing it below point 4 to a location level with the top of the engagement length, and by removing it in the region of the lower oil seal close to point 5 in figure 16. To test pressure-dependent density effects, the density equation from Molinar et al (1998) was implemented. Finally, the effect of coarser and denser finite element meshes was investigated. Although one would ideally like to use as fine a mesh as possible, such an approach is not feasible when run times are long and many repetitions of the analysis are required. Thus the mesh chosen for the base line model is dense enough to require run times of several hours, but not dense enough to produce intractable run times for repeat analyses. Tables 27 to 30 set out the results for the range of input variations which were investigated for the four cases. In the table headings the PTB's terminology is used to define the models: "Model 2" refers to the version with differing piston and cylinder properties, and "Model 3" to the version in which the properties are identical.

Euromet 463 project: predictions of base line models		
	Distortion coefficient ppm/MPa	**Piston fall rate mm/min**
Piston and cylinder differ		
Free deformation	0.7651	0.3150
Controlled clearance	0.3666	0.1605
Piston and cylinder identical		
Free deformation	0.9447	0.4091
Controlled clearance	0.4907	0.2023

Table 26: Compare predictions of base line models at 400 MPa

Figures 17 to 20 show the pressure distributions and gap widths as a function of position along the engagement length for the differing and identical piston and cylinder properties cases in both controlled clearance and free deformation modes. In each case it is the base line 400 MPa results which are presented.

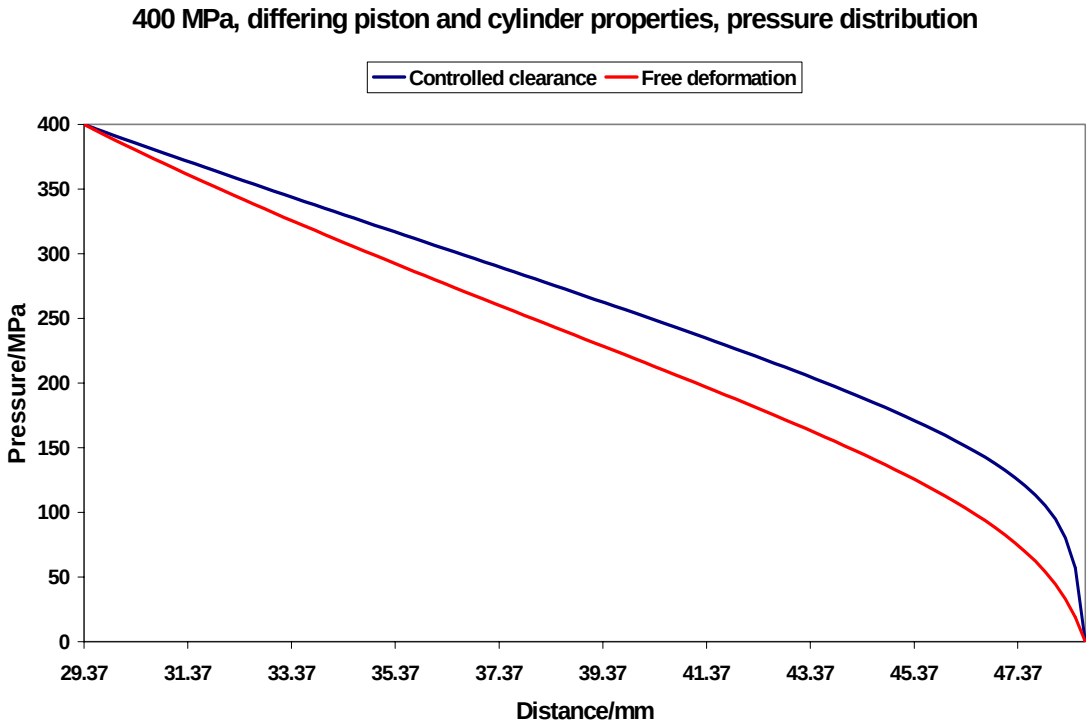

Figure 17: 400 MPa base line model, differing piston and cylinder properties, pressure distribution

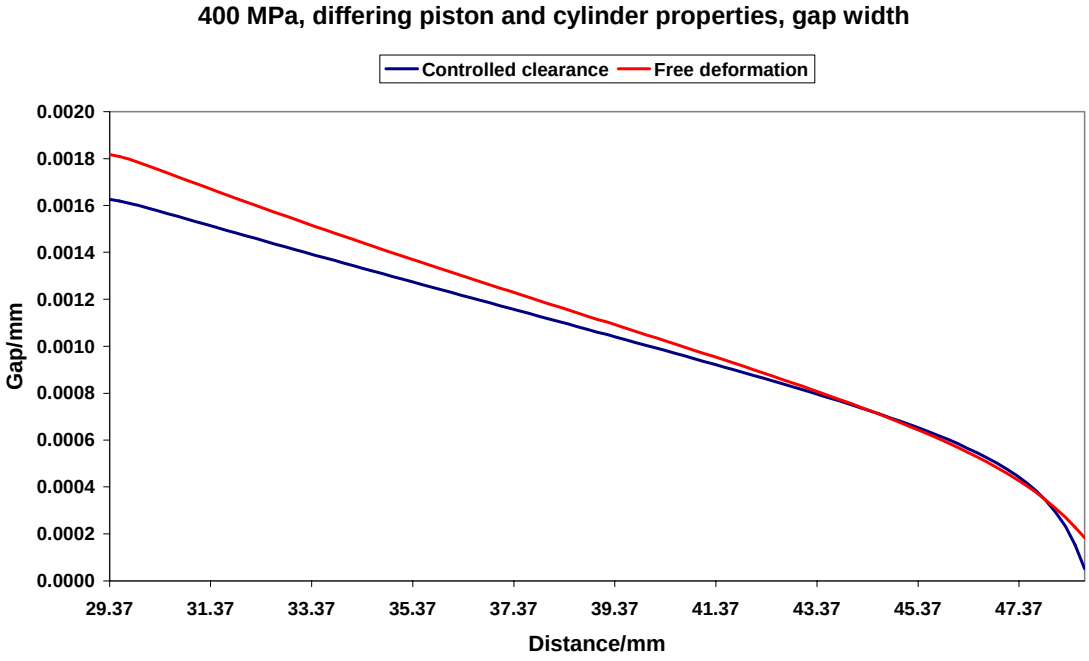

Figure 18: 400 MPa base line model, differing piston and cylinder properties, gap width

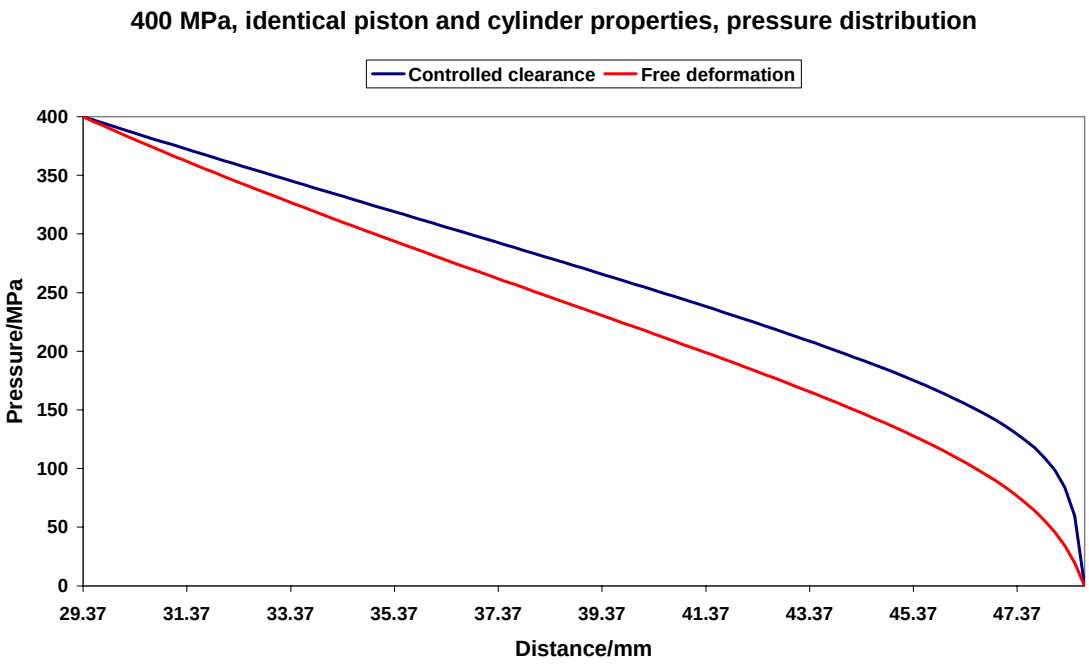

Figure 19: 400 MPa base line model, identical piston and cylinder properties, pressure distribution

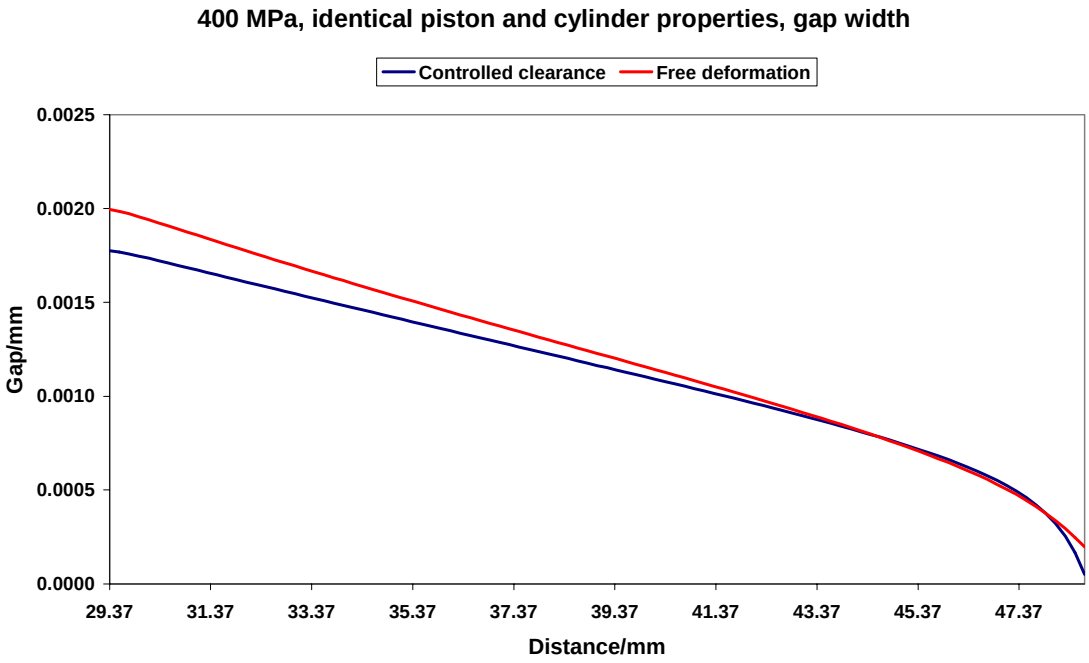

Figure 20: 400 MPa base line model, identical piston and cylinder properties, gap width

Model 2 uncertainties: 400 MPa controlled clearance FEA model, ideally round and straight gap of 0.32 microns

Factor or quantity	Range of variation	Range of output		% range of input	% range of output	
		Lambda/ppm/MPa	Fall rate/mm/min		Lambda	Fall rate
Young's modulus of piston	536 GPa to 550 GPa	0.3630 to 0.3703	0.1613 to 0.1593	± 1.3	± 1.0	± 0.8
Young's modulus of cylinder	620 GPa to 640 GPa	0.3777 to 0.3561	0.1640 to 0.1567	± 1.6	± 3.0	± 2.4
Young's modulus of cylinder sleeve	193 GPa to 207 GPa	0.3654 to 0.3679	0.1598 to 0.1608	± 3.5	± 0.4	± 0.5
Poisson's ratio of piston	0.236 to 0.240	0.3613 to 0.3722	0.1616 to 0.1589	± 0.9	± 1.5	± 1.0
Poisson's ratio of cylinder	0.218 to 0.222	0.3653 to 0.3680	0.1601 to 0.1609	± 1.0	± 0.4	± 0.3
Poisson's ratio of cylinder sleeve	0.27 to 0.31	0.3619 to 0.3714	0.1591 to 0.1619	± 7.0	± 1.3	± 0.9
Gap width	0.29 to 0.35 microns	0.3655 to 0.3679	0.1441 to 0.1786	± 9.4	± 0.4	± 11.3
Pressure variation	100 to 1000 MPa	0.3747 to 0.3596	Not applicable	N/A	± 2.0	N/A
Boundary conditions						
no pressure, line 1-2	N/A	0.3603	0.1588	N/A	-1.7	-1.1
jacket pressure, below point 4	N/A	0.4237	0.1749	N/A	+ 15.6	+ 9.0
jacket pressure, line 3-4	N/A	0.3400	0.1555	N/A	-7.3	-3.2
jacket pressure, lower oil seal	N/A	0.3646	0.1599	N/A	-0.6	-0.4
Pressure-dependent density	Molinar et al 1998	0.3665	0.1638	N/A	-0.03	+ 2.1
FEA mesh density	coarse; aspect	0.3713 to 0.3646	0.1655 to 0.1579	N/A	± 1.4	± 3.0

Table 27: Euromet 463 pressure balance: controlled clearance output variations

Model 2 uncertainties: 400 MPa free deformation FEA model, ideally round and straight gap of 0.32 microns

Factor or quantity	Range of variation	Range of output		% range of input	% range of output	
		Lambda/ppm/MPa	Fall rate/mm/min		Lambda	Fall rate
Young's modulus of piston	536 GPa to 550 GPa	0.7615 to 0.7686	0.3165 to 0.3136	± 1.3	± 0.5	± 0.5
Young's modulus of cylinder	620 GPa to 640 GPa	0.7815 to 0.7491	0.3230 to 0.3075	± 1.6	± 2.1	± 2.4
Young's modulus of cylinder sleeve	193 GPa to 207 GPa	0.7657 to 0.7644	0.3154 to 0.3147	± 3.5	± 0.1	± 0.1
Poisson's ratio of piston	0.236 to 0.240	0.7595 to 0.7706	0.3179 to 0.3122	± 0.9	± 0.8	± 0.9
Poisson's ratio of cylinder	0.218 to 0.222	0.7634 to 0.7667	0.3143 to 0.3158	± 1.0	± 0.3	± 0.3
Poisson's ratio of cylinder sleeve	0.27 to 0.31	0.7649 to 0.7653	0.3149 to 0.3151	± 7.0	± 0.1	± 0.1
Gap width	0.29 to 0.35 microns	0.7649 to 0.7653	0.2847 to 0.3482	± 9.4	± 0.1	± 10.5
Pressure variation	100 to 600 MPa	0.7642 to 0.7659	Not applicable	N/A	± 0.2	N/A
Boundary conditions no pressure, line 1-2	N/A	0.7574	0.3120	N/A	-1.0	-1.1
Pressure-dependent density	Molinar et al 1998	0.7650	0.3188	N/A	+ 0.01	+ 1.2
FEA mesh density	coarse	0.7668	0.3221	N/A	+ 0.2	+ 2.3

Table 28: Euromet 463 pressure balance, free deformation output variations

Model 3 uncertainties: 400 MPa controlled clearance FEA model, ideally round and straight gap of 0.32 microns

Factor or quantity	Range of variation	Range of output		% range of input	% range of output	
		Lambda/ppm/MPa	Fall rate/mm/min		Lambda	Fall rate
Young's modulus of piston	536 GPa to 550 GPa	0.4870 to 0.4944	0.2036 to 0.2009	± 1.3	± 0.8	± 0.7
Young's modulus of cylinder	536 GPa to 550 GPa	0.5015 to 0.4804	0.2060 to 0.1984	± 1.3	± 2.2	± 2.0
Young's modulus of cylinder sleeve	193 GPa to 207 GPa	0.4891 to 0.4924	0.2018 to 0.2025	± 3.5	± 0.3	± 0.3
Poisson's ratio of piston	0.236 to 0.240	0.4853 to 0.4963	0.2040 to 0.2003	± 0.9	± 1.1	± 1.0
Poisson's ratio of cylinder	0.236 to 0.240	0.4892 to 0.4923	0.2017 to 0.2027	± 0.9	± 0.3	± 0.3
Poisson's ratio of cylinder sleeve	0.27 to 0.31	0.4855 to 0.4959	0.2004 to 0.2041	± 7.0	± 1.1	± 1.0
Gap width	0.29 to 0.35 microns	0.4901 to 0.4914	0.1833 to 0.2230	± 9.4	± 0.2	± 10.2
Pressure variation	100 to 1000 MPa	0.4972 to 0.4860	Not applicable	N/A	N/A	± 1.3
Boundary conditions						
no pressure, line 1-2	N/A	0.4839	0.2000	N/A	-1.4	-1.2
jacket pressure, below point 4	N/A	0.5561	0.2203	N/A	+13.3	+ 8.9
jacket pressure, line 3-4	N/A	0.4602	0.1957	N/A	- 6.2	- 3.3
jacket pressure, lower oil seal	N/A	0.4885	0.2014	N/A	- 0.5	- 0.5
Pressure-dependent density	Molinar et al 1998	0.4908	0.2064	N/A	+ 0.02	+ 2.0
FEA mesh density	fine: coarse	0.4876 to 0.4974	0.1991 to 0.2086	N/A	± 1.4	± 3.1

Table 29: Euromet 463 pressure balance: identical piston and cylinder properties, controlled clearance output variations

Model 3 uncertainties: 400 MPa free deformation FEA model, ideally round and straight gap of 0.32 microns

Factor or quantity	Range of variation	Range of output		% range of input	% range of output	
		Lambda/ppm/MPa	Fall rate/mm/min		Lambda	Fall rate
Young's modulus of piston	536 GPa to 550 GPa	0.9411 to 0.9481	0.4108 to 0.4074	± 1.3	± 0.4	± 0.4
Young's modulus of cylinder	536 GPa to 550 GPa	0.9602 to 0.9295	0.4180 to 0.4005	± 1.3	± 1.6	± 2.1
Young's modulus of cylinder sleeve	193 GPa to 207 GPa	0.9455 to 0.9438	0.4096 to 0.4086	± 3.5	± 0.1	± 0.1
Poisson's ratio of piston	0.236 to 0.240	0.9391 to 0.9502	0.4125 to 0.4057	± 0.9	± 0.6	± 0.8
Poisson's ratio of cylinder	0.236 to 0.240	0.9428 to 0.9465	0.4080 to 0.4101	± 0.9	± 0.2	± 0.3
Poisson's ratio of cylinder sleeve	0.27 to 0.31	0.9444 to 0.9449	0.4089 to 0.4093	± 7.0	± 0.03	± 0.05
Gap width	0.29 to 0.35 microns	0.9446 to 0.9448	0.3731 to 0.4482	± 9.4	0	± 8.8
Pressure variation	100 to 600 MPa	0.9434 to 0.9458	Not applicable	N/A	± 0.14	N/A
Boundary conditions no pressure, line 1-2	N/A	0.9362	0.4051	N/A	- 0.9	- 1.0
Pressure-dependent density	Molinar et al 1998	0.9446	0.4142	N/A	- 0.01	+ 1.25
FEA mesh density	coarse	0.9477	0.4183	N/A	+ 0.3	+ 2.25

Table 30: Euromet 463 balance, identical properties for piston and cylinder, free deformation output variations

It is of interest to note the different effects which changes in cylinder materials properties have, when compared with the effects of changes in piston and cylinder sleeve properties, where the base line model predictions, as set out in table 26, are used as the reference from which variations are calculated. In the case in which the piston and cylinder are assumed to have different properties, a variation in Young's modulus of the cylinder by ± 1.6% produces a ± 3% variation in distortion coefficient and a ± 2.4% variation in the fall rate in the controlled clearance case. The equivalent results for the ± 1.6% input change in the free deformation case are ± 2.1% and ± 2.4 % respectively. When a 1.3% variation in Young's modulus is applied to the piston, the controlled clearance outputs are a ± 1.0 % variation in distortion coefficient and a ± 0.8% variation in fall rate. For the free deformation mode, the variations are ± 0.5% for the distortion coefficient and ± 0.5% for the piston fall rate. The model is also less sensitive to changes in the properties of the cylinder sleeve than in either the piston or the cylinder itself. The Young's modulus of the steel comprising the sleeve was varied by ± 3.5 %. The controlled clearance outputs were a ± 0.4% variation in distortion coefficient and a ± 0.5% variation in fall rate. The equivalent figure for the free deformation case were a ± 0.1% variation in distortion coefficient and a ± 0.1% variation in piston fall rate.

When the properties of the piston and cylinder were taken to be identical a similar outcome was observed. In controlled clearance mode a ± 1.3% variation in the Young's modulus of the cylinder leads to variations of ± 2.2% in the distortion coefficient and ± 2.0% variation in piston fall rate. The free deformation mode figures are ± 1.6% and ± 2.1% respectively. When the piston's Young's modulus is varied by ± 1.3% the predicted distortion coefficient varies by ± 0.8% and the piston fall rate by ± 0.7% in controlled clearance mode, and in free deformation mode the distortion coefficient varies by ± 0.4% and the fall rate varies by ± 0.4%. Once again, the cylinder sleeve is seen to have only a minor effect on the results. In controlled clearance mode a ± 3.5% variation in the Young's modulus of the cylinder sleeve leads to variations of ± 0.3% in distortion coefficient and also ± 0.3% in piston fall rate. The comparable free deformation mode variations are ± 0.1% for both the distortion coefficient and the fall rate.

Poisson's ratio variations show an effect opposite to that of Young's modulus variations. Here it is the properties of the piston which have the greatest effect on distortion coefficient and fall rate predictions. For the analyses in which the piston and cylinder were taken as having different properties a ± 0.9% variation in the piston's Poisson's ratio in controlled clearance mode led to predictions of variations of ± 1.5% in the distortion coefficient and ± 1.0% in fall rate. The equivalent outputs for the free deformation case were ± 0.8% for the distortion coefficient and ± 0.9% for the piston fall rate. In controlled clearance mode a ± 1.0% variation in the cylinder's Poisson's ratio produced output variations of ± 0.4% for the distortion coefficient and ± 0.3% for fall rate. The equivalent results for the free deformation case are ± 0.3% for distortion and ± 0.3% for fall rate. Once again, the effects of changes in material properties for the cylinder sleeve were seen to be less important. In the controlled clearance case a ± 7.0% variation in the Poisson's ratio of the cylinder sleeve produces a ± 1.3% variation in distortion coefficient and a ± 0.9% variation in fall rate. In the free deformation case, the comparable results for a ± 7.0% input variation were ± 0.1% for distortion coefficient and also ± 0.1% for piston fall rate.

For the case of identical piston and cylinder properties, it is still the piston's Poisson's ratio which has the dominant effect. In controlled clearance mode varying the piston's Poisson's

ratio by ± 0.9% produces a ± 1.1% variation in distortion coefficient and a ± 1.0% variation in fall rate. The equivalent free deformation outputs are ± 0.6% for distortion and ± 0.8% for fall rate. When the cylinder's Poisson's ratio is varied by ± 0.9%, the distortion coefficient varies by ± 0.3% in controlled clearance mode and ± 0.2% in free deformation mode and the fall rate varies by ± 0.3% in controlled clearance mode and by ± 0.3% in free deformation mode. Varying the cylinder sleeve Poisson's ratio by ± 7.0% produces a variation of distortion coefficient of ± 1.1% in controlled clearance mode and ± 0.03% in free deformation mode. The piston fall rate varies by ± 1.0% in controlled clearance mode and ± 0.05% in free deformation mode.

The effect on the distortion coefficient of varying the gap width by ± 9.4% from the base line model was small. The analysis of the case where the piston and cylinder were regarded as having different properties produces a variation in distortion coefficient of ± 0.4% in the controlled clearance case and ± 0.1% for the free deformation mode. The equivalent results for the identical properties case were ± 0.2% and 0% respectively. The larger gap width, 0.35 μm, as opposed to the base line value of 0.32 μm led naturally to increased piston fall rates varying from an increase of 8.8% for the free deformation mode where the piston and cylinder are treated as having identical properties to 11.3% in the controlled clearance, differing piston and cylinder properties case.

The distortion coefficient predictions are very insensitive to changes in line pressure. In the case of differing piston and cylinder properties a variation of line pressure from 100 MPa to 1 GPa produced a ± 2.0% variation in distortion coefficient in the controlled clearance case, with the higher distortion coefficients being predicted at lower pressure levels. In free deformation mode, the range of pressure variation was from 100 MPa to 600 MPa, and the distortion coefficient predictions varied by ± 0.2%. When the piston and cylinder were regarded as having identical properties, the distortion coefficient predictions in the controlled clearance case varied by ± 1.3% over the range from 100 MPa to 1 GPa and in the free deformation case they varied by ± 0.14% over the pressure range from 100 MPa to 600 MPa.

Exact definition of the boundary conditions, specifically the surfaces over which the jacket pressure is to be applied in the controlled clearance case, is shown to be a significant source of potential variation in the modelling predictions. The following variations to the base line model were investigated: allowing the surface adjacent to the upper oil seal to experience the full jacket pressure (between points 3 and 4 in figure 16), removing the line pressure from the curved surface in the region of point 5 in figure 16), and removing the pressure below point 4 to a level parallel with the top of the engagement length. The greatest effect is produced by removing the jacket pressure below point 4. In the case where the piston and cylinder are treated as having differing material properties, this produces an predicted increase in the distortion coefficient of + 15.6% and a predicted fall rate increase of + 9.0%. For the case in which the piston and cylinder properties are identical, the predicted increase in the distortion coefficient is + 13.3% above the base line model value and the fall rate is predicted to increase by + 8.9%. When the line between points 3 and 4 is regarded as experiencing the full jacket pressure, the distortion coefficient is predicted to decrease by 7.3% for the differing properties case and by 6.2% for the identical properties case. The equivalent decreases in predicted fall rate are 3.2% and 3.3% respectively. Removing the jacket pressure from the region of the lower oil seal has a much smaller effect. In the case in which the piston and cylinder have different properties the change in predicted distortion coefficient is - 0.6% and the predicted fall rate change is - 0.4%. In the analysis of the case in which the two

components are regarded as having identical properties, the predicted distortion coefficient change is - 0.5% and the fall rate change is also - 0.5%. These results emphasise the importance of correct definition of the boundary conditions for controlled clearance balances, especially in that part of the structure close to the top or low pressure end of the engagement length. It may be the case for a real device that the exact nature and extent of the applied pressures in the regions close to seals is not known and this would have consequences both for the modelling and for the comparison of modelling results with experiment. The changes in predicted distortion coefficients arising from plausible variations in controlled clearance boundary conditions far exceed those observed when material properties are varied within reasonable limits.

The final change in boundary conditions which was investigated was to remove the line pressure from the conical part of the lower cylinder structure, that is, the line between points 1 and 2 in figure 16. In the controlled clearance case this reduced the predicted distortion coefficient by 1.7 % for the differing materials case, and by 1.4% in the identical materials case. The equivalent fall rate reductions were -1.1% and -1.2% respectively. The free deformation model produced distortion coefficient reductions of 1.0% and 0.9% for the different and identical properties and cases, with the equivalent fall rate reductions being 1.1% and 1.0%.

The use of a pressure-dependent equation for the density of DHS (Molinar et al, 1998) made only the smallest changes to the predicted distortion coefficient, the largest predicted change being - 0.03% for the controlled clearance case in which the piston and cylinder were taken to have different properties. The largest change in predicted fall rate was + 2.1% for the same case.

Reducing the mesh density from (from 101 nodes to 61 nodes along the engagement length) in the free deformation cases increases the distortion coefficient by at most 0.3% (the identical piston and cylinder properties case) and a finer mesh reduces it by at most 0.6%. A coarser mesh increases the fall rate by 3.1% for the controlled clearance, identical properties case.

The variations in output which have been seen in this model of the PTB 1 GPa piston-cylinder are instructive because this balance has the most complicated structure of the balances modelled for the work reported here. It has the smallest gap width, the highest operating pressure, and is one of only two controlled-clearance balances to be analysed. Thus the output variations which have been observed are likely to represent the extremes which are to be obtained from finite element models of pressure balances. It is also instructive to note that when controlled clearance and free deformation mode outputs are compared, it is the free deformation model which always shows the smaller variation in output for a particular change in input.

7 COMPARISON WITH EXPERIMENT AND UNCERTAINTY BUDGETS

7.1 B2-816, B2-817 and D&H SERIAL NO. 1000: EXPERIMENT

Experimental determination of the effective area, and therefore the distortion coefficient of pressure balances is performed by "cross-floating" one pressure balance against another. If two balances are connected to a common pressure system and are "in equilibrium", then the ratio of the loads applied to the two balances will equal the ratio of the effective areas of the balances. If the effective area of one of the balances is already known, then the effective area of the other can be determined at the pressure at which the measurement is made.

Experimental determinations of the effective area have been carried out at NPL at various times for the balances which have been modelled in this report. Balance B2-817 has been cross-floated against B2-816 and an experimental distortion coefficient of 3.16 ± 0.25 ppm/MPa was measured for B2-817, where the uncertainty is stated at the 95% confidence level and B2-816 was assumed to have an undistorted area of 16.7997 ± 0.0004 mm^2. The distortion coefficient of the B2-817 stainless steel balance was predicted by finite element modelling to be 3.1932 ppm/MPa at the maximum line pressure of 140 MPa for a Young's modulus of 210 GPa and a Poisson's ratio of 0.3. Simple elastic theory predicts a distortion coefficient of 3.0412 for the same materials properties. In the case of this stainless steel balance, relatively small changes in the values of the materials parameters produce substantial changes in distortion coefficient. If the Poisson's ratio is held constant at 0.3, then a Young's modulus of 200 GPa produces a distortion coefficient of 3.3587 ppm/MPa and a value of 220 GPa for Young's modulus leads to a distortion coefficient prediction of 3.0430 ppm/MPa. If Young's modulus is held constant at 210 GPa while Poisson's ratio is varied, a distortion coefficient prediction of 3.1027 ppm/MPa is obtained for a Poisson's ratio of 0.291 and 3.2838 ppm/MPa is obtained from a Poisson's ratio of 0.309. It appears that a 5% change in the value of either materials property leads to a change in predicted distortion coefficient of approximately this value.

Although one can legitimately claim that there is agreement between the finite element predictions and experiment, it is clear that what is really needed is a good quality measurement (i.e. both accurate and precise) of the actual properties of the B2-817 piston and cylinder. In addition, it is important to recognise that whereas the experiment provides a single value for the distortion coefficient by means of a linear fit to data obtained over a range of pressures, the FEA modelling predicts that the distortion coefficient for this balance is pressure dependent, with a value of 3.0550 ppm/MPa at a line pressure of 14 MPa (see table 12), as compared to the value of 3.1932 ppm/MPa at 140 MPa.

The D&H serial no 1000 balance was calibrated three times against B2-816 over a period of three years. Experimentally determined distortion coefficients were 0.98 ± 0.18 ppm/MPa, 0.95 ± 0.18 ppm/MPa and 1.09 ±0.18 ppm/MPa, where uncertainties are again stated at the

95% confidence level. Although these values are all within the ± 0.18 ppm/MPa uncertainty range, the ratio of the highest to the lowest distortion coefficient value is 1.15. The "base line" FEA model employed a Young's modulus for the piston and cylinder of 583 GPa and Poisson's ratio of 0.23 at a line pressure of 100 MPa. This produced a distortion coefficient of 0.871 ppm/MPa. This value lies within the experimental uncertainties of the two lower experimental determinations but outside the error bars of the highest result, which was 1.09 ± 0.18 ppm/MPa. However a reduction in Young's modulus to 523 GPa from the base line value leads to an FEA prediction of the distortion coefficient of 0.968 ppm/MPa. A change in the base line Poisson's ratio from 0.23 to 0.258 produces a distortion coefficient prediction of 0.9646 ppm/MPa. Once again, the results highlight the need for accurate knowledge of the material properties of the piston and cylinder for FEA modelling.

A final experimental comparison can be made from results of calibrations of the B2-816 and B2-817 balances against a third balance, an NPL-manufactured 300 series balance D303-X303, where the D and X codes identify the pistons and cylinders which made up the NPL manufactured balance (the balance was designed to have interchangeable pistons and cylinders). The calibration of the B2-817 pressure balance against D303-X303 produced a distortion coefficient of 3.89 ± 0.47 ppm/MPa and the B2-816 calibration produced a distortion coefficient of 1.47 ± 0.47 ppm/MPa. Although both the predicted distortion coefficients are substantially higher than the values derived from FEA, and the experimentally determined value for B2-817 is higher than the results obtained in the calibration against B2-816 (3.16 ± 0.25 ppm/MPa), the difference between the two experimental values is in close agreement with FEA prediction. For the calibration against D303-X303 the distortion coefficient difference between B2-817 and B2-816 is 2.42 ppm/MPa (3.89 ppm/MPa - 1.47 ppm/MPa). The difference between the FEA predictions at the base line values and 140 MPa line pressure is 2.32 ppm/MPa (3.16 ppm/MPa - 0.84 ppm/MPa).

7.2 THE EUROMET 463 PROJECT BALANCE: EXPERIMENT

The PTB made available to participants in the Euromet 463 project the results of its own experiments on the D&H 7594 1 GPa pressure balance which was modelled in this study. It provided on the measured fall rate as a function of pressure for both controlled clearance and free deformation mode. Figures 21 and 22 set out the experimental results for both modes and comparisons with NPL's FEA predictions for both cases which were modelled, that is, the piston and cylinder with different material properties and with identical properties.

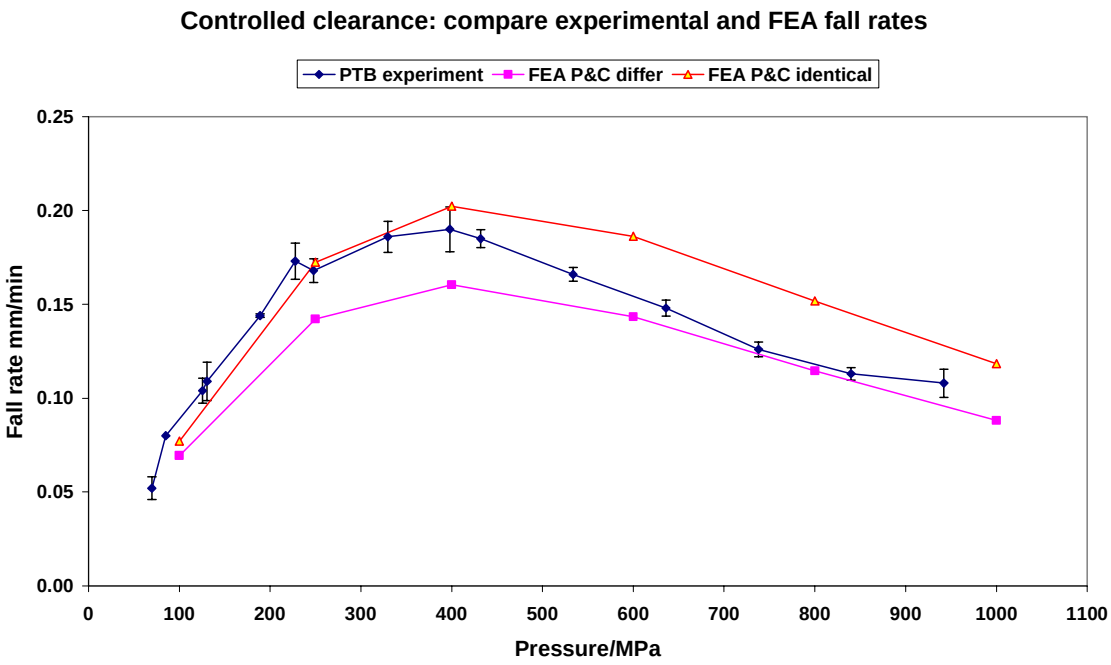

Figure 21: Euromet 463 project, compare PTB experimental controlled clearance fall rates with FEA predictions for differing and identical piston and cylinder properties

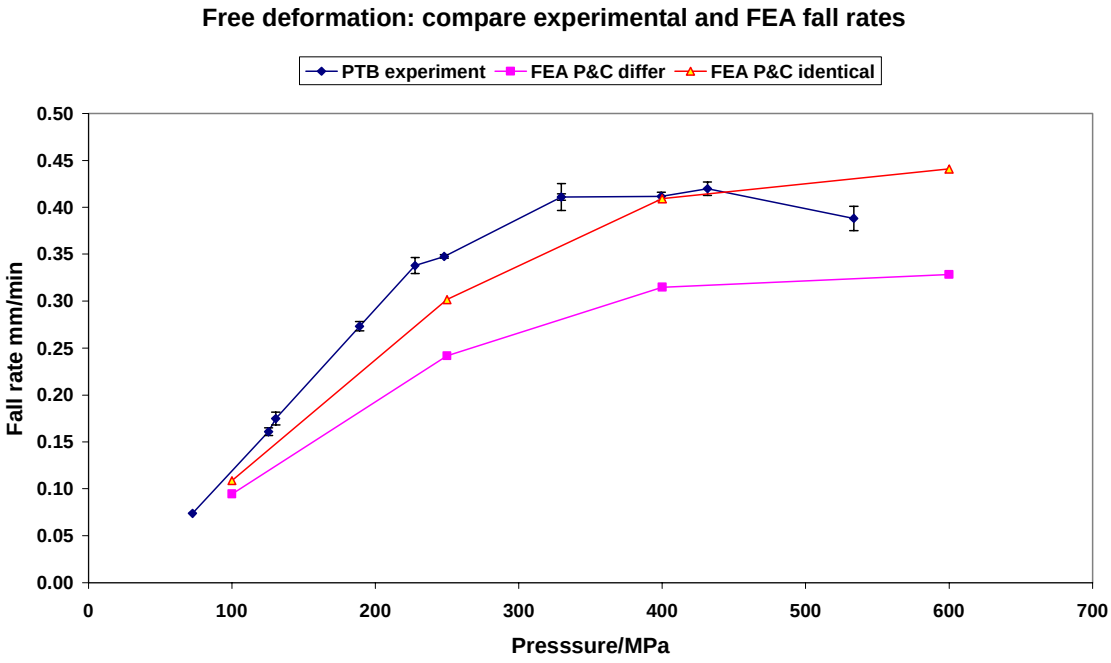

Figure 22: Euromet 463 project, compare PTB experiment free deformation fall rates with FEA predictions for differing and identical piston and cylinder properties

The uncertainties on the experimental data are one standard deviation of a series of repeat measurements. In the case of the controlled clearance results, above 250 MPa the experimental fall rates lie between the FEA predictions for the cases of differing and identical piston and cylinder properties. For the free deformation case, the experimental results are consistently higher than both FEA predictions at all pressures below 400 MPa.

It is of interest to note that the PTB made a series of fall rate measurements at low line pressures and, using the following equation, predicted the gap width to be 0.34 μm:

$$h = \left(\frac{6\eta r v l}{p} \right)^{1/3} \qquad (9)$$

where h is the gap width, η is viscosity, r is piston radius, v is fall rate, l is gap length and p is pressure, and it is assumed that the gap is constant and unaffected by distortion. The gap width which was employed in the FEA modelling was 0.32 μm. During the investigation of the sensitivity of the output of the FEA model to input variations it was observed that a 9.4% variation in gap width could lead to variations in fall rate ranging from ± 8.8 % to ± 11.3% depending on mode of operation of the balance and whether the piston and cylinder materials were considered to be different or identical.

The PTB also calibrated the D&H 7594 balance against two other pressure balances, a Ruska 400 MPa balance and a D&H 10 1 GPa balance. Both these balances are employed as reference standards within the PTB's pressure laboratories. The experimentally determined distortion coefficient of the D&H 7594 1 GPa balance in controlled clearance mode was 0.437 ± 0.012 ppm/MPa from the Ruska balance and 0.457 ± 0.023 pm/MPa for the D&H 10 balance, where the quoted uncertainties are type A standard uncertainties only. In addition, the D&H 7594 was calibrated against the Ruska balance in free deformation mode and this produced a distortion coefficient of 0.776 ± 0.011 ppm/MPa where the uncertainty once again takes into account only type A contributions.

The NPL FEA results for the base line models for the two cases of differing and identical piston and cylinder properties were set out in table 26. The FEA model predicted a controlled clearance distortion coefficient of 0.3666 ppm/MPa for the case in which the piston and cylinder differ in their properties and 0.4907 ppm/MPa when they have identical properties. In free deformation mode the FEA predictions were 0.7651 ppm/MPa for the case in which the piston and cylinder are assumed to have different properties and 0.9447 ppm/MPa for the identical properties case. In this mode closer agreement with experiment is achieved for the case of differing properties, but in controlled clearance mode the identical properties case produces closer agreement between FEA and experiment, although the agreement is not as good as in the free deformation, differing properties case. It was these observations which led the PTB to propose it might be the differing properties case which provided a truer representation of the pressure balance than the assumption that the properties of the piston and cylinder were identical, but that it also would be necessary to take into account the real shape of the piston and cylinder. However, to reconcile the FEA predictions with experiment, the influence of the real piston and cylinder profile data would have to be different in free deformation mode from controlled clearance mode. In free deformation mode, the effect would have to be small to maintain the agreement between FEA and experiment, but a large effect would be needed in controlled clearance mode.

It is also worth noting that the FEA modelling takes into account only the measured properties of the piston. The properties of the cylinder have not been measured but are taken to be those supplied by the manufacturer, who is not able to guarantee that the values in question apply to the actual balance being modelled. In addition, the Young's modulus and Poisson's ratio of the steel cylinder sleeve were not measured but assumed to be in agreement with book values of these properties. As we have seen, the FEA predictions show that the properties of the sleeve have minimal effect on the predicted distortion coefficient, so that exact knowledge of the sleeve properties is probably less important than accurate knowledge of piston and cylinder properties. However, the FEA modelling also demonstrated the importance of exact knowledge of the boundary conditions which define the extent of the surface over which the jacket pressure is applied in the controlled clearance case. It is difficult to envisage an experimental determination of the pressure loading which is applied to the cylinder sleeve. At present it is not possible to conclude that the FEA model truly reflects the manner in which the jacket pressure is applied.

7.3 UNCERTAINTY BUDGET: EUROMET PROJECT 463 BALANCE

Section 6.4 of this report summarised the effect on the predicted distortion coefficients and fall rates of varying the inputs to the Euromet 463 project FEA model. In this section of the report those results are presented as uncertainty budgets arising from the mathematical modelling process itself. The method adopted was to calculate semi-range values for each source of uncertainty identified in the tables in section 6.4 by taking the extremes of the ranges from those tables and dividing by two. The resulting semi-range values were regarded as possessing a rectangular distribution in every case. In cases such as materials properties, the gap width, pressure variations and mesh density, this process is straightforward.

The modelling uncertainty budgets for the Euromet project no 463 balance are set out below in tables 31 to 38. For the boundary condition variations, the range was calculated by noting the largest positive and negative changes to the distortion coefficient and fall rate predictions obtained for various alterations to the boundary conditions and treating these as the extremes of the observed ranges. In the case of the controlled clearance predictions, there were four variations in the boundary conditions which were analysed, so that it was simple to determine the largest positive and negative variations from the base line model and to divide this range by two to give the semi-range value required In the free deformation case only one variation in boundary conditions was investigated. The variation from the base line prediction in this case was taken as representing the semi-range value to be used in the uncertainty calculation.

For the investigation of the effect of variations in fluid properties, two cases were analysed. The first of these was to replace the pressure-independent density with the pressure-dependent density equation from Molinar et al (1998). The difference between the distortion coefficient and fall rate predictions in this case and those of the base line model was treated as the semi-range variation for the calculation of standard uncertainty, with a rectangular distribution once again assumed, although in reality only one variation from the base line case was calculated. To investigate variations arising from changes in pressure-dependent viscosity small changes were made to the exponent in equation 5. The predictions were re-run with

exponents of 8.80 and 8.82. This equation was obtained from a fit to empirical data and it seemed preferable to vary the exponents, rather than the constants in the equation. Varying the exponents ensures that the shape of the curve changes throughout the pressure range of interest, and so is a reasonable test of the effect of viscosity variations at all pressures. The base line value of the exponent was 8.81 and it was thus straightforward to obtain semi-range values from the difference between the predictions obtained for the 8.80 and 8.82 values.

The effect of FEA mesh density variations was investigated by varying the number of nodes defined along the engagement length of the piston-cylinder combination. The base line model contained 101 nodes along this length, and the effect of using 61 nodes and 141 nodes was also investigated. Increasing the number of nodes along the engagement length also leads to a denser mesh in the remaining structure of the balance, and thus to greatly increased run times. Ideally, it would have been preferable to run the model with as dense a mesh as possible. However, as the model has to be run many times to produce the output needed for the Euromet 463 project, it is impractical to use the densest meshes. A compromise has to be achieved and it is for this reason it is useful to specific an additional source of modelling uncertainty arising from mesh density variations.

The standard uncertainties for each source of modelling uncertainty were summed in quadrature and the expanded uncertainty obtained by taking a k value of 2. Separate uncertainty calculations were varied out for the controlled clearance and free deformation modes for both basic models (one assuming that the properties of the piston and cylinder differ and the other assuming they are identical). It is important to note that the standard uncertainties predicted for the controlled clearance cases are substantially larger than those for the free deformation case. This is because variations in the boundary conditions related to the application of the jacket pressure in the controlled clearance mode are the major contributor to the uncertainty budget.

Apart from the uncertainty contribution from the mesh density term, every other contribution to the uncertainty budget arises from a limitation on the information which is known about the pressure balance. If material properties or boundary conditions could be defined more precisely, then the predicted uncertainties would be reduced. Conversely, the less that is known about the true properties of a balance, the larger the uncertainties on the predicted distortion coefficient and fall rate become. To gain the most benefit from finite element modelling, especially when its results are to be used in calibration certificates and in calculations of calibration uncertainties, then substantial experimental work is needed to obtain the most precise quantification possible of materials properties and boundary conditions. Note, also, that even if inputs to the model can be precisely defined, the predicted uncertainties for controlled clearance mode will always exceed those of the free deformation mode of operation.

Euromet 463 project: D&H 7594 balance in controlled clearance mode, differing piston and cylinder properties					
Source of uncertainty	**Uncertainty or range of quantity**	**Value ± ppm/MPa**	**Probability distribution**	**Divisor**	**Standard uncertainty ±ppm/MPa**
Piston: Young's modulus	536 GPa to 550 GPa	0.0037	Rectangular	√3	0.0021
Piston: Poisson's ratio	0.236 to 0.240	0.0055	Rectangular	√3	0.0031
Cylinder: Young's modulus	620 GPa to 640 GPa	0.0108	Rectangular	√3	0.0062
Cylinder: Poisson's ratio	0.218 to 0.222	0.0014	Rectangular	√3	0.0008
Sleeve: Young's modulus	193 to 207 GPa	0.0013	Rectangular	√3	0.0007
Sleeve: Poisson's ratio	0.27 to 0.31	0.0048	Rectangular	√3	0.0027
Gap width	0.29 to 0.35 microns	0.0012	Rectangular	√3	0.0007
Pressure variation	100 MPa to 1000 MPa	0.0076	Rectangular	√3	0.0044
Boundary conditions		0.0419	Rectangular	√3	0.0242
Pressure-dependent density		0.0001	Rectangular	√3	0.0001
Oil viscosity variations	expt 8.80 to 8.82	0.0000	Rectangular	√3	0.0000
FE mesh density	61 to 141 nodes along engagement length	0.0034	Rectangular	√3	0.0019
Combined standard uncertainty			Normal assumed		0.0259
Expanded uncertainty			k=2		0.0517
Controlled clearance distortion coefficient = 0.3666 ± 0.0517 ppm/MPa					

Table 31: Controlled clearance mode, differing piston and cylinder properties, distortion coefficient expanded uncertainty

Euromet 463 project: D&H 7594 balance in controlled clearance mode, differing piston and cylinder properties					
Source of uncertainty	**Uncertainty or range of quantity**	**Value ± mm/min**	**Probability distribution**	**Divisor**	**Standard uncertainty ±mm/min**
Piston: Young's modulus	536 GPa to 550 GPa	0.0010	Rectangular	√3	0.0006
Piston: Poisson's ratio	0.236 to 0.240	0.0014	Rectangular	√3	0.0008
Cylinder: Young's modulus	620 GPa to 640 GPa	0.0037	Rectangular	√3	0.0021
Cylinder: Poisson's ratio	0.218 to 0.222	0.0004	Rectangular	√3	0.0002
Sleeve: Young's modulus	193 to 207 GPa	0.0005	Rectangular	√3	0.0003
Sleeve: Poisson's ratio	0.27 to 0.31	0.0014	Rectangular	√3	0.0008
Gap width	0.29 to 0.35 microns	0.0173	Rectangular	√3	0.0100
Pressure variation	not applicable	-	Rectangular	√3	
Boundary conditions		0.0097	Rectangular	√3	0.0056
Pressure-dependent density		0.0033	Rectangular	√3	0.0019
Oil viscosity variations	expt 8.80 to 8.82	0.0006	Rectangular	√3	0.0003
FE mesh density	61 to 141 nodes along engagement length	0.0038	Rectangular	√3	0.0022
Combined standard uncertainty			Normal assumed		0.0121
Expanded uncertainty			k=2		0.0241
Controlled clearance fall rate = 0.1605 ± 0.0241 mm/min					

Table 32: Controlled clearance mode, differing piston and cylinder properties, fall rate expanded uncertainty

Euromet 463 project: D&H 7594 balance in free deformation mode, differing piston and cylinder properties					
Source of uncertainty	**Uncertainty or range of quantity**	**Value ± ppm/MPa**	**Probability distribution**	**Divisor**	**Standard uncertainty ±ppm/MPa**
Piston: Young's modulus	536 GPa to 550 GPa	0.0036	Rectangular	√3	0.0020
Piston: Poisson's ratio	0.236 to 0.240	0.0056	Rectangular	√3	0.0032
Cylinder: Young's modulus	620 GPa to 640 GPa	0.0162	Rectangular	√3	0.0094
Cylinder: Poisson's ratio	0.218 to 0.222	0.0017	Rectangular	√3	0.0010
Sleeve: Young's modulus	193 to 207 GPa	0.0007	Rectangular	√3	0.0004
Sleeve: Poisson's ratio	0.27 to 0.31	0.0002	Rectangular	√3	0.0001
Gap width	0.29 to 0.35 microns	0.0002	Rectangular	√3	0.0001
Pressure variation	100 MPa to 1000 MPa	0.0009	Rectangular	√3	0.0005
Boundary conditions		0.0077	Rectangular	√3	0.0044
Pressure-dependent density		0.0001	Rectangular	√3	0.0001
Oil viscosity variations	expt 8.80 to 8.82	0.00005	Rectangular	√3	0.00003
FE mesh density	61 to 141 nodes along engagement length	0.0017	Rectangular	√3	0.0010
Combined standard uncertainty			Normal assumed		0.0111
Expanded uncertainty			k=2		0.0223
Free deformation distortion coefficient = 0.7651 ± 0.0223 ppm/MPa					

Table 33**: **Free deformation mode, differing piston and cylinder properties, distortion coefficient expanded uncertainty

Euromet 463 project: D&H 7594 balance in free deformation mode, differing piston and cylinder properties					
Source of uncertainty	**Uncertainty or range of quantity**	**Value ± mm/min**	**Probability distribution**	**Divisor**	**Standard uncertainty ±mm/min**
Piston: Young's modulus	536 GPa to 550 GPa	0.0015	Rectangular	√3	0.0008
Piston: Poisson's ratio	0.236 to 0.240	0.0029	Rectangular	√3	0.0016
Cylinder: Young's modulus	620 GPa to 640 GPa	0.0078	Rectangular	√3	0.0045
Cylinder: Poisson's ratio	0.218 to 0.222	0.0008	Rectangular	√3	0.0004
Sleeve: Young's modulus	193 to 207 GPa	0.0004	Rectangular	√3	0.0002
Sleeve: Poisson's ratio	0.27 to 0.31	0.0001	Rectangular	√3	0.0001
Gap width	0.29 to 0.35 microns	0.0318	Rectangular	√3	0.0183
Pressure variation	not applicable	-	Rectangular	√3	
Boundary conditions		0.0030	Rectangular	√3	0.0017
Pressure-dependent density		0.0038	Rectangular	√3	0.0022
Oil viscosity variations	expt 8.80 to 8.82	0.0012	Rectangular	√3	0.0007
FE mesh density	61 to 141 nodes along engagement length	0.0071	Rectangular	√3	0.0041
Combined standard uncertainty			Normal assumed		0.0196
Expanded uncertainty			k=2		0.0392
Free deformation fall rate = 0.3150 ± 0.0392 mm/min					

Table 34: Free deformation mode, differing piston and cylinder properties, fall rate expanded uncertainty

Euromet 463 project: D&H 7594 balance in controlled clearance mode, identical piston and cylinder properties					
Source of uncertainty	**Uncertainty or range of quantity**	**Value ± ppm/MPa**	**Probability distribution**	**Divisor**	**Standard uncertainty ±ppm/MPa**
Piston: Young's modulus	536 GPa to 550 GPa	0.0037	Rectangular	√3	0.0021
Piston: Poisson's ratio	0.236 to 0.240	0.0055	Rectangular	√3	0.0032
Cylinder: Young's modulus	536 GPa to 550 GPa	0.0106	Rectangular	√3	0.0061
Cylinder: Poisson's ratio	0.236 to 0.240	0.0016	Rectangular	√3	0.0009
Sleeve: Young's modulus	193 to 207 GPa	0.0017	Rectangular	√3	0.0010
Sleeve: Poisson's ratio	0.27 to 0.31	0.0052	Rectangular	√3	0.0030
Gap width	0.29 to 0.35 microns	0.0007	Rectangular	√3	0.0004
Pressure variation	100 MPa to 1000 MPa	0.0056	Rectangular	√3	0.0032
Boundary conditions		0.0480	Rectangular	√3	0.0277
Pressure-dependent density		0.0001	Rectangular	√3	0.0001
Oil viscosity variations	expt 8.80 to 8.82	0.00005	Rectangular	√3	0.00003
FE mesh density	61 to 141 nodes along engagement length	0.0049	Rectangular	√3	0.0028
Combined standard uncertainty			Normal assumed		0.0291
Expanded uncertainty			k=2		0.0582
Controlled clearance distortion coefficient = 0.4907 ± 0.0582 ppm/MPa					

Table 35: Controlled clearance mode, identical piston and cylinder properties, distortion coefficient expanded uncertainty

Euromet 463 project: D&H 7594 balance in controlled clearance mode, identical piston and cylinder properties					
Source of uncertainty	**Uncertainty or range of quantity**	**Value ± mm/min**	**Probability distribution**	**Divisor**	**Standard uncertainty ±mm/min**
Piston: Young's modulus	536 GPa to 550 GPa	0.0014	Rectangular	√3	0.0008
Piston: Poisson's ratio	0.236 to 0.240	0.0019	Rectangular	√3	0.0011
Cylinder: Young's modulus	536 GPa to 550 GPa	0.0038	Rectangular	√3	0.0022
Cylinder: Poisson's ratio	0.236 to 0.240	0.0005	Rectangular	√3	0.0003
Sleeve: Young's modulus	193 to 207 GPa	0.0004	Rectangular	√3	0.0002
Sleeve: Poisson's ratio	0.27 to 0.31	0.0019	Rectangular	√3	0.0011
Gap width	0.29 to 0.35 microns	0.0199	Rectangular	√3	0.0115
Pressure variation	not applicable		Rectangular	√3	
Boundary conditions		0.0123	Rectangular	√3	0.0071
Pressure-dependent density		0.0041	Rectangular	√3	0.0024
Oil viscosity variations	expt 8.80 to 8.82	0.0009	Rectangular	√3	0.0005
FE mesh density	61 to 141 nodes along engagement length	0.0095	Rectangular	√3	0.0055
Combined standard uncertainty			Normal assumed		0.0150
Expanded uncertainty			k=2		0.0300
Controlled clearance fall rate = 0.2023 ± 0.0300 mm/min					

Table 36: Controlled clearance mode, identical piston and cylinder properties, fall rate expanded uncertainty

Euromet 463 project: D&H 7594 balance in free deformation mode, identical piston and cylinder properties					
Source of uncertainty	**Uncertainty or range of quantity**	**Value ± ppm/MPa**	**Probability distribution**	**Divisor**	**Standard uncertainty ±ppm/MPa**
Piston: Young's modulus	536 GPa to 550 GPa	0.0035	Rectangular	√3	0.0020
Piston: Poisson's ratio	0.236 to 0.240	0.0056	Rectangular	√3	0.0032
Cylinder: Young's modulus	536 GPa to 550 GPa	0.0154	Rectangular	√3	0.0089
Cylinder: Poisson's ratio	0.236 to 0.240	0.0019	Rectangular	√3	0.0011
Sleeve: Young's modulus	193 to 207 GPa	0.0009	Rectangular	√3	0.0005
Sleeve: Poisson's ratio	0.27 to 0.31	0.0003	Rectangular	√3	0.0001
Gap width	0.29 to 0.35 microns	0.0001	Rectangular	√3	0.0001
Pressure variation	100 MPa to 1000 MPa		Rectangular	√3	0.0000
Boundary conditions		0.0020	Rectangular	√3	0.0012
Pressure-dependent density		0.0001	Rectangular	√3	0.0001
Oil viscosity variations	expt 8.80 to 8.82	0.00001	Rectangular	√3	0.00001
FE mesh density	61 to 141 nodes along engagement length	0.0030	Rectangular	√3	0.0017
Combined standard uncertainty			Normal assumed		0.0099
Expanded uncertainty			k=2		0.0199
Free deformation distortion coefficient = 0.9447 ± 0.0199 ppm/MPa					

Table 37: Free deformation mode, identical piston and cylinder properties, distortion coefficient expanded uncertainty

Euromet 463 project: D&H 7594 balance in free deformation mode, identical piston and cylinder properties					
Source of uncertainty	**Uncertainty or range of quantity**	**Value ± mm/min**	**Probability distribution**	**Divisor**	**Standard uncertainty ±mm/min**
Piston: Young's modulus	536 GPa to 550 GPa	0.0017	Rectangular	√3	0.0010
Piston: Poisson's ratio	0.236 to 0.240	0.0034	Rectangular	√3	0.0020
Cylinder: Young's modulus	536 GPa to 550 GPa	0.0088	Rectangular	√3	0.0051
Cylinder: Poisson's ratio	0.236 to 0.240	0.0011	Rectangular	√3	0.0006
Sleeve: Young's modulus	193 to 207 GPa	0.0005	Rectangular	√3	0.0003
Sleeve: Poisson's ratio	0.27 to 0.31	0.0002	Rectangular	√3	0.0001
Gap width	0.29 to 0.35 microns	0.0376	Rectangular	√3	0.0217
Pressure variation	not applicable	-	Rectangular	√3	
Boundary conditions		0.0040	Rectangular	√3	0.0023
Pressure-dependent density		0.0051	Rectangular	√3	0.0029
Oil viscosity variations	expt 8.80 to 8.82	0.0015	Rectangular	√3	0.0009
FE mesh density	61 to 141 nodes along engagement length	0.0092	Rectangular	√3	0.0053
Combined standard uncertainty			Normal assumed		0.0233
Expanded uncertainty			k=2		0.0466
Free deformation fall rate = 0.4091 ± 0.0466 mm/min					

Table 38: Free deformation mode, identical piston and cylinder properties, fall rate expanded uncertainty

7.4 UNCERTAINTY BUDGETS: NPL PRESSURE BALANCES

Uncertainty budgets were prepared for the three NPL pressure balances which have been analysed in this report in the same manner as was adopted for the Euromet project 463 balance, including the assumption of rectangular distributions for each source of uncertainty. All these balances operated in free deformation mode only and at lower pressures (maxima of 100 MPa to 140 MPa) compared with the 1 GPa balance modelled for the Euromet project. In addition, the full structure of the balances was not modelled, unlike the approach adopted for the Euromet project. As a result there are fewer parameters which can be varied. In the case of the NPL balances investigations have been carried out of the effects of changes in materials properties, gap width, applied line pressure and mesh density. Values for the effects of changes in fluid property (viscosity and density) have been taken as being identical to those observed for the Euromet balance. In addition, there is little scope in the models of the NPL balances for varying boundary conditions. In any case, as was shown by the Euromet project work, boundary condition effects are small for free deformation mode operation.

A more serious limitation of the models of NPL-owned balances is the lack of information concerning materials properties. This means that it is not possible to be as precise about Young's modulus and Poisson's ratio as it was for the Euromet balance. Relatively wide ranges for materials properties variations have been used in producing the uncertainty budgets, leading to modelling uncertainties on the distortion coefficient predictions of the order of 10% or greater. If more precise information becomes available in the future, it will be possible to re-work the uncertainty budgets using the results set out in chapter 6 of this report. Presented here are the results for distortion coefficient uncertainties only, as these are of directly relevance to the calibration process. Fall rate data have not been systematically recorded for the balances in question, so there is little benefit in providing uncertainty data for fall rate predictions.

Tables 39 to 41 set out the predicted distortion coefficient uncertainties for the NPL balances B2-816, B2-817 and D&H serial no 1000. Note the similarity of the results for the two tungsten carbide balances. In both cases the materials properties have been varied over the same ranges for the piston and cylinder and uncertainty contributions from sources other than materials property variations are negligible for both balances. The B2-816 balance distortion coefficient prediction is 0.8575 ± 0.0956 ppm/MPa and for the D&H serial no 1000 balance it is 0.8683 ± 0.0961 ppm/MPa. In both cases the uncertainty is ± 11% on the base line value. It appears in both cases that more precise values for the piston's Poisson's ratio and the cylinder's Young's modulus are the key to reducing the predicted uncertainties.

In the case of the B2-817 stainless steel balance, the piston's Poisson's ratio and the cylinder's Young's modulus are also the largest contributors to the uncertainty budget. What is also of interest in the stainless steel case is the relatively large effect that varying the gap width has compared with the tungsten carbide balances. However, the initial gap width for this balance is in any case smaller, 0.43 μm, whereas the tungsten carbide balances have initial gaps of 1 μm. Pressure variations also have a much greater effect on the predictions for this balance than for the tungsten carbide balances. For the tungsten carbide balances this effect was negligible but for the stainless steel balances varying the pressure from 14 MPa to 140 MPa has an effect on the predicted distortion coefficient comparable to that predicted for the

cylinder's Poisson's ratio variations. The results of this greater sensitivity to a wider range of inputs is that the uncertainty on the predicted distortion coefficient is more than ± 14% of the base line value.

The most important conclusion which can be drawn from this analysis of the NPL balances is that it is essential that the properties of the materials of which pressure balances are constructed are known as precisely as possible if it is intended that the results of finite element analysis are to be used in defining distortion-related terms in calibration results and on calibration certificates. The more precisely the properties are known the smaller the uncertainty on the distortion coefficient prediction.

B2-816 tungsten carbide balance: free deformation					
Source of uncertainty	**Uncertainty or range of quantity**	**Value ± ppm/MPa**	**Probability distribution**	**Divisor**	**Standard uncertainty ±ppm/MPa**
Piston: Young's modulus	553 GPa to 613 GPa	0.0139	Rectangular	√3	0.0080
Piston: Poisson's ratio	0.209 to 0.251	0.0541	Rectangular	√3	0.0312
Cylinder: Young's modulus	553 GPa to 613 GPa	0.0583	Rectangular	√3	0.0337
Cylinder: Poisson's ratio	0.209 to 0.251	0.0182	Rectangular	√3	0.0105
Gap width	0.95 to 1.05 microns	0.000050	Rectangular	√3	0.000029
Pressure variation	14 MPa to 140 MPa	0.00010	Rectangular	√3	0.00006
Pressure-dependent density	from Euromet 463 model	0.0001	Rectangular	√3	0.0001
Oil viscosity variations	from Euromet 463 model	0.00005	Rectangular	√3	0.00003
FE mesh density	145 to 271 nodes along engagement length	0.0004	Rectangular	√3	0.0002
Combined standard uncertainty			Normal assumed		0.0478
Expanded uncertainty			k=2		0.0956
Distortion coefficient = 0.8575 ± 0.0956 ppm/MPa					

Table 39: B2-816 pressure balance: distortion coefficient uncertainty from finite element analysis

B2-817 stainless steel balance: free deformation					
Source of uncertainty	**Uncertainty or range of quantity**	**Value ± ppm/MPa**	**Probability distribution**	**Divisor**	**Standard uncertainty ±ppm/MPa**
Piston: Young's modulus	190 GPa to 230 GPa	0.0111	Rectangular	√3	0.0064
Piston: Poisson's ratio	0.273 to 0.327	0.2035	Rectangular	√3	0.1175
Cylinder: Young's modulus	190 GPa to 230 GPa	0.3288	Rectangular	√3	0.1898
Cylinder: Poisson's ratio	0.273 to 0.327	0.0681	Rectangular	√3	0.0393
Gap width	0.38 to 0.48 microns	0.013100	Rectangular	√3	0.007563
Pressure variation	14 MPa to 140 MPa	0.06910	Rectangular	√3	0.03989
Pressure-dependent density	from Euromet 463 model	0.0001	Rectangular	√3	0.0001
Oil viscosity variations	from Euromet 463 model	0.00005	Rectangular	√3	0.00003
FE mesh density	145 to 271 nodes along engagement length	0.0002	Rectangular	√3	0.0001
Combined standard uncertainty			Normal assumed		0.2304
Expanded uncertainty			k=2		0.4608
Distortion coefficient = 3.1932 ± 0.4608 ppm/MPa					

Table 40: ***B2-817 pressure balance: distortion coefficient uncertainty from finite element analysis***

D&H serial no 1000 tungsten carbide balance: free deformation					
Source of uncertainty	**Uncertainty or range of quantity**	**Value ± ppm/MPa**	**Probability distribution**	**Divisor**	**Standard uncertainty ±ppm/MPa**
Piston: Young's modulus	553 GPa to 613 GPa	0.0141	Rectangular	√3	0.0081
Piston: Poisson's ratio	0.209 to 0.251	0.0541	Rectangular	√3	0.0312
Cylinder: Young's modulus	553 GPa to 613 GPa	0.0589	Rectangular	√3	0.0340
Cylinder: Poisson's ratio	0.209 to 0.251	0.0182	Rectangular	√3	0.0105
Gap width	0.95 to 1.05 microns	0.000005	Rectangular	√3	0.000003
Pressure variation	10 MPa to 100 MPa	0.00005	Rectangular	√3	0.00003
Pressure-dependent density	from Euromet 463 model	0.0001	Rectangular	√3	0.0001
Oil viscosity variations	from Euromet 463 model	0.00005	Rectangular	√3	0.00003
FE mesh density	137 to 271 nodes along engagement length	0.0002	Rectangular	√3	0.0001
Combined standard uncertainty			Normal assumed		0.0480
Expanded uncertainty			k=2		0.0961
Distortion coefficient = 0.8683 ± 0.0961 ppm/MPa					

Table 41**: **B2-817 pressure balance: distortion coefficient uncertainty from finite element analysis

8 FEASIBILITY OF THREE-DIMENSIONAL MODELLING

8.1 INTRODUCTION

All the work described in this report, and indeed all finite element modelling of pressure balances that has been reported in the scientific literature to date, has assumed that balances are axisymmetric. Such an approach can be regarded as representing three-dimensional behaviour for the case in which there are no geometrical variations with angle about the axis of symmetry of the FEA model. If such variations exist, then true three-dimensional modelling is required. In addition, pressure balance modelling ignores the fact that the piston and cylinder rotate with respect to each other.

It is not only the structure of the pressure balance which is simplified by the axisymmetric assumption. As a consequence of this approach, fluid flow along the gap is treated as a one-dimensional problem, with pressure being dependent only on one co-ordinate, the distance along the engagement length. Pressure is assumed not to vary radially across the gap, and any effects which might be due to rotation of the balance are ignored. It is important to appreciate that the FEA model is being used simply to provide the parameters which are needed to evaluate equation 4 - the pressure distribution as a function of position along the engagement length, and the changes in radius of the piston and cylinder along the engagement length, based on the assumptions outlined above. In addition, this approach implicitly accepts all the simplifications and idealisations which lie behind equation 4 itself.

Given the observation set out above, it is clear that an attempt to take into account the real shapes of pistons and cylinders and their rotational behaviour would require current approaches to modelling, both those theories set out in Dadson, Lewis and Peggs (1982) and finite element methods themselves to be re-worked from first principles. In reality, it is perhaps more productive to try to define the range of piston and cylinder geometries, pressure ranges and boundary conditions over which the current methodologies can be regarded as adequate representations of the real behaviour of pressure balances and to restrict their application to this limited range of cases.

8.2 DEFINING THE UNDISTORTED AREA

The question of the definition of the undistorted area of a pressure balance prior to loading is one which has to be resolved for the transition from axisymmetric modelling to full three-dimensional modelling. Although limited attempts have been made (Dadson et al, 1982, Buonanno et al, 1999**)** to consider conically shaped or tilted piston and cylinders, it has almost always been the case that mathematical modelling begins with the assumption of ideally round and straight piston and cylinders to which exact values of the component radius can be assigned. Even when detailed dimensioning of piston and cylinders has been carried out it is still the practice to reduce the results of such work to a single value of radius with an associated measurement uncertainty.

Equation 4, which is used to calculated the distorted effective area requires one to assign a single value for the undistorted radius and the undistorted gap width, r_O and h_O. Thus, even if one has full three-dimensional geometry data for a piston and cylinder, the use of this

equation builds the assumption of ideal roundness and straightness into the mathematical model.

8.3 AXIAL SYMMETRY AND 3-D MODELLING

One approach to the use of three-dimensional geometry information in finite element modelling is to allow the radius of the piston and of the cylinder to vary axially. However, this method still has the disadvantage that a single radius value has to be assigned for each "slice" of the piston and cylinder model, thus forcing each segment to be perfectly round. One still has to assign single values for the undistorted radius and gap width, and calculations of the radial piston and cylinder distortions along the engagement length are based on the assumption of axial symmetry. For piston and cylinders which possess some asymmetry - detailed measurements often identify concave and convex surfaces - an axisymmetric model may depart substantially from reality.

It is likely that failure to represent true three-dimensional shapes may have a greater effect on finite element predictions of fall rates than of distortion coefficients. Firstly, the fall rate is proportional to the third power of the gap width. Secondly, the fall rate is an absolute value which depends on the volume of fluid enclosed between the piston and cylinder. Failure to represent the true geometry will lead to wrong estimates of this volume. Finally, the distortion coefficient is calculated from changes in shapes of the piston and cylinder rather than absolute shapes, that is, it is variations from the undistorted shape arising from pressure loading which are used in equation 4, rather than the absolute shape itself. For pistons and cylinders whose departures from roundness and straightness are small compared with their radii, it is likely that the magnitude of the changes in shape as a function of position along the engagement length are likely to be very similar to those of the ideally round and straight case, that is, the d(u+U)/dx term within the integral in equation 4, is likely not to vary greatly between the "real" and the "ideal" case at each position along the engagement length, particularly for those designs of pressure balance in which the radial distortion is proportional to or approximately proportional to the applied pressure.

8.4 THE EUROMET 463 EXPERIENCE

One of the questions which the Euromet 463 project addressed is the question of whether differences between experimental results and the predictions of finite element analysis were due to the need to take into account the real shapes of the piston and cylinder. The PTB obtained measurements of roundness and straight of the piston and cylinder from their "Geometrical standards" section. It became clear from measurements of straightness at eight positions around the piston and cylinder, each position being separated by a 45^{O} rotation from the previous position, that the piston and cylinder appeared to possess a "banana" shape and consideration of the measurements alone suggests that the piston would not fit inside the cylinder. However, if the data sets are not considered separately, but are taken in pairs representing sets measured at 180^{O} from each other and each pair is averaged to produce an estimated "average" radius for that pair of measurements, then the piston appears to fit inside the cylinder. Figure 23 shows the eight measured profiles of the cylinder at each angle and figure 24 presents the profiles for the piston. The radius data in the figures are expressed in

nanometres and the PTB estimated that the standard uncertainties of the data are at least ± 60 nm for the cylinder and ± 40 nm for the piston.

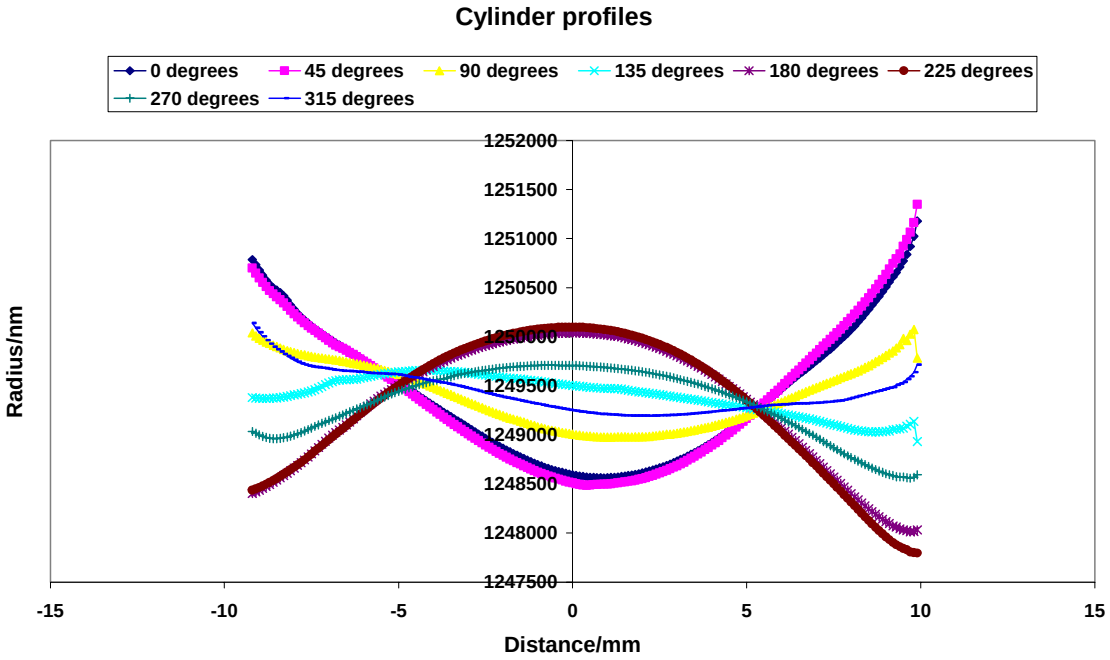

Figure 23: Euromet project 463 pressure balance, measured cylinder profile at eight angles

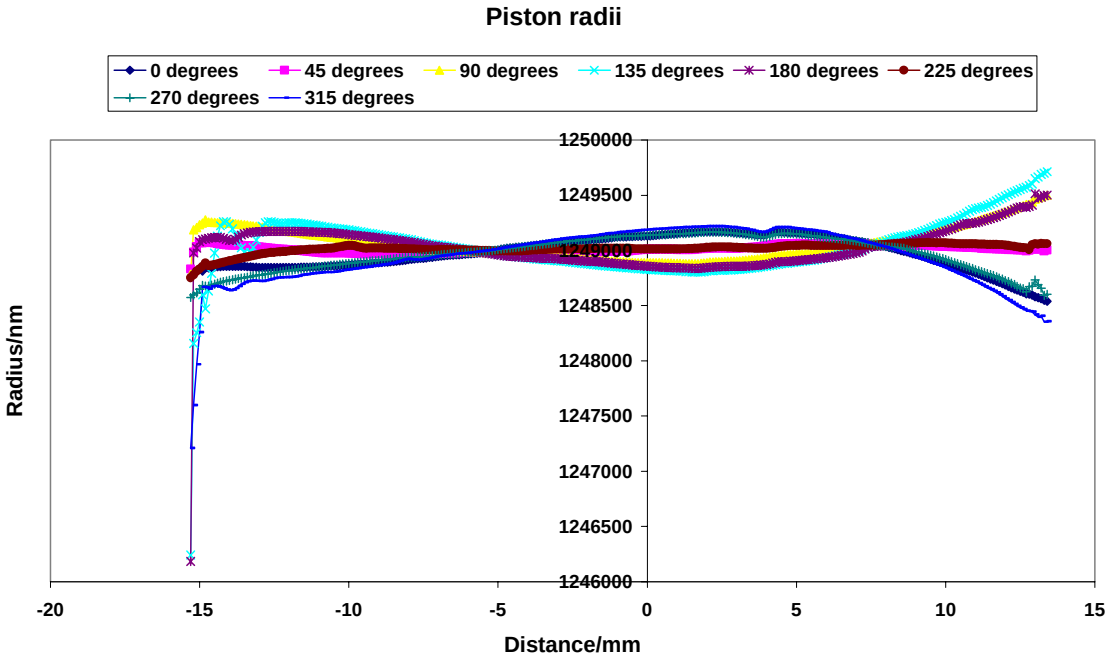

Figure 24: Euromet project 463 pressure balance, measured piston profile at eight angles

If the diametrically opposed angles are averaged for the piston and cylinder then the results shown in figures 25 and 26 are obtained. In this case, there is no interference between the piston and cylinder at any point along the engagement length.

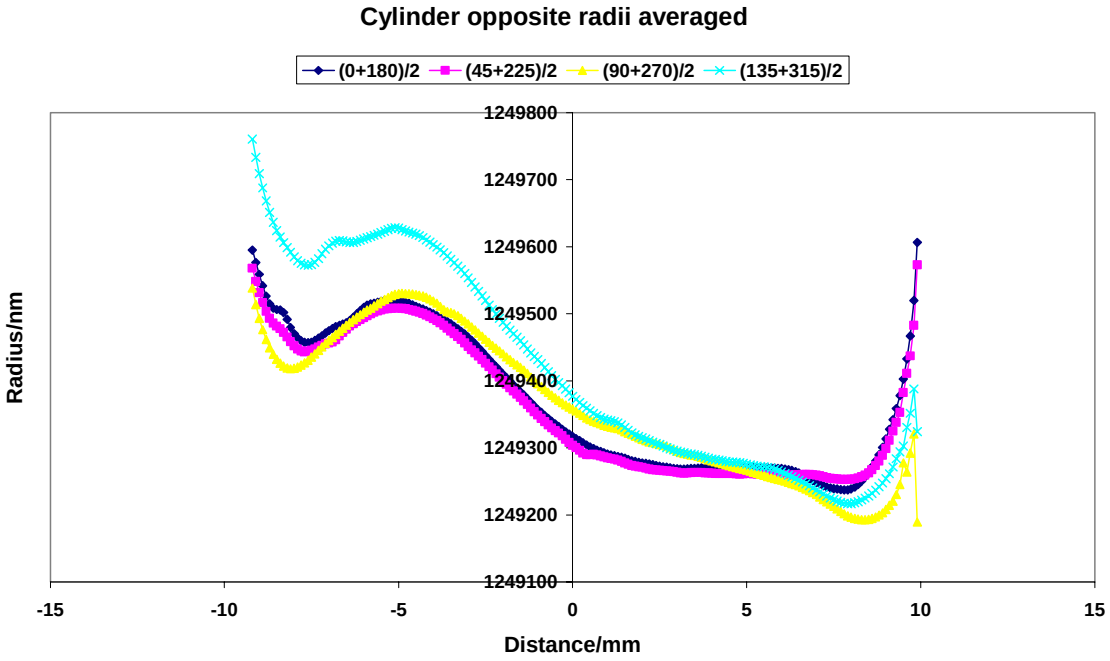

Figure 25: Euromet 463 cylinder measured radii, opposite angles averaged

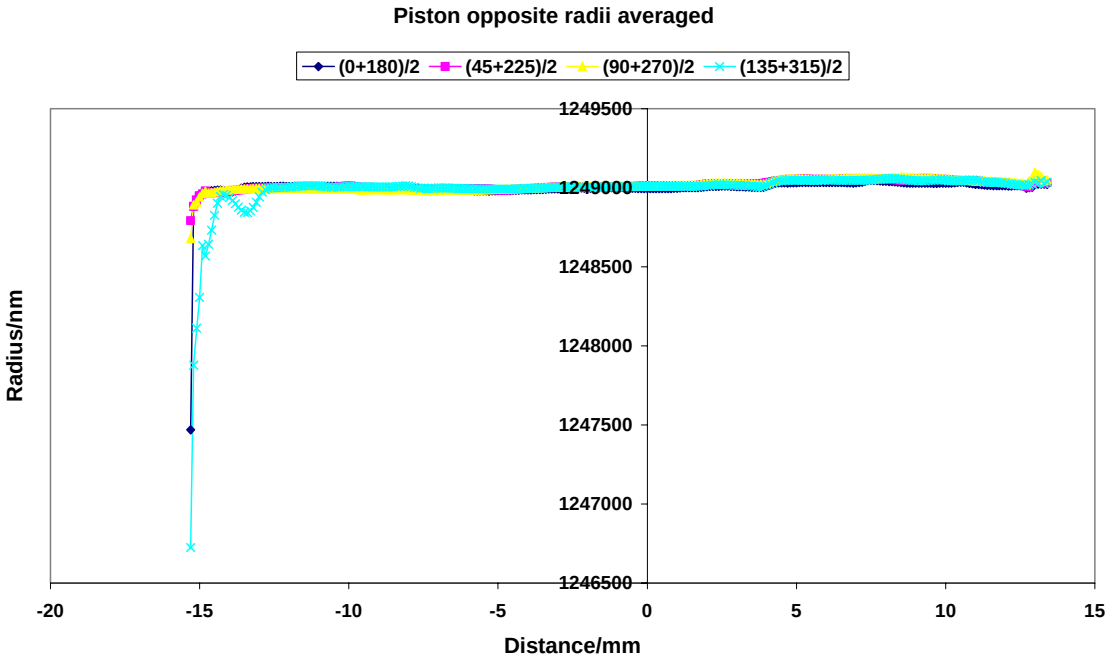

Figure 26: Euromet 463 piston measured radii, opposite angles averaged

The co-ordinator of the Euromet project suggested that for the purposes of the project it would be sufficient to average all eight sets of straightness data for the piston and cylinder, thus producing a single averaged profile for the piston and cylinder. Although this has the advantage of producing a single case which has to be analysed, it is clear from the figures presented above that such a reduction of the data leads to an axisymmetric profile which

cannot be regarded as representative of the true piston and cylinder profiles in any way. Figure 27 shows the piston and cylinder profiles which are obtained after averaging over all the data sets.

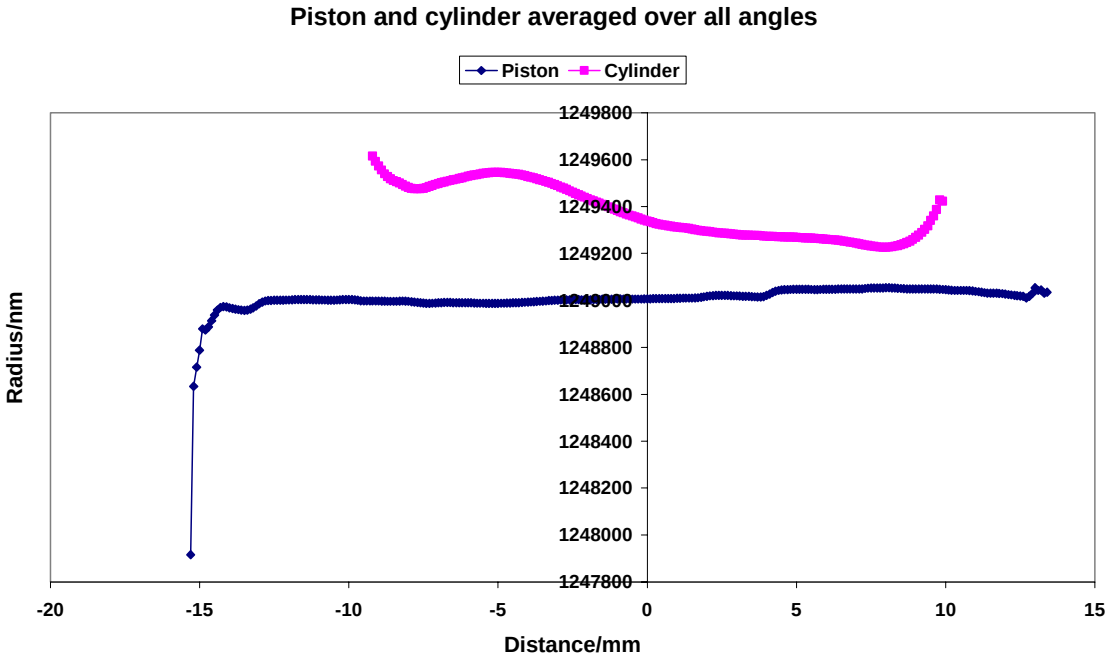

Figure 27: Euromet project 463, averaged piston and cylinder profiles

It is clear from figure 27 that, whereas the averaged piston profile is reasonably straight, the shape of the averaged cylinder profile bears no relationship to any of the individual cylinder profiles. It is likely that this failure to represent the characteristics of the real balance will have a greater effect on finite element predictions of fall rate than on the distortion coefficient prediction. As the distortion calculation takes into account only changes in radial co-ordinates of the piston and cylinder as a result of pressure loading, rather than absolute displacement, the difference between the predicted changes for the ideally round and straight case and the calculation using the averaged profiles is likely to be small.

It is not a straightforward task to adapt the finite element model for the ideally round and straight case to take account of the new co-ordinate positions in the region of the engagement length which are required to implement to measured profiles. The ANSYS software does not allow the co-ordinates of nodes simply to be reassigned. The model has to be built again from the start. In addition, the departure from ideal roundness and straightness means that it is not possible to define large areas and volumes which can be meshed using automatic meshing techniques. A third problem is that the positions along the piston and cylinder at which roundness and straightness measurements were made do not necessarily correspond to node positions in the finite element model, and in any case, one requires the ability to investigate a range of mesh densities in the model. To overcome this last problem the piston and cylinder profiles were represented as splines using the Matlab programming language, and Matlab's spline fitting routines were employed to generate the required piston and cylinder radius values at each nodal point of interest. The Matlab results were then copied into the ANSYS macros used to generate the finite element mesh. As was pointed out earlier in this chapter, even when one is work with measured profiles, it is still necessary to assign a single value for

the piston radius and the gap width to be able to calculate the distortion coefficient. This was done by calculating the average radius and gap along the engagement length. In addition to the profiles obtained by averaging all eight sets of straightness data for the piston and cylinder (figure 27), the four pairs of profiles obtained by averaging opposite angles (figures 25 and 26 were also investigated).

The results of the modelling based on measured profiles are set out in tables 42 and 43. Table 42 presents the predicted distortion coefficient and fall rate for the 400 MPa controlled clearance model for the case in which the piston and cylinder are regarded as having different materials properties. The table sets out the results obtained from averaging all eight angles and also those from averaging opposite pairs of angles. For the purposes of comparison, the predicted results for the ideally round and straight geometry were: distortion coefficient 0.3666 ppm/MPa, fall rate 0.1605 mm/min. The undistorted area value, A_O, was 4.90206 mm^2. Note the relative small effect that using the measured data has on the predicted distortion coefficient. The maximum range of the data for the five sets of results is 0.0083 ppm/MPa (0.3714 - 0.3631). If this range is regarded as representing a variation of ± 0.0042 ppm/MPa in the distortion coefficient, then in comparison to the average of the five values in the table (0.3673 ppm/MPa), this variation is ±1.14%. The fall rate predicted show a greater variation. The range is 0.0296 mm/min. As before, if we regard this as a variation of ±0.0148 mm/min, this represents ± 10% of the average fall rate obtained from the five values listed in the table. Note that all the predicted fall rates for the measured data sets are lower than those obtained from the ideally round and straight model.

Differing piston and cylinder properties: Measured profiles			
Source data	Ao/mm^2	Lambda/ ppm/MPa	Fall rate/ mm/min
All angles averaged	4.90244	0.3673	0.1478
Angles 0 and 180 averaged	4.90238	0.3714	0.1596
Angles 45 and 225 averaged	4.90238	0.3679	0.1483
Angles 90 and 270 averaged	4.40240	0.3631	0.1300
Angles 135 and 315 averaged	4.90260	0.3666	0.1536

Table 42: FEA predictions from measured profiles, differing piston and cylinder properties

Table 43 sets out similar results for the 400 MPa controlled clearance model for identical piston and cylinder properties. For comparison, the base line results for the ideally round and straight case are: 0.4907 ppm/MPa for the predicted distortion coefficient, and 0.2023 mm/min for the predicted fall rate. The range of the distortion coefficient values is 0.0071 ppm/MPa. If this is regarded as representing a variation of ± 0.0035 ppm/MPa, the variation represents ± 0.71% of the average value of 0.4905 ppm/MPa. For the fall rate predictions derived from the measured profiles, the range of the predicted fall rate values is 0.0357 mm/min. If this is taken to be a variation of ±0.0018 mm/min, then the variation with respect to the average value of 0.1801 mm/min is ±10%. Once again, the predicted fall rates obtained from the measured profiles are all lower than the value predicted for the ideally round and straight case, 0.2023 mm/min.

Identical piston and cylinder properties: Measured profiles			
Source data	Ao/mm^2	Lambda/ ppm/MPa	Fall rate/ mm/min
All angles averaged	4.90244	0.4900	0.1886
Angles 0 and 180 averaged	4.90238	0.4939	0.1596
Angles 45 and 225 averaged	4.90238	0.4923	0.1888
Angles 90 and 270 averaged	4.40240	0.4868	0.1673
Angles 135 and 315 averaged	4.90260	0.4895	0.1953

Table 43: FEA predictions from measured profiles: identical piston and cylinder properties

A possible explanation of the relative insensitivity of the distortion coefficient to variations in piston and cylinder profiles is that the distortion coefficient is derived from the changes in the piston and cylinder radius arising from pressure loading and not from the absolute local value of the radius. This can be understood from figures 28 and 29. The first figure is for the 400 MPa controlled clearance model with differing piston and cylinder properties for the ideally round and straight case. It shows both the radius of the undistorted piston and cylinder and the radius of distorted piston and cylinder as a function of position along the engagement length. The second figure presents the same data for the case in which the undistorted piston and cylinder profiles have been obtained averaging over all angles, that is, it shows the profiles relevant to the results set out in the first line of table 42 above. Notice that the differences between the undistorted and distorted radii are very similar in the two figures although the absolute values of the radii, especially for the cylinder, differ substantially.

Finally, it is to be expected that the fall rate prediction would show greater variation than the distortion coefficient predictions. Not only is the fall rate proportional to the third power of the gap width, but it is an absolute quantity whose value is determined by the volume of fluid which can flow along the gap. Variations in gap geometry will have a greater effect on fall rate than they have on the distortion coefficient.

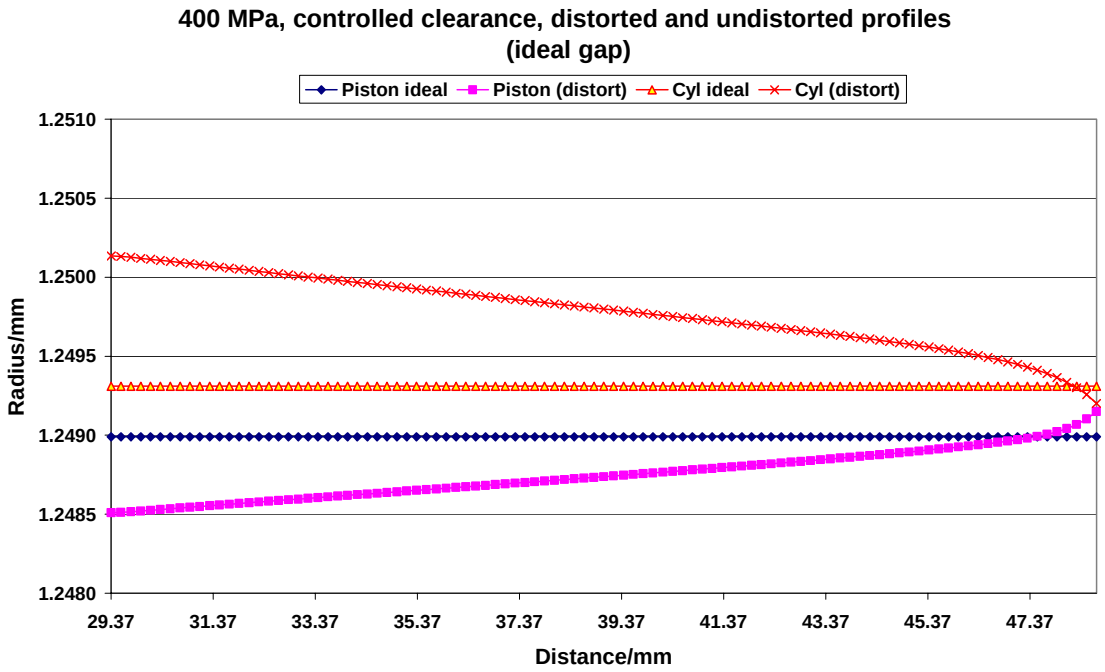

Figure 28: Prediction of the manner in which piston and cylinder distort, ideal gap

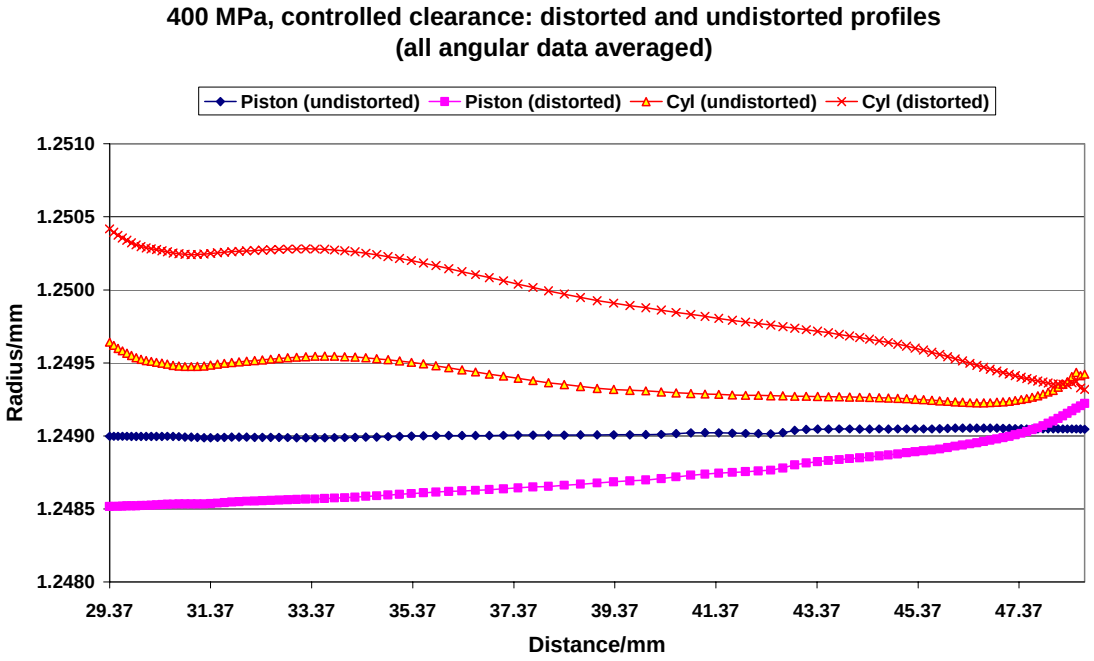

Figure 29: Prediction of the manner in which piston and cylinder distort, measured gap (averaged over all angles)

8.5 USING MEASURED PROFILE DATA: CONCLUSIONS

Current approaches to the finite element modelling of pressure balances all rely on the assumption of axial symmetry and all ignore the relative movement of the piston and cylinder, and therefore, of the pressure-transmitting fluid. In addition, the equations which are used to derive the distortion coefficient also assume axial symmetry and indeed ideal roundness and straightness, as single values are used for the piston radius and the gap width. Measured three-dimensional profile data have to be forced to fit into these prior assumptions. The most straightforward way of doing this is to reduce the measured profile data to a series of axisymmetric slices, which are stacked along the same perpendicular axis to form the piston and cylinder shapes. However, as has been shown in the case of the Euromet 463 project, the result of this process is a piston and cylinder configuration which is in not representative of the real pressure balance.

The process of building the axisymmetric slices into a finite element modelling is time consuming, as one cannot take full advantage of automatic mesh generation facilities to mesh large areas of the structure rapidly, and it is necessary to derive equations, such as splines or polynomials, from curve fitting to the measured profiles so that radius values can be derived for the piston and cylinder at the nodal positions required by the finite element model.

It also appears that distortion coefficient predictions obtained from measured profiles may not differ substantially from those obtained for the ideally round and straight case. In cases in which the measured profiles do not depart greatly from the ideal shape, this is to be expected. The methods adopted by Dadson, Lewis and Peggs (1982), in which ideal geometry is assumed, have been applied to a wide range of real devices over several decades, and for practical purposes have been shown to be adequate for almost all types of oil-based balance. If small departures from roundness and straightness led to large changes in distortion coefficient, this would have tended to invalidate their approach, which has gained general acceptance in the metrology community. In addition, if the use of measured piston and cylinder profiles as inputs to FEA models is to be adopted by NMIs, then it is necessary to reach agreement on how this is to be done in the context of axisymmetric models and their limitations, which have been reviewed in this chapter.

9 CONCLUSIONS

9.1 SUMMARY OF CONCLUSIONS OF CURRENT PROJECT

This report has described in detail the use of ANSYS finite element software to model a range of oil-operate balances, three of which are owned and operated by NPL and the fourth by the PTB. Predictions of the distortion coefficients and their sensitivity to variations in input parameters, especially materials properties and boundary conditions, have been derived for all the modelled balances. Finite element methods have the advantage that they can take into account complex engineering structures and allow realistic restraints and boundary conditions to be applied to the meshed structure. However, it is clear that the outputs of the modelling can only be as good as the available input information.

The main conclusions of the work reported here can be summarised as follows:

- For oil-operated tungsten carbide balances of simple structure in free deformation mode, there is little advantage in using finite element modelling over more simple analytical equations for predicting distortion coefficients.
- For balances made from less stiff materials, such as steel, finite element methods are to be preferred, as the simple analytical equations based on elastic theory are less reliable in this case.
- For balances with complex geometries, and which are operated at high pressures and with small gaps in controlled clearance mode, finite element analysis can provide good predictions of distortion coefficients and fall rates.
- For tungsten carbide balances in particular, variations in gap width and in line pressure have little effect on the predicted distortion coefficients. This is not so for the stainless steel balance which was modelled, which showed a dependence of the distortion coefficient on both these parameters.
- If the outputs of finite element models are to be relied upon for deriving distortion coefficient uncertainties for calibration certificates, it is essential that accurate and precise measurements data exist for Young's modulus and Poisson's ratio of all component materials. Uncertainties in knowledge of material properties are the dominant factor in the distortion coefficient uncertainties derived from mathematical modelling.
- To model controlled clearance balances accurately it is necessary to be able to define the boundary conditions in a manner which represents how the jacket pressure is actually applied. Exact representation of the pressure loading in the region of oil-seals and at the top of the engagement length is essential for reliable results.
- Attempts to represent the real three-dimensional shapes of pistons and cylinders in axisymmetric models are problematic. They cannot reflect the true shape of the piston and cylinder and ignore the effect of relative motion of the piston and cylinder, and therefore of the fluid. For cases in which the measured profiles do not show large departures from the ideally round and straight case there may be little benefit to be gained from persisting with axisymmetric models, as in any case, distortion coefficients are calculated using theory which assumes ideal roundness and straightness of the initial undistorted piston and cylinder.

- For the balances modelled during the course of this project, variations in fluid properties, i.e. viscosity as a function of pressure, and density, have very little effect on distortion coefficient predictions. Fall rate predictions are more sensitive to these parameters.

9.2 RECOMMENDATIONS FOR FUTURE WORK

Mathematical modelling of pressure balances, as it is currently carried out by metrology laboratories, has a number of limitations which have been identified in this report. Although the finite element method provides a powerful tool for investigating the sensitivity of distortion coefficients and fall rates to various features of the structure and use of the balance (material properties, pressure loading, and geometry, for example), it has a number of limitations. Effectively, its current use is simply to derive numerical results for the displacement of the cylinder and piston under pressure, which are then used in distortion coefficient equations which have been derived using many simplifications and assumptions. Thus the defects of these equations are built into the manner in which the finite element results are used.

At present the interaction between the fluid and the balance is treated as an uncoupled problem. The fluid pressure distribution problem is solved to derive a pressure distribution, which is then applied to the balance structure. A new distorted shape is derived, which allows a new pressure distribution to be calculated that can then be applied to the balance. Iteration is necessary to converge to a final prediction of the distorted shape of the balance. This can be a lengthy process. To obtain results for the Euromet 463 balance at 1000 MPa line pressure more than 400 iterations are needed, so that it can take many hours to obtain results. However, it is not clear that it is possible to solve the fluid pressure distribution problem and the structural distortion problem in a coupled manner, given that the fluid pressure distribution depends on the shape of the piston-cylinder gap. To begin the calculation, an initial guess at the pressure distribution has to be made, and at the start of the calculation this is known only at two points, the opposite ends of the engagement length. The need for iterative solution techniques is likely to make three-dimensional finite element modelling intractable without improvements in computing power, as the move from two to three dimensions would lead to a substantial increase in the size of the problem to be solved even ignoring the fact that the piston and cylinder move relative to each other.

There is a need to revisit the basic theory on which the derivation of the distortion coefficient relies if one wishes to investigate real piston and cylinder shapes in three dimensions, rather than to assume that all pistons and cylinders are ideally round and straight. One needs to begin again with the forces which a piston experiences - the forces acting on its end, the frictional force exerted by the fluid as it moves, the vertical component of the fluid pressure acting on the distorted piston - and derive distortion coefficient equations which do not assume axial symmetry. It is also necessary to review the limitations of the current techniques for representing the fluid. Current approaches assume laminar flow of a viscous fluid experiencing a one-dimensional pressure gradient. The only fluid parameters used in modelling are the pressure depend viscosity and density. It is likely that this approach is inadequate for gaps of nanometric dimensions at high pressures. Furthermore, current modelling ignores the fact that common pressure transmitting fluids such as DHS possess

long chain molecules, so that the nature of the fluid flow depends on the orientation of molecules and their interactions with each other.

In the view of the author, finite element modelling of pressure balances as it is currently performed, is useful for investigating the sensitivity of distortion coefficients and fall rates to changes in a limited range of balance properties, but it cannot give a true picture of how a balance behaves in practice. It is therefore important to appreciate that finite element methods can only answer a limited range of questions about the behaviour of pressure balances. A more comprehensive understanding, especially one which can be applied to balances operating at high pressures and with nanometric gaps, requires revision and refinement of existing theories.

10 ACKNOWLEDGEMENTS

The work carried out by Dr Ade Idowu in developing ANSYS finite element models of pressure balances during the course of previous DTI programmes provided an excellent foundation for the results reported here. In addition, the author would like to thank the Department of Trade and Industry's National Measurement System Directorate for its support for this research.

REFERENCES

Buonanno G, Dell'Isola M, Maghenzani R, Finite element analysis of pressure distortion coefficient and piston fall rate in a simple pressure balance, Metrologia, Vol. 36, No. 6, pp 579-584, 1999

Buonanno G, Dell'Isola M, Iagulli G, A finite element method to evaluate the pressure distortion coefficient in pressure balances, High Temperatures – High Pressures, Vol. 31, No. 2, pp 131-143, 1999

City University, A preliminary report on modelling more pressure balances, City University School of Engineering Report, May 1991

Dadson R S, Greig R G P, Horner A, Developments in the accurate measurement of high pressures, Metrologia, pp 55-68, 1965

Dadson R S, Lewis S L, Peggs G N, The Pressure Balance: Theory and Practice, London, HMSO, 1982

Doi H, Fujiwara Y, Miyake K and Oosawa Y, Systematic investigation of elastic moduli of WC-Co alloys, Met. Trans. A. pp 1417-1425, 1970

Drysdale C.V. et al, The mechanical properties of fluids, Blackie and Son, 1925

Heydemann P L M, Welch, B E, Pressure Measurements III – piston gages, pp 147-202, in Experimental Thermodynamics. Volume II, Experimental thermodynamics of non-reacting fluids, eds, Le Neindre B, Vodar B, Butterworths, 1975

Min Gon Kim, Lamb J, The effects of pressure and temperature on the viscosities of liquids composed of long-chain molecules, Journal of the Korean Physical Society, vol. 18, no. 2 pp 109-122, 1985

Molinar G, Sabuga W, Robinson G, Legras J C, Comparison of methods for calculating distortion in pressure balances up to 400 MPa – EUROMET Project 256, Metrologia, Vol 35, No. 5 , pp 739-759, 1998

Molinar G F, Maghenzani R, Urbanski M, Wisniewski R, Buonanno G, Dell'Isola M, Elastic distortions of a mixed (simple and re-entrant) piston-cylinder unit for pressure measurements up to 2.6 GPa, Metrologia, Vol. 36, No. 6, pp 595-590, 1999

Robinson G M, Second NPL analysis of the distortion of pressure balances as part of EUROMET Project 256, NPL Report MOM 120, National Physical Laboratory, Teddington, UK, July 1996

Robinson G M, Finite element prediction of the distortion coefficients of pressure balances, XIV IMEKO World Congress, Tampere, Finland, 1-6 June 1997

Sabuga W, Elastic distortion calculations at PTB on LNE 200 MPa balances as part of Euromet project 256, PTB-W-63 report, 1995, Physikalisch-Technische Bundesanstalt, Braunschweig, Germany

Sabuga W, Elastic distortion calculations at PTB on a PTB 400 MPa balance as part of Euromet project 256, PTB-W-60 report, 1995, Physikalisch-Technische Bundesanstalt, Braunschweig, Germany

Sabuga W, Determination of the elastic properties of piston gauges using the strain gauges method, Proceedings of the 17th International Conference on Mass, Torque and Pressure Measurements, IMEKO TC3, Istanbul, pp 380-385, September 2001

Samaan N D, Abdullah F, Characterisation of a 1 GPa piston-cylinder unit, Measurement, Vol. 23, No. 3, pp179-183, 1998

Samaan N D, Mathematical modelling of instruments for pressure metrology, Ph D thesis, City University, London, UK, 1990

Samaan N D, Computer-aided modelling of pressure balances, Metrologia, Vol 30. No. 6, pp 641-644, 1994

Stuart P R , The influence of fluid viscosity on the distortion of piston-cylinder assemblies in pressure balances, Proceedings of a seminar on high pressure metrology, published in BIPM monograph 89/1, pp 31-40, Paris, May 1989

APPENDIX A: DIAGRAMS OF MODELLED BALANCES

This appendix presents ANSYS drawings of the main volumes and meshes for each of the finite element models of pressure balances discussed in this report. All the models shown are axisymmetric so that to form the full three-dimensional shape one has to rotate the areas shown in the figures about the vertical axis of symmetry in the model. For the Euromet 256, B2-816, B2-817 and DH serial no. 1000 balances only the piston and cylinder have been modelled. In the case of the Euromet project no 463 balance it will be seen that it is necessary to include more detail of the structure of the balance to obtain reliable results.

The meshes shown in these figures are less dense than those used in practice during the course of the modelling to allow the reader to distinguish the main features of the meshing methods which were employed.

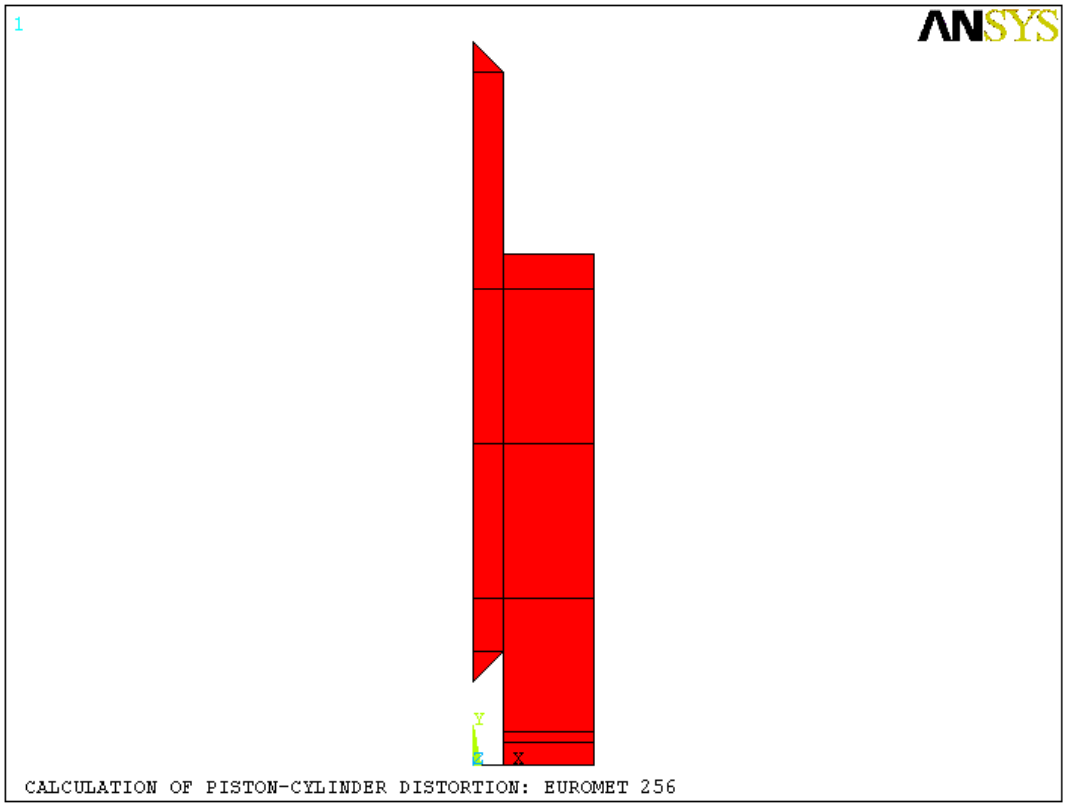

Figure A1: Euromet project no 256 pressure balance: piston and cylinder volumes

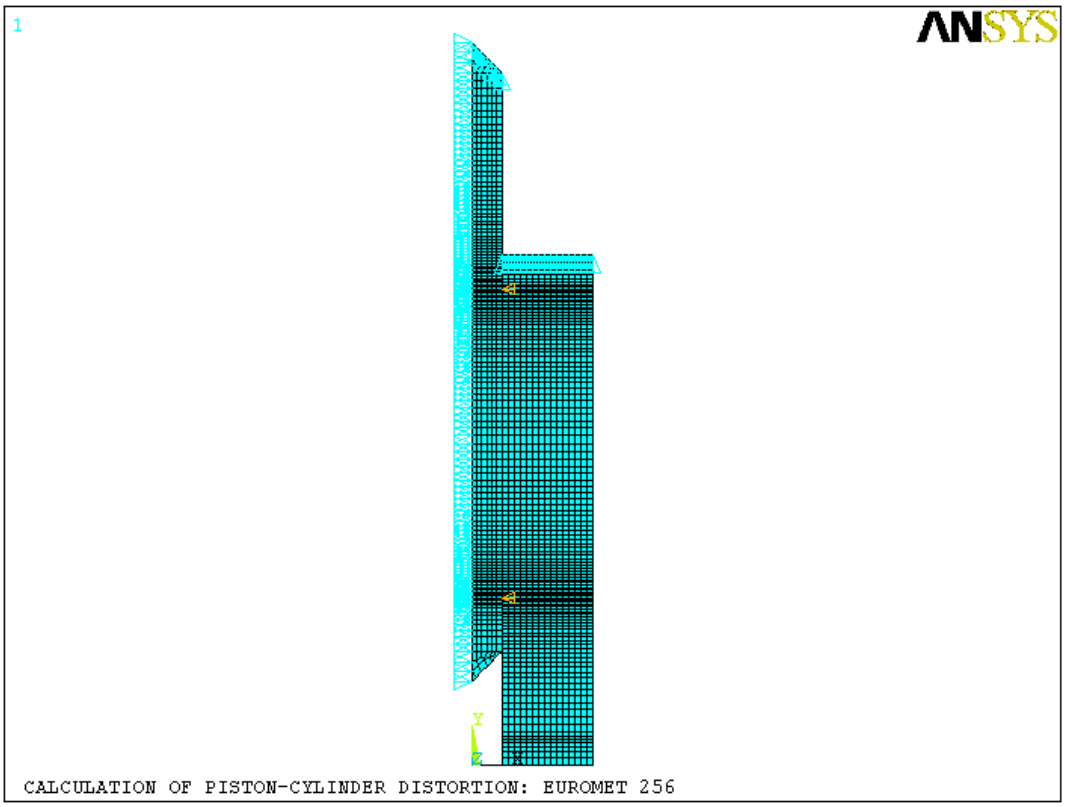

Figure A2: Euromet project no 256 pressure balance: piston and cylinder mesh

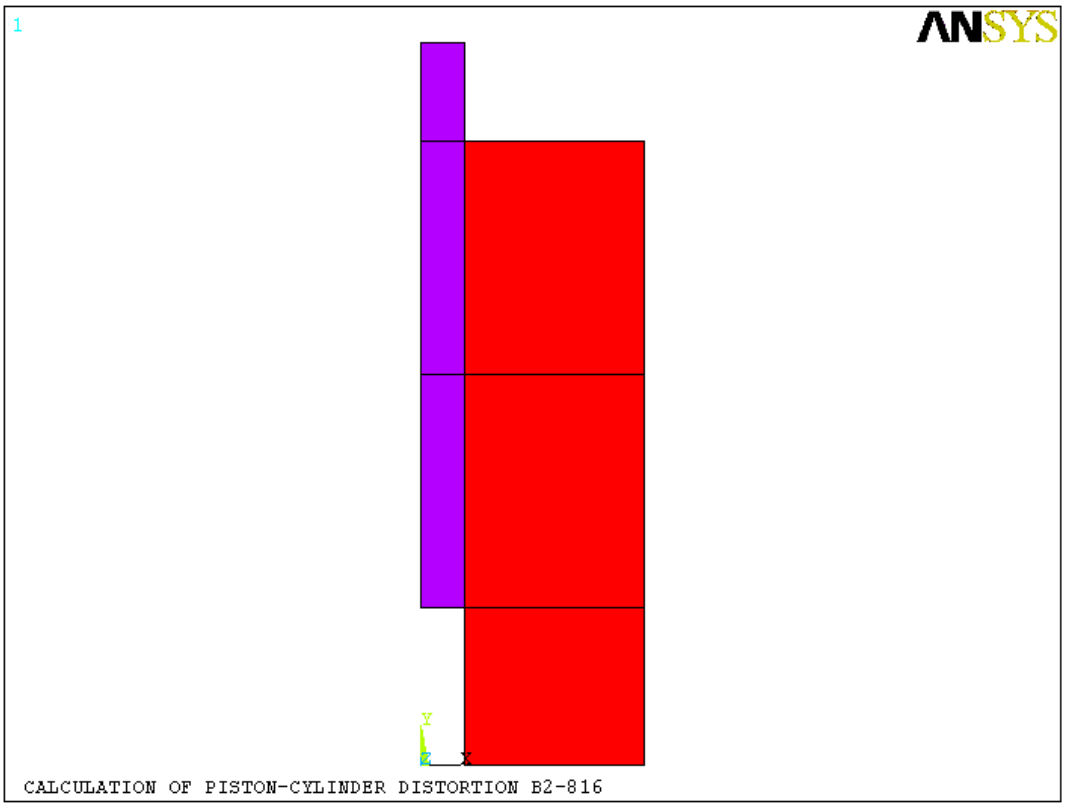

Figure A3: B2-816 pressure balance: piston and cylinder volumes

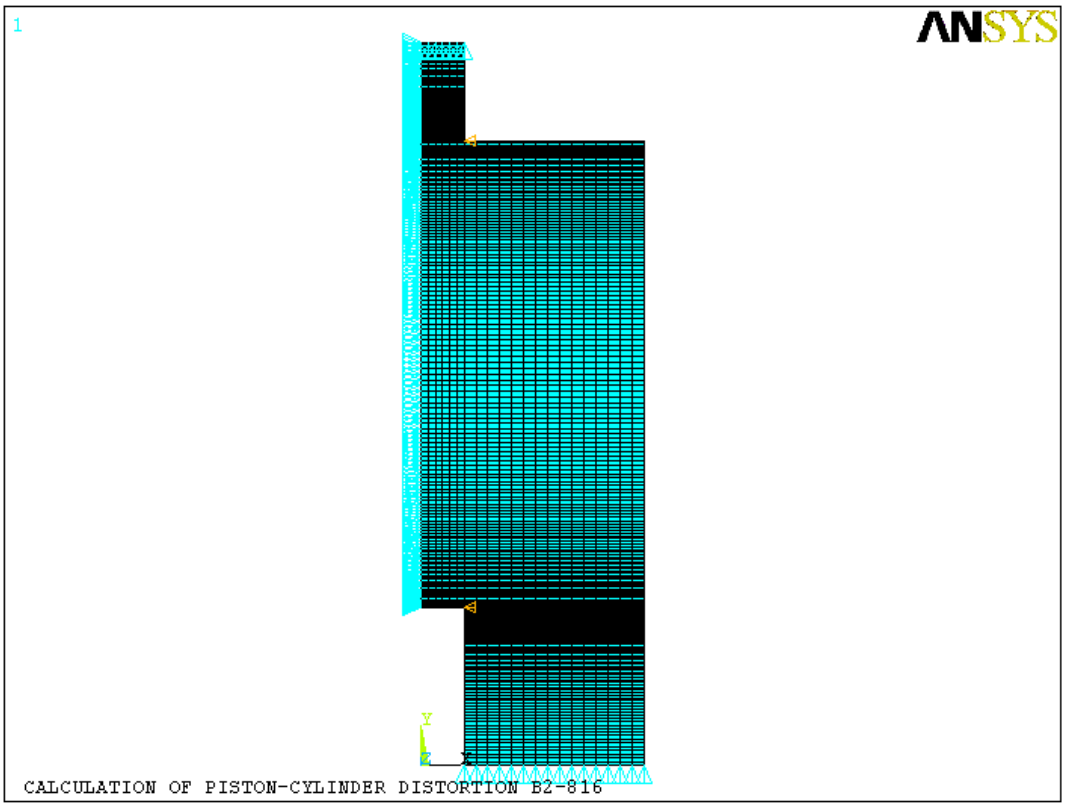

Figure A4: B2-816 pressure balance: piston and cylinder mesh

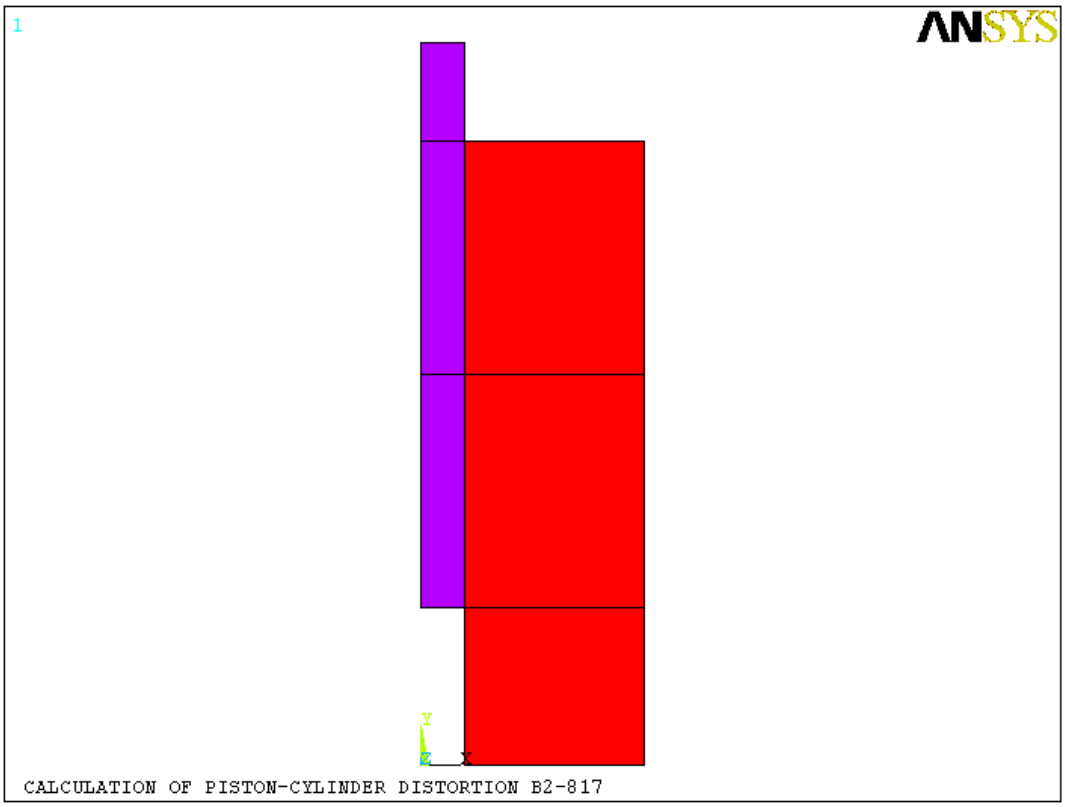

Figure A5: B2-817 pressure balance: piston and cylinder volumes

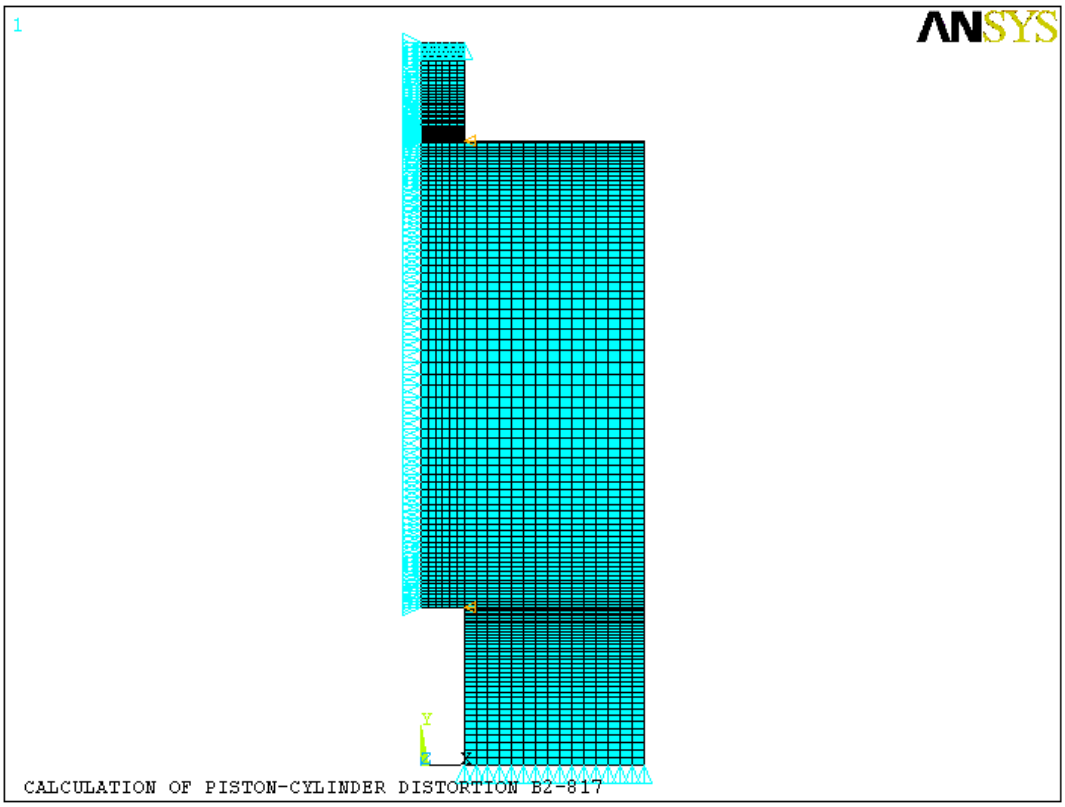

Figure A6: B2-817 pressure balance: piston and cylinder mesh

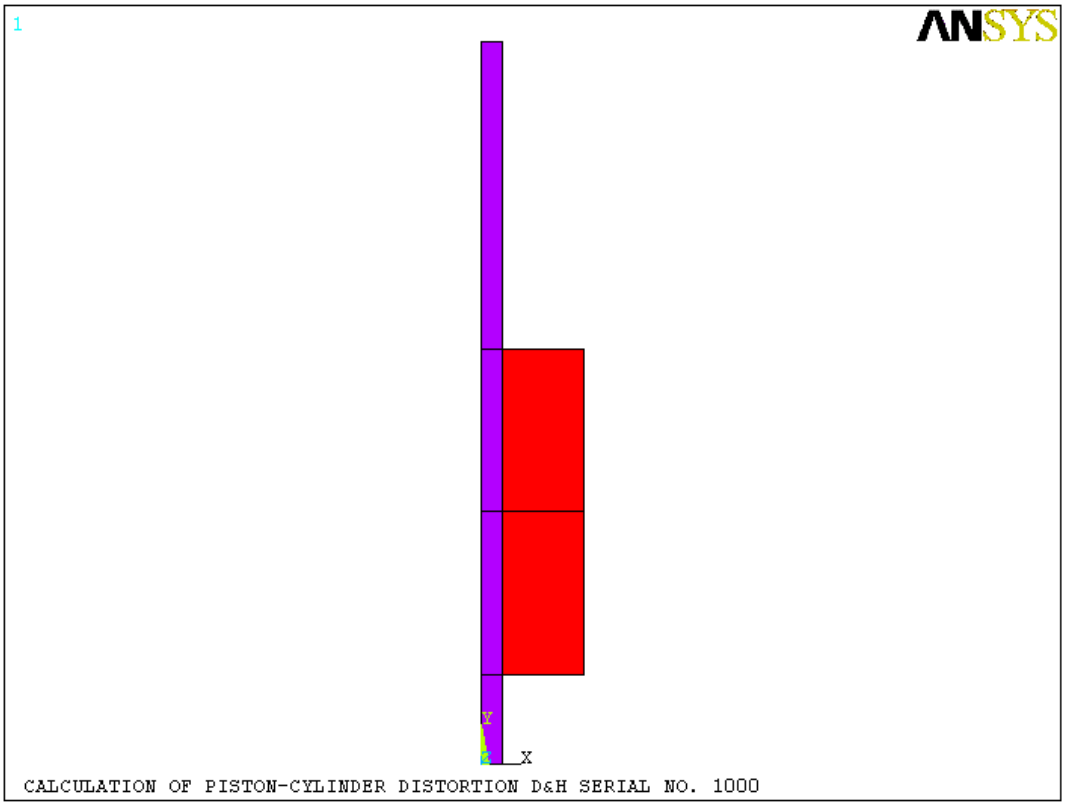

Figure A7: D&H serial no 1000 pressure balance: piston and cylinder volumes

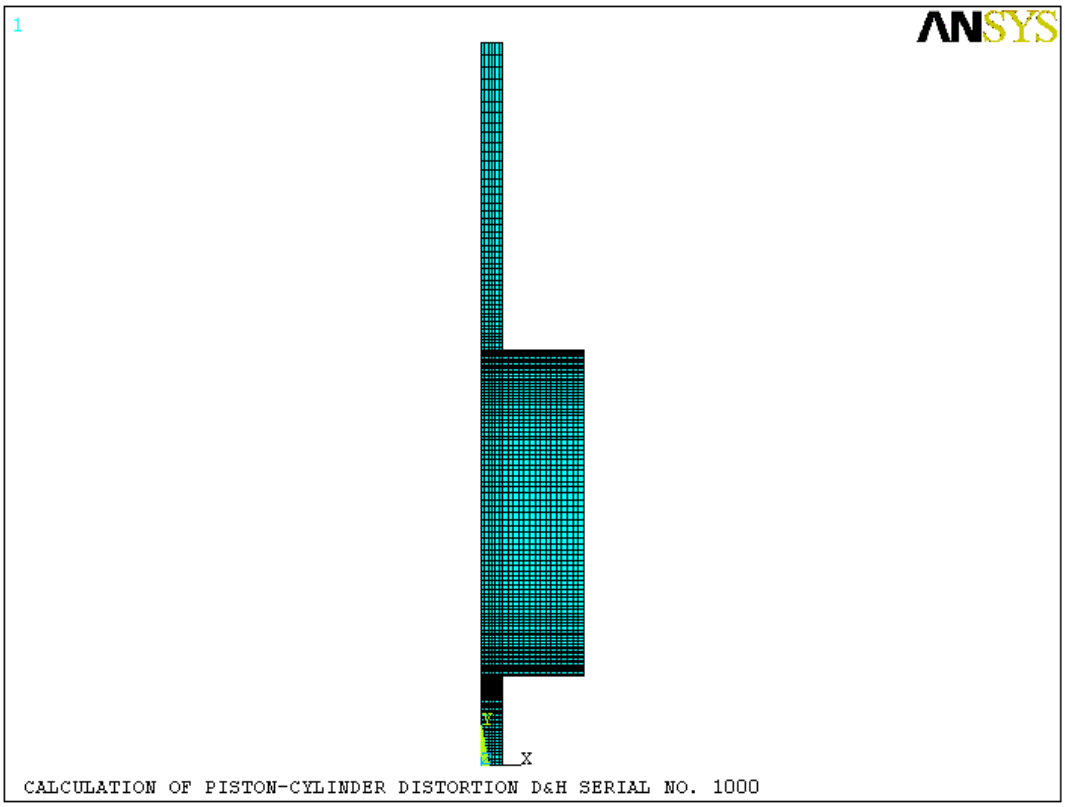

Figure A8: D&H serial no 1000 pressure balance: piston and cylinder mesh

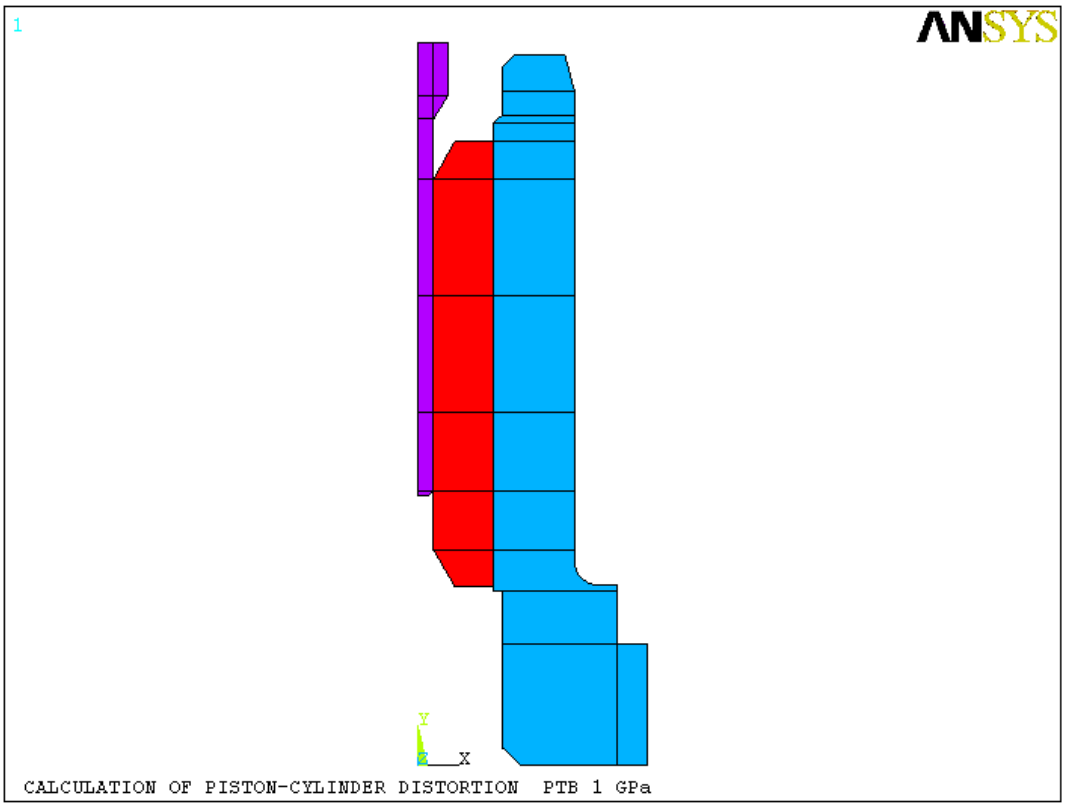

Figure A9: Euromet project no 463 pressure balance: piston and cylinder volumes

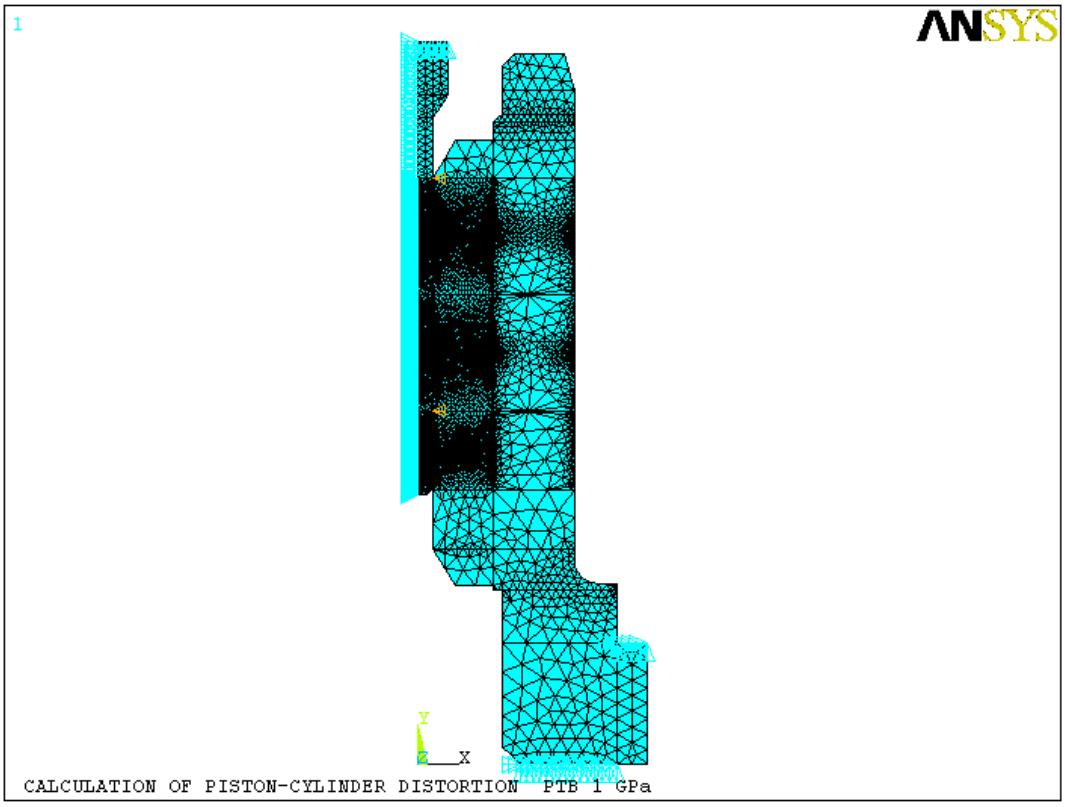

Figure A10: Euromet project no 463 pressure balance: piston and cylinder mesh